Applications of Field Theory to Reaction Diffusion Models and Driven Diffusive Systems

Sayak Mukherjee

Dissertation submitted to the Faculty of the
Virginia Polytechnic Institute and State University
in partial fulfillment of the requirements for the degree of

Doctor of Philosophy
in
Physics

Beate Schmittmann, Chair
Uwe. C. Täuber
Rahul Kulkarni
Tatsu Takeuchi

August 25, 2009
Blacksburg, Virginia

Keywords: Field Theory, Model A, Directed Percolation, Renormalization Group, Tasep, Power spectrum

Applications of Field Theory to Reaction Diffusion Models and Driven Diffusive Systems

Sayak Mukherjee

(ABSTRACT)

In this thesis, we focus on the steady state properties of two systems which are genuinely out of equilibrium. The first project is an application of dynamic field theory to a specific non equilibrium critical phenomenon, while the second project involves both simulations and analytical calculations. The methods of field theory are used on both these projects. In the first part of this thesis, we investigate a generalization of the well-known field theory for directed percolation (DP). The DP theory is known to describe an evolving population, near extinction. We have coupled this evolving population to an environment with its own nontrivial spatio-temporal dynamics. Here, we consider the special case where the environment follows a simple relaxational (model A) dynamics. We find two marginal couplings with upper critical dimension of four, which couple the two theories in a nontrivial way. While the Wilson-Fisher fixed point remains completely unaffected, a mismatch of time scales destabilizes the usual DP fixed point. Some open questions and future work remain.

In the second project, we focus on a simple particle transport model far from equilibrium, namely, the totally asymmetric simple exclusion process (TASEP). While its stationary properties are well studied, many of its dynamic features remain unexplored. Here, we focus on the power spectrum of the total particle occupancy in the system. This quantity exhibits unexpected oscillations in the low density phase . Using standard Monte Carlo simulations and analytic calculations, we probe the dependence of these oscillations on boundary effects, the system size, and the overall particle density. Our simulations are fitted to the predictions of a linearized theory for the fluctuation of the particle density. Two of the fit parameters, namely the diffusion constant and the noise strength, deviate from their naive bare values [6]. In particular, the former increases significantly with the system size. Since this behavior can only be caused by nonlinear effects, we calculate the lowest order corrections in perturbation theory. Several open questions and future work are discussed.

This work is supported by the NSF through Grant Nos. DMR-0414122 and DMR-0705152.

Dedication

I dedicate my work to my father, Bholanath Mukherjee and my mother, Udita Mukherjee.

Acknowledgments

First and foremost, I would like to thank my advisor Dr. Beate Schmittmann for her constant help and support through out my PhD career. She always encouraged stimulating discussions and independent thinking. She has been a mentor. I have learnt a great deal from her and I hope I can live up to her expectations for the years to come.
I would like to thank my committee member Dr. Uwe. C. Täuber. He has been extremely supportive. He always trusted in my abilities and helped me navigate through the ups and downs in my PhD career. I learned field theory from him. His presence in my research career is of singular importance.
A special thank you goes to my committee member Dr. Tatsu Takeuchi. He read my thesis with utmost care and patience. His suggestions were extremely helpful.

I would like to acknowledge my very good friends Sven Dorosz and Thierry Platini for helpful and insightful discussions. They read preliminary drafts of my thesis a multiple times. They have been a constant source of motivation. I have learnt a lot from Sven. He is not only a good friend but also a very dedicated and independent researcher. Without him life would have been terribly mundane.
I would also like to thank Dr. Royce Zia for helpful discussions. Amanda Rohm Daquila and George Daquila helped me a lot. They proof read my thesis and made valuable comments. Thank you, both of you. Both of you have been great friends to keep up with.
I would like to thank Xiaohua Xu for her help and support. She edited my thesis and contributed unconditionally.
Our graduate co-ordinator Christa Thomas has helped me with all the official paper works. Without her I would never have gotten things done on time.

Contents

1 Introduction **1**

2 Background and Overview **4**

2.1 Introduction 4

2.2 The Model 5

2.3 Mean Field Approximation 6

2.4 Mean Field Scaling Exponents 6

2.5 Mapping to Field Theory 7

2.6 The Environment Dynamics 10

2.7 Dynamical Functional for Model A 11

2.8 Critical Exponents 12

2.9 Previous Works with Fluctuating Backgrounds 12

3 Universal Properties of Population Dynamics With Fluctuating Resource **14**

3.1 Perturbation Theory 15

3.2 Fixed Points 22

4 Totally Asymmetric Simple Exclusion Process **25**

4.1 Introduction 25

4.2 Model 25

4.3 The Steady State for TASEP on a Ring 26

4.4 Interface Equivalence 27

4.5 Steady State for an Open TASEP 29

4.6 The Power Spectrum 30

5 Simulation Results and Theoretical Outlook **35**

5.1 Simulation and Results 35

5.1.1 Dependence on System Size 36

5.1.2 Dependence on Density 37

5.1.3 Effect of the Boundary 39

5.1.4 Periodic TASEP with a Window in the Middle 40

5.1.5 Density Dependence of the Power Spectrum of a TASEP on a Ring with a Window in the Middle 42

5.2 Linear Theory 44

5.3 The Fitting Parameter D 46

5.4 Perturbation Theory 47

5.5 The Discrete Case 50

6 Summary and Conclusion **53**

A Detailed Calculation of the Beta Function **60**

B Calculation of the Diagram (5.14) to One-Loop Order **64**

List of Figures

2.1 The reaction rules for the model under consideration. In our model the rules are, a species undergoes reproduction $A \to 2A$, death $A \to \emptyset$ and competition $2A \to A$ with rates σ, μ and α respectively. 5

3.1 The elements of perturbation theory. The black lines are model A propagators. The blue lines are the population dynamics propagators. 15

3.2 Primitively divergent diagrams to one loop order 16

4.1 The phase diagram of an open TASEP. The high density, low density and the maximal current phases are represented by acronyms HD, LD and MC respectively. 30

4.2 Typical time series for $N(t)$, for $L = 600$, in the two distinct regimes: MC and LD. The data have been generated by us but a similar image was originally published in [6]. 31

4.3 The power spectrum of an open TASEP in the MC phase is shown in black. The rates $\alpha = 0.6$ and $\beta = 0.7$. The system size is $L = 600$. We show the power spectrum of an open TASEP of the same length in the LD phase in red. The rates are $\alpha = 0.1$ and $\beta = 0.7$. The data have been generated by us but a similar image was originally published in [6]. 32

4.4 Fit for the linear theory using A and D as a fitting parameter a) L=100 , b) L = 200. The parameters are $\alpha = 0.1$ and $\beta = 0.7$. $\omega = 2\pi m/T$. 33

5.1 Log-log plot of the power spectrum for the open TASEP in the low density phase for different system sizes L. $\alpha = 0.2$ and $\beta = 0.7$. 36

5.2 Log-log plot of the location of the first minimum for different system sizes L starting from 100 up to 900. $\alpha = 0.2$ and $\beta = 0.7$. The red line is the best fit, to a function of the form C_0/L^{δ}. The blue line is a plot of A_0/L . 37

5.3 Log-log plot of the power spectrum of an open TASEP of length $L = 400$ for different densities. 38

5.4 Linear plot of a) location of the first minimum and b) location of the second minimum as a function of ρ for system size $L = 400$. The parameters are $\alpha = 0.2$ and $\beta = 0.7$. A linear function was used to fit the above data, the functional form of which was obtained from Eqn (4.25). For the panel left panel the plot is for the function $163.84 - 327.68\bar{\rho}$. For the right panel the plot is for function $327.68 - 655.36\bar{\rho}$. $T = 65536$. 38

5.5 Log-log plot of the power spectrum. a) Open TASEP of length $L = 100$ and an open TASEP of length $L = 2000$ with a window of length $l = 100$. b) Open TASEP of length $L = 200$ and an open TASEP of length $L = 2000$ with a window of length $l = 200$. The parameters are $\alpha = 0.2$ and $\beta = 0.7$. For the TASEPs with the windows, the power spectra are calculated only inside the window and not for the whole system. 39

5.6 Log-log plot of the power spectrum of an open TASEP of $L = 2000$ and $l = 300$ placed at different locations starting from lattice site 300 to lattice site 1500. The plot also shows the graph for $L = 300$. The parameters are $\alpha = 0.01$ and $\beta = 0.7$. 40

5.7 Log-log plot of the power spectrum of an a) open TASEP of $L = 100$ and a periodic TASEP of window $l = 100$ b) open TASEP of $L = 200$ and a periodic TASEP of window $l = 200$, $\rho = \alpha = 0.2$. The system size of the periodic TASEP is $L = 2000$. 41

5.8 Log-log plot of the power spectrum of a periodic TASEP a) window $l = 200$ for different system sizes b) the same graph with x-axis rescaled as ωL. The sector displayed, shows the location of small ω oscillations collapse. $\rho = 0.2$. 41

5.9 Log-log plot of the power spectrum of a periodic TASEP a) system size $L = 2000$ for different window sizes b) the same graph with x-axis rescaled as ωl. The sector displayed, shows the location of large ω oscillations collapse. $\rho = 0.2$. 42

5.10 Log-log plot of the power spectrum of a periodic TASEP of length $L = 2000$ and window size $l = 400$ for different densities. 43

5.11 Linear plot of a) location of the first maximum b) location of the second maximum as a function of ρ for window size $l = 400$ of a periodic TASEP. 43

5.12 Log-log plot of the power spectrum of a periodic TASEP along with its fit for $L = 2000$, a) window size $l = 300$ b) window $l = 400$, $\bar{\rho} = 0.2$ with D as a fitting parameter. $D = 6.0$ and 6.4 respectively for a) and b) 45

5.13 The dots are the extracted values of the diffusion constant D. The solid lines are fits. a) Linear plot of the diffusion constant Vs the system size for three different densities. The diffusion constant is extracted by fitting the log of Eqn (4.25). to the log of the data obtained from simulation. The three plots are fitted with a power law of the form $y = A + Bx^{\delta}$. The exponents for the three data sets are roughly 0.3. b) Linear plot of the diffusion constant as a function of the system size for three different densities. The diffusion constant is extracted by fitting the function above to the raw data. 47

5.14 Two point Feynman graph to one loop order. 49

Chapter 1

Introduction

Our modern understanding of the macroscopic world around us has been largely facilitated by classical thermodynamics and equilibrium statistical mechanics. The field of thermodynamics, which has been both empirical and very fundamental, has been tremendously successful in describing and comprehending equilibrium processes. Equilibrium phenomena are mainly characterized by vanishing transport of material and energy between the system and the environment (there is a more technical and more precise definition of the equilibrium based on the probabilities of the configurations and the rates associated with the transitions from one configuration to another in phase space). Systems in equilibrium are all around us, starting from a perfect salt crystal to a mug of coffee left to itself for a fair amount of time. The question that naturally arises is how to connect the thermodynamic properties like temperature, internal energy and so on with the microscopic details of the systems under investigation. Ideally one can write down a Newton's or a Schrödinger's equation for all the degrees of freedom and try to extract meaningful quantities by solving those equations. But due to the presence of a macroscopically large number of constituent particles, this approach will have limited success. Instead, we have to resort to the methods of statistical physics for studying the properties of many body systems. In equilibrium there is a framework which adequately serves this purpose. The probability of a microscopic configuration C is given by the Gibbs measure $P_{eq}(C) \sim e^{-H(C)/k_BT}$, where $H(C)$ is the microscopic Hamiltonian associated with the configuration, and k_BT denotes the temperature T multiplied by the Boltzmann constant. The ergodic hypothesis (time average is equal to the ensemble average) then allows us to calculate the thermodynamic quantities of interest from the configurational sum of the above distribution, also known as the partition sum.
But many interesting systems are not in equilibrium. Examples of *non-equilibrium* systems can be found on all length scales, from thousands of kilometers to scales which are a million times smaller. The systems, such as weather patterns, biological structures, glasses are examples of non-equilibrium systems. Unlike equilibrium, where there is no net transport, non-equilibrium entails influx and out-flux of energy and matter to and from the system. The hurricane, for example, can consume a huge amount of heat from the ocean before it makes a landfall. An iron bar connected to two heat reservoirs maintained at different temperatures can serve as a simple but classic example of a non-equilibrium

system. Any life form consumes food to survive, maintaining a non-equilibrium condition. In order to describe both an equilibrium and a non-equilibrium process by one generic governing equation, it is instructive to look at the time evolution of the time dependent probability $P(C,t)$ for a given configuration C. The equation is known as the master equation and has the form [1]

$$\frac{dP(C,t)}{dt} = \sum_{C'} \Big[w(C' \to C)P(C',t) - w(C \to C')P(C,t) \Big], \tag{1.1}$$

where $w(C' \to C)$ is the real non-negative incoming transition rate from the configuration C' to C and $w(C \to C')$ is the real non-negative outgoing transition rate from the configuration C to C'. Due to the conservation of probability we can identify the expression $K^* = w(C' \to C)P(C',t) - w(C \to C')P(C,t)$ inside the brackets as the net probability current from C' to C. Now, a steady state corresponds to a probability distribution that is independent of time. Looking at Eqn(1.1) one can readily see that the left hand side is identically zero for all configurations provided the sum total on the right hand side is zero or the terms K^*'s, are individually zero for any pair of configurations C' and C. The later condition

$$\frac{P(C',t)}{P(C,t)} = \frac{w(C \to C')}{w(C' \to C)} \qquad \text{for} \qquad \forall \ \mathrm{C}, \mathrm{C}', \tag{1.2}$$

goes by the name of *detailed balance* [1]. It turns out that if a system satisfies detailed balance, its long time probability distribution is given by the Gibbs measure.
In the absence of detailed balance, the system, however, can settle down into a non-equilibrium steady state, described by a time independent probability distribution but with a net non-zero probability current between any two pair of configurations. In non-equilibrium the stationary probability distribution is not given by the Gibbs measure and the distribution function has to be derived from the master equation. Due to the violation of detailed balance, solving the master equation can be an exceedingly difficult task.
We have worked on two models whose long time probability distributions are not given by the Gibbs measure. My first model is a reaction diffusion model whereas my second model is a driven diffusive model. Reaction diffusion models in the context of non-equilibrium physics describe evolving populations or chemical reactions in materials. The processes under consideration can be diverse, ranging from the evolution of a colony of bacteria or social networks, to chemical reactions like the fluorescence of certain liquids or amorphous semiconductors. The reactants/particles in these models are distributed on a lattice or in continuum. The choice of a lattice is strictly for convenience (for the purpose of computer simulation and also analytical calculations). The reactants/particles are allowed to hop (discrete case) or undergo diffusion (continuum). They are made to react following certain dynamic rules motivated from real life situations. The particles in these models are not physical particles and reactions are not necessarily chemical in nature. The particular model that we will look at is known to describe the evolution of a population on a uniform environment/background, on the brink of extinction [2, 3]. When the appropriate reaction rates are tuned the system undergoes a second order phase transition to a passive state where all the population eventually dies out. The questions that naturally arise are; what happens when the environment is no longer uniform but has its own dynamics ? How does a fluctuating environment affect the stability of the transition mentioned above ?

Studying the stability of the phase transition in this model under a particular choice of environment dynamics will be my area of focus for the first half of my dissertation. There are two essential ingredients : a) the population dynamics model and b) the environment dynamics. In chapter 2 we will describe our model and the environment dynamics. We will also summarize the known results for both the population dynamics model and the environment dynamics in that chapter. In chapter 3 we will present our own work in detail.

Our next project is on a specific driven diffusive model. Examples of transport processes are ubiquitous in nature ranging from the directed walk of the ribosomes along the mRNA strand to the transport of goods along the interstates. Driven diffusive models are used in modeling transport processes. The transport processes are modeled by particles hopping on a lattice or diffusing in continuum, respecting exclusion. The system is subjected to an external force due to which the particles undergo asymmetric hopping or biased diffusion. The specific model that we will study is known as the *totally asymmetric simple exclusion process* or in brief the TASEP model [4, 5]. There are two variants of the TASEP model, namely the closed and the open TASEP. Closed TASEP is a system on a ring, whereas for the open TASEP the system is coupled to two particle reservoirs at its two ends. Both closed and open TASEP are out of equilibrium systems as they support macroscopic particle transport even in a steady state. Unlike most of the non-equilibrium models one encounters, the steady state distribution of the TASEP model is known analytically. The steady state of the open TASEP is very rich. It exhibits multiple phases, phase co-existence and phase transitions. Our work in this model is motivated from a recent paper [6]. The authors of Ref [6] looked at the power spectrum of the total number of particles in an open TASEP. They found interesting features in the power spectrum undetected previously. In chapter 4 we will describe the model is detail, summarize a few known results and outline the recent finding by Adams et al. [6], along with a few open questions that prompted our work. In chapter 5 we will undertake a more thorough study of the power spectrum using rigorous Monte-Carlo simulations and analytic techniques. We will analyze the power spectrum for both the open and the closed TASEP. We will explicitly show how the power spectrum depends on the system size and the density of the particles. The boundary effects will be studied. Finally we will carry out some analytic calculations to address the open question in the Adams et al. work.

Chapter 2

Background and Overview

2.1 Introduction

Understanding continuous phase transitions, where all the relevant degrees of freedom participate co-operatively over large length scales has been a major challenge of equilibrium statistical mechanics. The most popular example of this kind of phenomena is the order-disorder transition in the two dimensional Ising model, where the correlation length diverges as the critical temperature is approached. The physics at criticality is described in terms of universal scaling laws and critical exponents. Different materials with different microscopic interactions were found to have the same type of singular behavior at the critical point. They are characterized by the same critical exponents which only depend on the number of spatial dimensions, the underlying symmetries and the range of interaction. All uniaxial three-dimensional magnets with short ranged interactions for example, have the same set of critical exponents. Based on these features, systems can be classified into different *universality classes*, defined by the critical exponents and scaling laws.

Examples of continuous phase transitions are not confined within processes at thermal equilibrium. Examples of non equilibrium phase transitions [7, 8] range from traffic jam [9] to spreading of infectious disease [10]. The concept of universality can be carried over to non equilibrium critical phenomena as well. One expects the universality classes to be more diverse than their equilibrium counterparts as they are governed in addition by the symmetry properties of the evolution dynamics (Ising model has two universality classes namely the model A and model B depending on whether the dynamics is relaxational or conserved).

The model that will be an essential ingredient in my work describes an evolving population on the brink of extinction [2, 3]. The system undergoes a second order phase transition to an inactive state as the relative death rate approaches its critical value. In the inactive state the dynamics ceases and the system cannot evolve back. As this passive state can only be approached but can never be left, this model entails a non-equilibrium phase transition. In the following section we will describe the model and underline some of the works that are already in the literature.

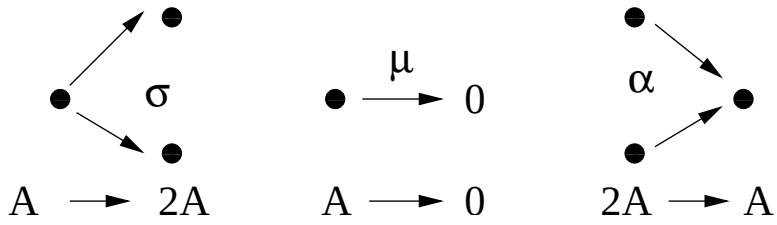

Figure 2.1: The reaction rules for the model under consideration. In our model the rules are, a species undergoes reproduction $A \to 2A$, death $A \to \emptyset$ and competition $2A \to A$ with rates σ, μ and α respectively.

2.2 The Model

The model describes spreading of an infectious disease without immunization. A species of bacteria A is distributed on a hypercubic lattice. At time $t = 0$ the density distribution is given by a Poisson distribution. The organisms perform a random walk with a unit rate λ/a^2 (a is the lattice constant). They interact only when they occupy the same lattice sites. The on-site reaction rules are : a) they can reproduce ($A \to 2A$) with a rate σ, b) they can die out ($A \to 0$, where 0 denotes an inert species) with a rate μ, c) they can have a competition for survival ($2A \to A$) with a rate α. The model does not have any occupation restriction. The dynamics is diagrammatically shown in Fig (2.1). At a given instant of time t any configuration C is given by a string of occupation numbers $\eta = (\eta_1, \eta_2, ...)$. Denoting the probability of a configuration by $P(\{\eta\}, t)$, the time evolution of the probability is given by the master equation

$$\begin{aligned}
\partial_t P(\{\eta_i\}, t) &= Diff + \sigma \sum_i [(\eta_i - 1)P(..., \eta_i - 1, .., t) - \eta_i P(..., \eta_i, .., t)] \\
&+ \alpha \sum_i [(\eta_i + 1)\eta_i P(..., \eta_i + 1, .., t) - \eta_i(\eta_i - 1)P(.., \eta_i .., t)] \\
&+ \mu \sum_i [(\eta_i + 1)P(.., \eta_i + 1.., t) - \eta_i P(.., \eta_i, .., t)]. \qquad (2.1)
\end{aligned}$$

The first bracket represents the reproduction term while the second and the third are the the contributions of the overcrowding effect and the death. The index i stands for the lattice site. The diffusion term is given below

$$\begin{aligned}
Diff &= \frac{\lambda}{a^2} \sum_{<ij>} [(\eta_i + 1)P(.., \eta_i + 1, \eta_j - 1, .., t) - \eta_i P(\{\eta\}, t) \\
&\quad + (\eta_j + 1)P(.., \eta_i - 1, \eta_j + 1.., t) - \eta_j P(\{\eta\}, t)]. \qquad (2.2)
\end{aligned}$$

The sum is over the nearest neighbor sites. The first term is the contribution from the particles from site i to j. The second term corresponds to a hop from j to i.
This master equation cannot be solved exactly. In the absence of any exact solution we are left with no choice but to resort to approximation methods. One of the most extensively used approximation schemes is called the mean field approach. In the mean field method one assumes homogeneous mixing of the reactants so that the rate of reaction

is proportional to the product of the concentrations of the reactants. This is a valid approximation as long as the effects of diffusive mixing of the reactants are way stronger than the correlations induced by the reactions.

2.3 Mean Field Approximation

The mean field equation for the reaction diffusion model under consideration can be constructed in a straightforward way just by looking at the gain and loss terms. The rate equation is

$$\partial_t a(t) = (\sigma - \mu)a(t) - \alpha a^2(t), \tag{2.3}$$

where $a(t)$ represents the mean particle density at time t. With the initial density a_0, Eqn (2.3) is solved by

$$a(t) = \frac{(\sigma - \mu)a_0 e^{(\sigma-\mu)t}}{\sigma - \mu - \alpha a_0 + \alpha a_0 e^{(\sigma-\mu)t}}. \tag{2.4}$$

The above equation has two fixed points for $(\sigma-\mu) > 0$: an unstable fixed point for $a = 0$, and a stable fixed point for $a = (\sigma - \mu)/\alpha$ where there are finite number of particles in the asymptotic limit. In the limit of a vanishing relative reproduction $(\sigma - \mu) \to 0$, the time variation of the density is given by

$$\lim_{(\sigma-\mu)\to 0} a(t) = \frac{1}{1 + \alpha a_0 t}, \tag{2.5}$$

i.e. the particle density decays as $a(t) \sim t^{-1}$. For $(\sigma - \mu) < 0$, the fixed point for $a = 0$ becomes stable and the population eventually dies out. Though the mean field theory is exact for infinite dimensions, it gives wrong predictions for dimensions below an upper critical dimension for the problem at hand. In the case of the diffusion limited pair annihilation process $A + A \to 0$, for example, the mean field predicts a decay of the particle density as $a(t) \sim t^{-1}$. In one dimension it was found to decay as $t^{-1/2}$. This is due to the correlation effect produced by the reactions to diffusion.

2.4 Mean Field Scaling Exponents

Continuous phase transition entails absence of any length scale due to the divergence of the correlation length at the critical point. In the 2-d Ising model, for example, the correlation length diverges as $\xi \sim |T - T_c|^{-\nu}$. In the order-disorder transition, the magnetization in the ordered phase vanishes as $m \sim |T - T_c|^{\beta}$. The concept of scaling function and critical exponent is not confined to equilibrium phase transitions only. They can be directly carried over to the case of dynamic phase transition. In our model, the order parameter is the coarse grained density of particles $\rho(x, t)$. The steady state density in the active phase vanishes as $\rho^{\text{steady}} \sim (\sigma - \sigma_c)^{\beta}$ when $(\sigma - \sigma_c) \to 0$, marking a dynamic continuous active-inactive phase transition. The difference between the non-equilibrium phenomena like the population model above and the equilibrium models like the two dimensional Ising model is that, the former is characterized by two correlation lengths as

opposed to just one. They are the spatial correlation length $\xi_{\rm sp}$ and the temporal correlation length $\xi_{\rm time}$. Close to the critical point these correlation lengths diverge as a function of $(\sigma - \sigma_c)$,

$$\xi_{\rm sp} \sim (\sigma - \sigma_c)^{-\nu_{\rm sp}}, \qquad \xi_{\rm time} \sim (\sigma - \sigma_{\rm c})^{-\nu_{\rm time}}, \tag{2.6}$$

with $\nu_{\rm sp} \neq \nu_{\rm time}$. In the scaling regime, the two lengths are related by $\xi_{\rm time} \sim \xi_{\rm sp}^z$, where $z = \nu_{\rm time}/\nu_{\rm sp}$ is the dynamic exponent. The exponent β and $\nu_{\rm time}$ in the mean field approximation for the DP process are, $\beta = 1$ and $\nu_{\rm time} = 1$. The dynamic exponent for the mean field model is $z = 2$. As mentioned above, diffusive mixing is not strong enough, especially in low dimensional systems. Fluctuations were found to play a decisive role in low dimensional systems leading to qualitative change in the physics. In order to investigate the role of fluctuations, more sophisticated techniques like field theory [8, 11, 12, 13] and renormalization group (RG) methods are called for.

2.5 Mapping to Field Theory

This section illustrates the mapping of the model to the field theory, starting from the very basic master equation. This mapping is exact and assumes nothing beyond the existence of a naive continuum limit. The method described here is due to Doi and Peliti [14, 15]. For a more elaborate discussion please see [12, 13]. The approach is adopted from [13].

We start off with the same master equation Eqn (2.1), (2.2). As the on-site particle numbers change only by integers, the algebraic structure of the second quantized ladder operator can be used to serve our end. The action of the ladder operator changes the particle number at a given lattice by unity. As we are working in a bosonic framework (no occupation restriction) we can introduce the bosonic creation and annihilation operators following the usual bosonic commutation relations, $[a_i, a_j] = 0 = [a_i^\dagger, a_j^\dagger]$ and $[a_i, a_j^\dagger] = \delta_{ij}$. Empty lattice sites are characterized by the vacuum state $|0\rangle$. The annihilation operator kills the state whereas the creation operator puts a particle in it. So $a_i|0\rangle = 0$ and $a_i^\dagger|0\rangle = |1\rangle$. A site i with η_i particles in it, is defined by the state vector $|\eta_i\rangle = (a_i^\dagger)^{\eta_i}|0\rangle$. Operation of the creation and annihilation operator on a general state vector is summarized as follows

$$a_i|\eta_i\rangle = \eta_i|\eta_i - 1\rangle \tag{2.7}$$
$$a_i^\dagger|\eta_i\rangle = |\eta_i + 1\rangle. \tag{2.8}$$

The vector describing the state of the whole stochastic system is given by

$$|\phi(t)\rangle = \sum_{\{\eta\}} P(\{\eta\}, t) \prod_i (a_i^\dagger)^{\eta_i}|0\rangle. \tag{2.9}$$

As a result the master equation can be cast into an imaginary time Schrödinger equation

$$\partial_t|\phi(t)\rangle = -\hat{H}|\phi(t)\rangle, \tag{2.10}$$

where the non-Hermitian quasi-Hamiltonian is given by

$$\begin{aligned}\hat{H} &= \frac{\lambda}{h^2}\sum_{<ij>}(a_i^\dagger - a_j^\dagger)(a_i - a_j) \\ &- \sigma\sum_i[(a_i^\dagger)^2 a_i - a_i^\dagger a_i] - \mu\sum_i[a_i - a_i^\dagger a_i] \\ &- \alpha\sum_i[a_i^\dagger a_i^2 - (a_i^\dagger)^2 a_i^2]. \end{aligned} \tag{2.11}$$

Our goal is to find the ensemble average $\bar{O}$ of an observable at time t. To this end we define a projection operator $\langle P|$ such that $\langle P|a_i^\dagger = \langle P|$ and $\langle P|0\rangle = 1$, leading to

$$\langle P| = \langle 0|e^{\sum_i a_i}. \tag{2.12}$$

Thus the average of an observable O is given by,

$$\bar{O} = \sum_{\{\eta\}} P(\{\eta\},t)O(\{\eta\}) = \sum_{\{\eta\}} P(\{\eta\},t)\langle P|\hat{O}\prod_i (a_i^\dagger)^{\eta_i}|0\rangle = \langle P|\hat{O}|\phi(t)\rangle, \tag{2.13}$$

where the operator $\hat{O}$ has been obtained by substituting $\eta_i \to a_i^\dagger a_i$ in $O(\{n\})$. The condition $\langle P|\hat{H} = 0$ ensures probability conservation. In order to obtain the field theory from the second quantization we follow the same scheme as in many body quantum mechanics. Discussions pertaining to reaction diffusion models are given by Peliti [15].

The temporal evolution of the state vector is sliced into N time slices $\Delta t = t/N$,

$$|\phi(t)\rangle = e^{-\hat{H}t}|\phi(0)\rangle = \lim_{\Delta t\to 0} e^{(-\hat{H}\Delta t)^N}|\phi(0)\rangle. \tag{2.14}$$

Now inserting the completeness relationship of the coherent states between each time step, we obtain

$$\bar{O}(t) = \lim_{\Delta t\to 0}\int(\prod_{i,k} d^2\phi_{i,k})\langle 1|\hat{O}|\{\phi\}_t\rangle\left[\prod_{k=\Delta t}^{t}\langle\{\phi\}_k|e^{-\hat{H}\Delta t}|\{\phi\}_{k-\Delta t}\rangle\right]\langle\{\phi\}_0|\phi(0)\rangle, \tag{2.15}$$

where ϕ is the complex eigenvalue of the annihilation operator $a|\phi\rangle = \phi|\phi\rangle$, and $\{\phi\} = (\phi_1, \phi_2, \phi_3...)$ denotes a set of coherent state eigenvalues, one for each annihilation operator. The index k is the index of time that increases in steps of Δt.

Evaluating this expression, we obtain the field theory action for the above mentioned reaction-diffusion model

$$J[\phi,\phi^*] = \sum_i\left(-\phi_i(t_f) + \int_0^{t_f} dt\,[\phi_i^*\partial_t\phi_i + H(\{\phi_i^*\},\{\phi_i\})] - \bar{\eta}_0\phi_i^*(0)\right), \tag{2.16}$$

where $\bar{\eta}_0$ is the average initial density. Now taking the continuum limit, i.e. $\phi_i(t) \to$

$\psi(x,t), \phi_i^* \to \hat{\psi}(x,t)$, we have

$$\begin{aligned} J[\hat{\psi},\psi] &= \int d^dx \int dt \left[\hat{\psi}\left(\partial_t - \lambda\bigtriangledown^2)\psi + H_\tau(\{\hat{\psi}\},\{\psi\}\right)\right] \\ &= \int d^dx \int dt \left[\hat{\psi}(\partial_t - \lambda\bigtriangledown^2)\psi - \mu(1-\hat{\psi})\psi + \sigma(1-\hat{\psi})\hat{\psi}\psi\right. \\ &- \left.\alpha(1-\hat{\psi})\hat{\psi}\psi^2\right]. \end{aligned} \tag{2.17}$$

The classical equations of motion can be obtained from $\delta J/\delta\psi = 0 = \delta J/\delta\hat{\psi}$. This implies the classical solution of $\hat{\psi} = 1$. Shifting $\hat{\psi}$ about the classical value and rescaling ψ accordingly as $\hat{\psi}(x,t) = 1 + \sqrt{\frac{\sigma}{\alpha}}\tilde{s}(x,t)$ and $\psi(x,t) = \sqrt{\frac{\alpha}{\sigma}}s(x,t)$ we obtain,

$$J[\tilde{s},s] = \int d^dx \int dt \left(\tilde{s}[\partial_t + \lambda(\tau - \bigtriangledown^2)]s - \frac{\lambda g}{2}(\tilde{s}-s)\tilde{s}s + \alpha\tilde{s}^2s^2\right), \tag{2.18}$$

where $(\lambda g)/2 = \sqrt{\sigma\alpha}$ and $\tau = (\mu - \sigma)/\lambda$. If we had followed the standard derivation from a Langevin equation, the correlations of the Langevin noise would have to be given by

$$\langle\zeta(x,t)\zeta(x^{'},t^{'})\rangle = \lambda g s(x,t)\delta^d(x-x^{'})\delta(t-t^{'}). \tag{2.19}$$

The noise correlation function is proportional to the density field $s(x,t)$ to ensure that the dynamics ceases once the absorbing state has been reached. We measure length in inverse of wave number and time in units that make the diffusion constant λ dimensionless. In units of an arbitrary momentum scale μ, we have $[x] = \mu^{-1}$, $[\lambda] = \mu^0$, $[t] = \mu^{-2}$, $[\omega] = \mu^2$ and $[J] = \mu^0$. Hence the fields scale as $[s] = [\tilde{s}] = \mu^{d/2}$, which in turn implies $[g/2] = \mu^{2-d/2}$ and $[\alpha] = \mu^{2-d}$.

The three point coupling constant g/2 is marginal at four dimensions which is in fact the upper critical dimension, d_c, for this theory. The coupling constant α however is marginal at two dimensions, rendering it irrelevant for our theory in the renormalization group sense. Hence, that term will be omitted from now on. The ensuing theory is also called the *Reggeon Field Theory*. The action $J[s,\tilde{s}]$ is invariant under the transformation $s(x,t) \leftrightarrow -\tilde{s}(x,-t)$, also known as the *rapidity reversal* symmetry. As a consequence of this symmetry the fields $\tilde{s}$ and s, have the same scaling properties. But from this point we will use different notations $g/2$ and $\bar{g}/2$ for $\tilde{s}s^2$ and $\tilde{s}^2s$ coupling strengths respectively. This will allow us to break the *rapidity reversal* symmetry. Employing standard $\epsilon = d_c - d$ expansion to one-loop order we can find out the critical exponents for the theory described by the dynamic functional (2.18). They are

$$\begin{aligned} \beta &= 1 - \epsilon/6 + O(\epsilon^2) \\ \nu_{\text{space}} &= 1/2 + \epsilon/16 + O(\epsilon^2) \\ \nu_{\text{time}} &= 1 + \epsilon/12 + O(\epsilon^2). \end{aligned} \tag{2.20}$$

The above model has been studied extensively by Cardy, Sugar, Janssen and others [16, 17]. For a detailed review on the inactive state transition see Hinrichsen [19]. For two loop approximation and further references see Janssen and Täuber [20].
The inactive/absorbing state transition described by the model above belongs to a much

broader class of absorbing state transitions known as the *directed percolation* (DP) [21] transition. Directed percolation is basically a spreading process like the spreading of forest fire or infectious disease. The spreading process can either survive or can die down. A majority of competing processes with an absorbing state transition belong to the DP universality class defined by the exponents in Eqn (2.20). The static $d+1$ dimensional DP can also be viewed as a dynamic reaction diffusion process [22] in d space dimensions and 1 time dimension, the direction of anisotropy being replaced by the direction in time. The DP universality class is extremely robust. Many different models for contact processes, epidemics without immunization, and forest fires belong to the DP universality class. Any spreading process described by a positive scalar order parameter with a short range interaction, in absence of any extra symmetry like quenched randomness, belongs to the DP universality class [17, 18]. For a detailed review and further references see [19].

The discussion of this model so far relied crucially on the one assumption that the system sits on a uniform environment/background. The effect of a non-dynamic environment has been encoded in the constant values of the parameters σ, μ, α. A natural extension of this well studied problem can be achieved if we include fluctuations in the background. The result will heavily depend on the choice of the background dynamics. We will study the effect of an environment described by model A [7] dynamics on the stability of the DP transition. Before we present our result we introduce model A dynamics.

2.6 The Environment Dynamics

Model A dynamics (spin flip) is a relaxation dynamics. The coarse-grained Hamiltonian for model A dynamics is given by the Ginzburg-Landau-Wilson Hamiltonian [23, 24, 25, 26]

$$H[\phi] = \int d^d x \left[\frac{r}{2}\phi^2(x,t) + \frac{1}{2}[\bigtriangledown\phi(x,t)]^2 + \frac{u}{4!}\phi^4(x,t) \right], \tag{2.21}$$

where $\phi(x,t)$ is the local coarse-grained order parameter and u, the four-point coupling strength, provides the restoring force. The quantity r is a control parameter which controls the distance from the mean field critical point. The minimum energy configuration corresponds to a spatially flat order parameter. The second term then corresponds to the cost in energy for having a spatially non-uniform order parameter. The dynamics for model A is given by the non-linear Langevin equation [27]

$$\partial_t \phi(x,t) = -\gamma \frac{\delta H}{\delta \phi(x,t)} + \zeta(x,t), \tag{2.22}$$

where ζ is the stochastic force. In order to assure that the system relaxes back to equilibrium we impose the following conditions

$$\langle \zeta(x,t) \rangle = 0, \qquad < \zeta(x^{'},t^{'})\zeta(x,t) >= 2\gamma k_B T \delta^d(x-x^{'})\delta(t-t^{'}). \tag{2.23}$$

2.7 Dynamical Functional for Model A

We start with the non-linear Langevin equation of the form

$$\partial_t \phi(x,t) = F[\phi] + \zeta, \tag{2.24}$$

where F is the relaxation force. All the effects of the fast degrees of freedom have been encapsulated inside the noise term $\zeta(x,t)$. In order to compute the ensemble average of an observable O, we take the following course.
The noise correlation can be obtained from the distribution

$$W[\zeta] \propto \exp\left(-\frac{1}{4}\int d^d x \int dt \zeta(x,t)(\gamma k_B T)^{-1}\zeta(x,t)\right). \tag{2.25}$$

We intend to find $\int D[\zeta]O[\phi[\zeta]]W[\zeta]$. The Jacobian of transformation from $\{\zeta\} \to \{\phi\}$ has been dropped as it is unity for the forward discretization of the Langevin equation. The field ϕ obeys the Langevin equation at all points in space and time and that has been imposed by inserting an unity for each point in space and time

$$\begin{aligned} 1 &= \int D[\phi] \prod_{x,t} \delta\left(\partial_t \phi(x,t) + \gamma \frac{\delta H}{\delta \phi(x,t)} - \zeta(x,t)\right) \\ 1 &= \int D[\phi] \int D[i\tilde{\phi}] \exp\left[-\int d^d x \int dt \tilde{\phi}\left[\partial_t \phi(x,t) + \gamma \frac{\delta H}{\delta \phi(x,t)} - \zeta(x,t)\right]\right], \end{aligned} \tag{2.26}$$

where $\tilde{\phi}$ is called the *Martin-Siggia-Rose* response field [28].

So inserting this unity inside the functional integral for the average we have,

$$\begin{aligned} \langle O \rangle &= \int D[i\tilde{\phi}] \int D[\phi] \exp\left[-\int d^d x \int dt \tilde{\phi}\left(\partial_t \phi + \gamma \frac{\delta H}{\delta \phi(x,t)}\right)\right] \\ &\times O[\phi[\zeta]] \int D[\zeta] \exp\left(-\int d^d x \int dt \left[\frac{1}{4}\int d^d x \int dt \zeta(x,t)(\gamma k_B T)^{-1}\zeta(x,t)\right]\right) \\ &\times \int D[\zeta] \exp\left[\int d^d x \int dt \tilde{\phi}(x,t)\zeta(x,t)\right]. \end{aligned} \tag{2.27}$$

The action for *model A* is extracted after performing the noise integral, which leads to

$$J[\tilde{\phi},\phi] = \int d^d x \int dt \left(\tilde{\phi}\left[\partial_t \phi + \gamma \frac{\delta H}{\delta \phi(x,t)}\right] - \tilde{\phi}(\gamma k_B T)\tilde{\phi}\right). \tag{2.28}$$

From now on we are going to take $k_B T = 1$. The functional obtained above goes by the name of *Janssen- De Dominicis response functional* [29, 30]. The free part of the action is

$$J_0[\tilde{\phi},\phi] = \int d^d x \int dt \left(\tilde{\phi}[\partial_t \phi - \gamma(\tau - \bigtriangledown^2)]\phi - \gamma\tilde{\phi}^2\right), \tag{2.29}$$

the anharmonic part is given by,

$$J_{\text{int}}[\tilde{\phi},\phi] = \gamma\frac{u}{6}\int d^d x \int dt \tilde{\phi}\phi^3. \tag{2.30}$$

We again go through the naive dimensional analysis to find out the marginal couplings in units of an arbitrary length scale μ: $[x] = \mu^{-1}$, $[q] = \mu$, $[D] = \mu^0$, $[t] = \mu^{-2}$, $[\omega] = \mu^2$, $[A] = \mu^0$. Hence the fields scale as $[\tilde{\phi}(x,t)] = \mu^{1+\frac{d}{2}}$ and $[\phi(x,t)] = \mu^{-1+\frac{d}{2}}$. The couplings scale as $[\tau] = \mu^2$, $[u] = \mu^{4-d}$. So we see that once again $d_c = 4$. At four dimensions the anharmonic coupling is marginal. For more details see [31].

2.8 Critical Exponents

The model A is a dynamic model for order-disorder phase transition. The correlation length close to a critical point, is given by $\xi(r)_{\text{space}} \sim |r|^{-\nu}$, where r is the distance from the critical point and ν is the correlation length critical exponent. As in any continuous phase transition, the order-disorder transition is marked by the divergence of the correlation length ξ. The critical two-point correlation in space is given by $C(x) \sim |x|^{-(d-2+\eta)}$, where η is the Fisher exponent. The exponent β, defined as $m \sim |r|^{\beta}$, where m is the average magnetization, is related to ν and η by the scaling law. As the correlation length diverges, it affects the relaxation of the ordered domains. As T_c is approached, the typical characteristic time scale ξ_{time} for relaxation of the order parameter increases as well. This is known as the critical slowing down and is given by $\xi_{\text{time}} \sim \xi^z_{\text{space}} \sim |r|^{-z\nu}$, where z is the dynamic exponent. The critical exponents for the model A can be extracted from its dynamic functional following standard RG techniques. To two-loop in $\epsilon = 4-d$ expansion, the exponents are

$$\eta = \epsilon^2/54 + O(\epsilon^3) \tag{2.31}$$

$$\frac{1}{\nu_{\text{space}}} = 2 - \epsilon/3 + O(\epsilon^2) \tag{2.32}$$

$$z = 2 + [6\ln(4/3) - 1 + O(\epsilon)]\eta. \tag{2.33}$$

The fixed point characterized by the critical exponent above also goes by the name of Wilson-Fisher fixed point [32].

2.9 Previous Works with Fluctuating Backgrounds

Quenched Disorder: The reaction diffusion model assumes that the rates of reaction are invariant in space and time. In reality however the rates of reproduction or death are intimately intertwined with the availability of food, health care, and many other different factors. In order to achieve a more realistic model, it is important to investigate the role of quenched randomness on the critical properties of DP. For a spatially quenched disorder, the disorder field $\psi(x)$ is defined as

$$\overline{\psi(x')\psi(x)} = f\delta^d(x' - x), \tag{2.34}$$

where the bar represents the average over independent realizations of the disorder field. Janssen showed [33] that this amounts to adding a marginal term $-\lambda^2 f \int d^dx \left[\int dt\tilde{s}s\right]^2$,

in the dynamic functional. This model has only runaway solutions in the physical domain [33]. His findings reconfirmed the numerical results of Moreira and Dickman [34]. Thus quenched randomness severely disturbs the DP fixed point.

DP coupled to a Conserved Diffusive Field: The DP fixed point goes to a new stable fixed point when it is coupled to a conserved diffusive field. Using field theoretic analysis, Kree et al. [35] showed that the dynamic exponent z is 2 to one-loop order. They also showed that the exponent $\beta_{new} > \beta_{DP}$. This basically amounts to saying that the temporal fluctuations of the DP field is governed primarily by diffusion and the mean density of active sites goes to zero with a larger exponent than the DP counterpart. The work of van Wijland et al. [36] was along similar tracks. They considered a multi-species model, comprised of particles A and B, having reactions of type $A + B \to 2B$ and $B \to A$. The particles can diffuse with diffusion constants D_A and D_B. They showed that the critical behavior for $D_A < D_B$ is governed by a new fixed point and a new scaling law. For the case of $D_A = D_B$ the critical behavior is given by Kree et al. [35]. The system does not have any stable solution for $D_A > D_B$.

Our efforts are similar in spirit to the works mentioned above. In spite of the works that have been done, DP coupled to model A has escaped careful scrutiny. In chapter 3 we will report on the consequences of this coupling. We will couple the two theories and then look for novel marginal couplings at the upper critical dimension of the two theories that might destabilize the well known directed percolation and the Wilson-Fisher fixed points.

Chapter 3

Universal Properties of Population Dynamics With Fluctuating Resource

In this chapter we will present our work. The results have been published in [37]. We will refer to DP as the population dynamics (PD) model and model A will be our nutrient dynamics. The words like nutrient, environment, or resource will all be used interchangeably to describe the fluctuating field coupled to DP. The reason for our choice of model A is primarily the fact that both the population dynamics model and model A have upper critical dimensions of 4. This facilitates the coupling of the two field theories. If we had miss matched upper critical dimensions, then marginal couplings of one theory could have been an either irrelevant or relevant couplings of the other.

So far the discussions about the population dynamics calculations, except for some notable cases mentioned in chapter 2, crucially relied on the assumption that the environment it sits in has no structure of its own. The effect of the uniform environment has been captured in the constant reproduction, death, and over-crowding rates. It is however instructive to impose a dynamics on the environment thus making the rates depend on the nutrient density. Basically it amounts to saying, an individual will get more(less) food depending on its position in the lattice and its age. In doing so, the environment dynamics will be affected too.

In more technical terms we will seek novel marginal couplings, involving both the population dynamics and model A fields that might de-stabilize the well known transition from active to absorbing state. It is natural to assume that the critical control parameters will be modified and we can write down an expansion of r and τ about their mean field values, much in the same spirit as a Landau expansion

$$r = r_0 + vs + ..., \tag{3.1}$$

$$\tau = \tau_0 + \kappa\phi + w\phi^2/2! \quad . \tag{3.2}$$

In the above expansion we have respected the absorbing state condition, hence the term linear in $\tilde{s}$ has been omitted. Dimensional analysis shows that $[\kappa] \sim \mu^{\frac{6-d}{2}}$, $[v] \sim \mu^{\frac{4-d}{2}}$,

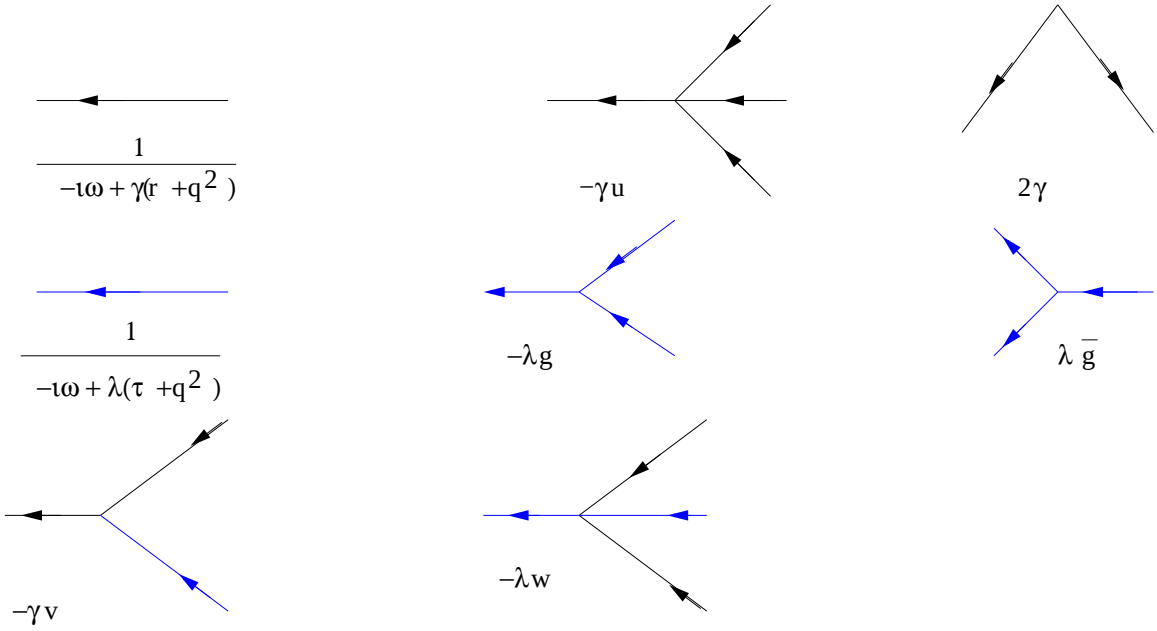

Figure 3.1: The elements of perturbation theory. The black lines are model A propagators. The blue lines are the population dynamics propagators.

and $[w] \sim \mu^{4-d}$. The coupling κ is relevant in $d = 4$ and must be tuned to zero to access the critical point. However, if we demand the existence of an up-down Ising symmetry, we can set κ to zero. The higher order terms are ignored as they are irrelevant in the renormalization group sense. Collecting all the terms, our model is given by,

$$J\{\tilde{\phi}, \phi, \tilde{s}, s\} = J_A\{\tilde{\phi}, \phi\} + J_{PD}\{\tilde{s}, s\} + J_{int}\{\tilde{\phi}, \phi, \tilde{s}, s\}$$

where

$$J_{\text{int}}(\tilde{\phi}, \phi, \tilde{s}, s) = \int \left[\gamma v \tilde{\phi}\phi s + \frac{1}{2}\lambda w \tilde{s} s \phi^2\right]. \tag{3.3}$$

In the path integral formulation, correlation functions and response functions can be determined by calculating the path integrals with the weight $\exp(-J)$, where the dynamic functional J describes the considered stochastic process. The interaction terms will be treated perturbatively.

3.1 Perturbation Theory

Following the standard procedure, the bilinear term in the action above is recognized as the Gaussian, or, the free theory term. The rest of the terms in the exponential $e^{-(J_{\text{free}}+J_{\text{nonlinear}})}$ are expanded in a power series and averaged with the statistical weight $e^{-J_{\text{free}}}$. The non-linearity induces corrections to the free theory that are represented conveniently by means of Feynman diagrams. The propagator and the vertices of the diagrammatical perturbation expansion are shown in Fig (3.1). Vertices are the nonlinear couplings that connect propagators together. We can use the time and the wave vector

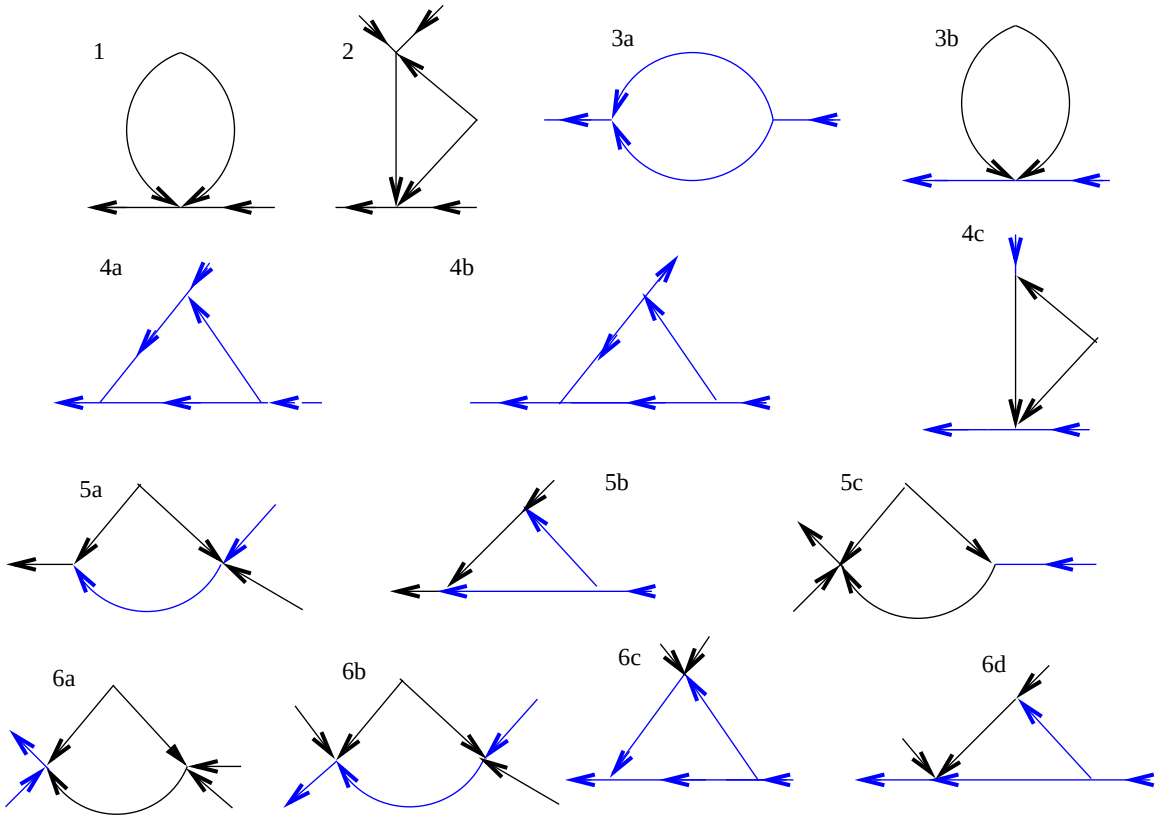

Figure 3.2: Primitively divergent diagrams to one loop order

picture as well, where the propagator and the noise correlator are represented as a function of momentum and time as opposed to momentum and frequency. The propagators in the momentum-time representation read

$$G_{\rm A}(q,t) = \theta(t)\exp\left[-\gamma(r+q^2)t\right], \tag{3.4}$$
$$G_{\rm PD}(q,t) = \theta(t)\exp\left[-\lambda(\tau+q^2)t\right]. \tag{3.5}$$

The Heaviside step function is defined with $\theta(t=0)=0$. This follows from the Itô discretization of the path integral and ensures causality. We will now calculate the one-loop order terms of our theory. The objects of perturbation theory which have to be calculated are the vertex functions, the amputated 1-particle irreducible graphs as a function of frequency and wave vector q. All the graphs will be calculated to one loop order. The vertex functions will be denoted by $\Gamma_{ij,kl}$, where the first pair of legs are the model A legs whereas the next pair are population dynamics legs. The first index in both the pairs represent the tilde field. The primitively divergent one-loop diagrams are shown in Fig (3.2). The self energy term is,

$$\text{Fig}(3.2.1) = -\frac{\gamma u}{2}\int d^dk \frac{1}{r+k^2}. \tag{3.6}$$

The diagram is quadratically divergent. The quadratic divergence however can be absorbed into the shift of the mean field critical distance r. In order to do so, we will use

the fact that the susceptibility diverges at the critical point. It can be shown that,

$$\gamma\chi^{-1} = \lim_{q,\omega\to 0} \Gamma_{11,00}(q,\omega) = 0, \tag{3.7}$$

where $\Gamma_{11,00} = G_0(-q,-\omega)^{-1} - \Sigma(-q,-\omega)$. So at r_c we have,

$$\begin{aligned} 0 &= r_c + \frac{u}{2}\int d^dk \frac{1}{r_c + k^2} + O(u^2), \\ r_c &= -\frac{u}{2}\int d^dk \frac{1}{r_c + k^2}. \end{aligned}$$

To $O(u)$

$$r_c = -\frac{u}{2}\int d^dk \frac{1}{k^2} + O(u^2). \tag{3.8}$$

We define a new variable $\hat{r} = r - r_c$. The two point vertex function after the appropriate r_c shift reads as,

$$\Gamma_{11,00}(q,\omega) = i\omega + \gamma(\hat{r} + q^2) - \frac{\gamma\hat{r}u}{2}\int d^dk \frac{1}{k^2(\hat{r} + k^2)}. \tag{3.9}$$

The integral above can be evaluated using Feynman parametrization,

$$\begin{aligned} \frac{\gamma\hat{r}u}{2}\int d^dk \frac{1}{k^2(\hat{r} + k^2)} &= \frac{1}{2}\gamma\hat{r}u\int_0^1 dx \int d^dk \frac{1}{(k^2 + \hat{r}x)^2} \\ &= \frac{1}{2}\gamma u\hat{r}^{1-\epsilon/2}\frac{S_d\Gamma(1+\frac{\epsilon}{2})\Gamma(\frac{d}{2})}{(2\pi)^d\Gamma(2)(1-\frac{\epsilon}{2})\epsilon}, \end{aligned} \tag{3.10}$$

where S_d is the surface area of the d dimensional unit sphere, given by $S_d = 2\pi^{d/2}/\Gamma(d/2)$. Here we have employed the standard ϵ expansion along with the minimal subtraction. We kept the contribution which diverges, as ϵ goes to zero. For the extraction of the divergence in the diagram we set the external momentum and frequency to zero.

$$\begin{aligned} \text{Fig(3.2.2)} &= \frac{3\gamma u^2}{2}\int d^dk \frac{1}{(\hat{r} + k^2)^2} + O(u^3) \\ &= \frac{3\gamma u^2}{2}\frac{S_d}{(2\pi)^d}\frac{\Gamma(1+\frac{\epsilon}{2})\Gamma(\frac{d}{2})}{\Gamma(2)\epsilon}\hat{r}^{-\epsilon/2}. \end{aligned} \tag{3.11}$$

The self energy correction for population dynamics after absorbing the quadratic divergence in the shift of τ, we have,

$$\begin{aligned} \Gamma_{00,11}(q,\omega) = i\omega + \lambda(\hat{\tau} + q^2) - \Bigg(&\frac{1}{8}\lambda g\bar{g}\left[\frac{i\omega}{\lambda} + 2\hat{\tau} + \frac{q^2}{2}\right]\int d^dk \frac{1}{k^2(k^2 + \hat{\tau})} \\ &+ \frac{1}{2}\lambda w\hat{r}\int d^dk \frac{1}{k^2(k^2 + \hat{r})}\Bigg). \end{aligned} \tag{3.12}$$

$\hat{\tau} = \tau - \tau_c$. The divergent contribution to the $\Gamma_{00,12}$ and the $\Gamma_{00,21}$ are

$$\text{Fig(3.2.4a)} = \frac{1}{2}\lambda g^2 \bar{g} \frac{S_d}{(2\pi)^d} \frac{\Gamma(1+\frac{\epsilon}{2})\Gamma(\frac{d}{2})}{\Gamma(2)\epsilon} \hat{\tau}^{-\frac{\epsilon}{2}}, \tag{3.13}$$

$$\text{Fig(3.2.4b)} = -\frac{1}{2}\lambda g \bar{g}^2 \frac{S_d}{(2\pi)^d} \frac{\Gamma(1+\frac{\epsilon}{2})\Gamma(\frac{d}{2})}{\Gamma(2)\epsilon} \hat{\tau}^{-\frac{\epsilon}{2}}, \tag{3.14}$$

$$\text{Fig(3.2.4c)} = \lambda w v \frac{S_d}{(2\pi)^d} \frac{\Gamma(1+\frac{\epsilon}{2})\Gamma(\frac{d}{2})}{\Gamma(2)\epsilon} \hat{r}^{-\frac{\epsilon}{2}}. \tag{3.15}$$

The divergent contribution to the $\Gamma_{11,01}$ are

$$\text{Fig(3.2.5a)} = \frac{(\lambda w)(\gamma v)}{\gamma + \lambda} \frac{S_d}{(2\pi)^d} \frac{\Gamma(1+\frac{\epsilon}{2})\Gamma(\frac{d}{2})}{\Gamma(2)\epsilon} \mu^{-\epsilon}, \tag{3.16}$$

$$\text{Fig(3.2.5b)} = \frac{(\gamma v)^2(\lambda \bar{g})}{\lambda(\lambda + \gamma)} \frac{S_d}{(2\pi)^d} \frac{\Gamma(1+\frac{\epsilon}{2})\Gamma(\frac{d}{2})}{\Gamma(2)} \frac{1}{2\epsilon} \mu^{-\epsilon}, \tag{3.17}$$

$$\text{Fig(3.2.5c)} = \frac{1}{2\epsilon}\gamma u v \frac{S_d}{(2\pi)^d} \frac{\Gamma(1+\frac{\epsilon}{2})\Gamma(\frac{d}{2})}{\Gamma(2)} \hat{r}^{-\epsilon/2}. \tag{3.18}$$

The contributions to the $\Gamma_{02,11}$ are,

$$\text{Fig(3.2.6a)} = \frac{\lambda w u}{2\epsilon} \frac{S_d}{(2\pi)^d} \frac{\Gamma(1+\frac{\epsilon}{2})\Gamma(\frac{d}{2})}{\Gamma(2)} \hat{r}^{-\frac{\epsilon}{2}}, \tag{3.19}$$

$$\text{Fig(3.2.6b)} = \frac{2(\lambda w)^2}{\lambda + \gamma} \frac{S_d}{(2\pi)^d} \frac{\Gamma(1+\frac{\epsilon}{2})\Gamma(\frac{d}{2})}{\Gamma(2)\epsilon} \mu^{-\epsilon}, \tag{3.20}$$

$$\text{Fig(3.2.6c)} = \frac{\lambda g \bar{g} w}{4\epsilon} \frac{S_d}{(2\pi)^d} \frac{\Gamma(1+\frac{\epsilon}{2})\Gamma(\frac{d}{2})}{\Gamma(2)} \hat{\tau}^{-\frac{\epsilon}{2}}, \tag{3.21}$$

$$\text{Fig(3.2.6d)} = \frac{(\lambda w)(\gamma v)(\lambda \bar{g})}{\lambda(\lambda + \gamma)} \frac{S_d}{(2\pi)^d} \frac{\Gamma(1+\frac{\epsilon}{2})\Gamma(\frac{d}{2})}{\Gamma(2)\epsilon} \mu^{-\epsilon}. \tag{3.22}$$

We are now in a position to write down the full vertex functions. The model A two-point function after an appropriate r_c shift, is given by,

$$\Gamma_{11,00} = i\omega + \gamma(\hat{r} + q^2) - \frac{1}{2}\gamma G_\epsilon u \hat{r}^{1-\epsilon/2} \frac{1}{\epsilon}, \tag{3.23}$$

where the geometric constant G_ϵ is defined as,

$$G_\epsilon = \frac{S_d \Gamma(1+\frac{\epsilon}{2})\Gamma(\frac{d}{2})}{(2\pi)^d \Gamma(2)}. \tag{3.24}$$

Similarly the model A four-point function to one loop order is given by,

$$\Gamma_{13,00} = -\gamma u + \frac{3}{2}\gamma u^2 G_\epsilon \hat{r}^{-\epsilon/2} \frac{1}{\epsilon}. \tag{3.25}$$

The two-point function for DP after appropriate subtraction, including the new diagram from w, reads as,

$$\Gamma_{00,11} = i\omega + \lambda(\hat{\tau} + q^2) - \frac{1}{8}\lambda g \bar{g} \left[\frac{i\omega}{\lambda} + 2\hat{\tau} + \frac{q^2}{2}\right] \hat{\tau}^{-\epsilon/2} G_\epsilon \frac{1}{\epsilon} - \frac{1}{2}\lambda w \hat{r}^{1-\frac{\epsilon}{2}} G_\epsilon \frac{1}{\epsilon}. \tag{3.26}$$

Similarly the two three-point functions are given by,

$$\Gamma_{00,12} = -\lambda g + \frac{1}{2}\lambda g^2 \bar{g} G_\epsilon \hat{\tau}^{-\epsilon/2} \frac{1}{\epsilon} + \lambda w v \hat{r}^{-\frac{\epsilon}{2}} G_\epsilon \frac{1}{\epsilon}, \tag{3.27}$$

$$\Gamma_{00,21} = \lambda \bar{g} - \frac{1}{2}\lambda g \bar{g}^2 G_\epsilon \hat{\tau}^{-\epsilon/2} \frac{1}{\epsilon}. \tag{3.28}$$

The correction to the new couplings are shown below.

$$\Gamma_{11,01} = -\gamma v + \frac{(\lambda w)(\gamma v)}{\lambda+\gamma} G_\epsilon \frac{1}{\epsilon} \mu^{-\epsilon} + \frac{(\gamma v)^2 (\lambda \bar{g})}{2\lambda(\lambda+\gamma)} G_\epsilon \frac{1}{\epsilon} \mu^{-\epsilon} + \frac{1}{2}\gamma u v G_\epsilon \frac{1}{\epsilon} \hat{r}^{-\epsilon/2}, \tag{3.29}$$

$$\begin{aligned} \Gamma_{02,11} &= -\lambda w + \frac{\lambda w u}{2} G_\epsilon \frac{1}{\epsilon} \hat{r}^{-\epsilon/2} + \frac{2(\lambda^2 w^2)}{\lambda+\gamma} G_\epsilon \frac{1}{\epsilon} \mu^{-\epsilon} + \frac{\lambda g \bar{g} w}{4} G_\epsilon \frac{1}{\epsilon} \hat{\tau}^{-\epsilon/2} \\ &+ \frac{(\lambda w)(\gamma v)(\lambda \bar{g})}{\lambda(\lambda+\gamma)} G_\epsilon \frac{1}{\epsilon} \mu^{-\epsilon}. \end{aligned} \tag{3.30}$$

Now, we will write down our renormalization scheme. We change the notation: the bare quantities stay the same while the renormalized quantities are written with a subscript R. Beginning with the known model A renormalization, we have,

$$\begin{aligned} \phi &= Z_\phi^{1/2} \phi_R, \qquad \tilde{\phi} = Z_{\tilde{\phi}}^{1/2} \tilde{\phi}_R, \qquad \gamma = Z_\phi^{1/2} Z_{\tilde{\phi}}^{-1/2} Z_\gamma \gamma_R, \\ \hat{r} &= Z_\phi^{-1} Z_r \hat{r}_R, \qquad G_\epsilon u = Z_\phi^{-2} Z_\gamma^{-1} Z_u u_R \mu^\epsilon. \end{aligned} \tag{3.31}$$

For the population dynamics field we have,

$$\begin{aligned} s &= Z_s^{1/2} s_R, \qquad \tilde{s} = Z_{\tilde{s}}^{1/2} \tilde{s}_R, \qquad \lambda = Z_s^{-1/2} Z_{\tilde{s}}^{-1/2} Z_\lambda \lambda_R, \\ \hat{\tau} &= Z_\lambda^{-1} [Z_\tau \hat{\tau}_R + Y_\tau \hat{r}_R], \qquad \sqrt{G_\epsilon} g = Z_s^{-1/2} Z_\lambda^{-1} Z_g g_R \mu^{\epsilon/2}, \\ \sqrt{G_\epsilon} \bar{g} &= Z_{\tilde{s}}^{-1/2} Z_\lambda^{-1} Z_{\bar{g}} \bar{g}_R \mu^{\epsilon/2}. \end{aligned} \tag{3.32}$$

For the new couplings we define the renormalization constants as follows

$$\begin{aligned} \sqrt{G_\epsilon} v &= Z_\phi^{-1} Z_s^{-1/2} Z_\gamma^{-1} Z_v v_R \mu^{\epsilon/2}, \\ G_\epsilon w &= Z_\phi^{-1} Z_\lambda^{-1} Z_w w_R \mu^\epsilon. \end{aligned} \tag{3.33}$$

It is not hard to see that under the coupling outlined above, model A does not pick up any corrections. So the well known model A renormalization stays the same. The multiplicative renormalization constants are [31]

$$Z_\phi, Z_{\tilde{\phi}} = 1 + O(u^2), \tag{3.34}$$

$$Z_{\hat{r}} = 1 + \frac{u_R}{2\epsilon}, \tag{3.35}$$

$$Z_u = 1 + \frac{3u_R}{2\epsilon}. \tag{3.36}$$

Employing similar technique for the population dynamics functions we have

$$\begin{aligned} \Gamma_{00,11} &= \left[Z_{\tilde{s}}^{1/2} Z_s^{1/2} - \frac{g_R \bar{g}_R}{8\epsilon} \right] i\omega + \left[Z_{\tilde{s}}^{1/2} Z_s^{1/2} Z_s^{-1/2} Z_{\tilde{s}}^{-1/2} Z_\lambda \lambda_R - \frac{1}{16\epsilon} \lambda_R g_R \bar{g}_R \right] q^2 \\ &+ Z_{\tilde{s}}^{1/2} Z_s^{1/2} Z_s^{-1/2} Z_{\tilde{s}}^{-1/2} Z_\lambda \lambda_R Z_\lambda^{-1} \left[Z_\tau \hat{\tau}_R + Y_\tau \hat{r}_R \right] - \frac{1}{4\epsilon} \lambda_R g_R \bar{g}_R \hat{\tau}_R \\ &- \frac{1}{2} \lambda_R w_R \hat{r}_R \frac{1}{\epsilon}. \end{aligned} \tag{3.37}$$

$$\Gamma_{00,12} = Z_{\tilde{s}}^{1/2} Z_s \Big[-Z_s^{-1/2} Z_{\tilde{s}}^{-1/2} Z_\lambda \lambda_R Z_s^{-1/2} Z_\lambda^{-1} \left(Z_g g_R + Y_g v_R \right) \mu^{\epsilon/2} G_\epsilon^{-1/2} + \frac{1}{2} \lambda_R g_R^2 \bar{g}_R \mu^{\epsilon/2} G_\epsilon^{-1/2} \frac{1}{\epsilon} + \lambda_R w_R v_R G_\epsilon^{-1/2} \mu^{\epsilon/2} \frac{1}{\epsilon} \Big]. \tag{3.38}$$

$$\Gamma_{00,21} = Z_{\tilde{s}} Z_s^{1/2} \Big[Z_s^{-1/2} Z_{\tilde{s}}^{-1/2} Z_\lambda \lambda_R Z_{\tilde{s}}^{-1/2} Z_\lambda^{-1} Z_{\bar{g}} \bar{g}_R \mu^{\epsilon/2} G_\epsilon^{-1/2} - \frac{1}{2} \lambda_R g_R \bar{g}_R^2 G_\epsilon^{-1/2} \mu^{\epsilon/2} \frac{1}{\epsilon} \Big]. \tag{3.39}$$

We can read off the renormalization factors

$$Z_{\tilde{s}}^{1/2} Z_s^{1/2} = 1 + \frac{g_R \bar{g}_R}{8\epsilon} + O((g_R \bar{g}_R)^2) \tag{3.40}$$

$$Z_\lambda = 1 + \frac{1}{16\epsilon} g_R \bar{g}_R + O((g_R \bar{g}_R)^2) \tag{3.41}$$

$$Z_\tau = 1 + \frac{1}{4\epsilon} g_R \bar{g}_R + O((g_R \bar{g}_R)^2); Y_\tau = \frac{w_R}{2\epsilon} + O(w_R^2) \tag{3.42}$$

$$Z_g = 1 + \frac{1}{2\epsilon} g_R \bar{g}_R + w_R v_R \frac{1}{\epsilon} g_R^{-1} + O((g_R \bar{g}_R)^2) \tag{3.43}$$

$$Z_{\bar{g}} = 1 + \frac{1}{2\epsilon} g_R \bar{g}_R + O((g_R \bar{g}_R)^2). \tag{3.44}$$

For the mixed couplings we have,

$$\Gamma_{11,01} = -\gamma_R Z_v v_R \mu^{\epsilon/2} G_\epsilon^{-1/2} + \frac{(\lambda_R w_R)(\gamma_R v_R)}{\lambda_R + \gamma_R} G_\epsilon^{-1/2} \frac{1}{\epsilon} \mu^{\epsilon/2} + \frac{(\gamma_R v_R)^2 (\lambda_R \bar{g}_R)}{2\lambda_R (\lambda_R + \gamma_R)} G_\epsilon^{-1/2} \frac{1}{\epsilon} \mu^{\epsilon/2} + \frac{1}{2} \gamma_R u_R v_R G_\epsilon^{-1/2} \mu^{\epsilon/2} \frac{1}{\epsilon}. \tag{3.45}$$

$$\Gamma_{02,11} = Z_\phi Z_{\tilde{s}}^{1/2} Z_s^{1/2} \Big[-Z_s^{-1/2} Z_{\tilde{s}}^{-1/2} Z_\lambda \lambda_R Z_\phi^{-1} Z_\lambda^{-1} Z_w w_R \mu^\epsilon G_\epsilon^{-1} + \frac{2(\lambda_R^2 w_R^2) G_\epsilon^{-1} \mu^\epsilon}{(\lambda_R + \gamma_R)\epsilon} + \frac{\lambda_R g_R \bar{g}_R w_R G_\epsilon^{-1} \mu^\epsilon}{4\epsilon} + \frac{(\lambda_R w_R)(\gamma_R v_R)(\lambda_R \bar{g}_R) G_\epsilon^{-1} \mu^\epsilon}{\lambda_R (\lambda_R + \gamma_R)\epsilon} + \frac{\lambda_R w_R u_R}{2} G_\epsilon^{-1} \frac{1}{\epsilon} \mu^\epsilon \Big]. \tag{3.46}$$

So we have,

$$Z_v = 1 + \frac{(\lambda_R w_R)}{\lambda_R + \gamma_R} \frac{1}{\epsilon} + \frac{(\gamma_R v_R)(\bar{g}_R)}{2(\lambda_R + \gamma_R)} \frac{1}{\epsilon} + \frac{u_R}{2\epsilon} + O((v_R \bar{g}_R)^2). \tag{3.47}$$

$$Z_w = 1 + \frac{(2\lambda_R w_R)}{\lambda_R + \gamma_R} \frac{1}{\epsilon} + \frac{g_R \bar{g}_R}{4} \frac{1}{\epsilon} + \frac{(\gamma_R v_R)(\bar{g}_R)}{(\lambda_R + \gamma_R)} \frac{1}{\epsilon} + \frac{u_R}{2} \frac{1}{\epsilon} + O(w_R^2). \tag{3.48}$$

We define dimensionless coupling parameters and the ratio of two time scales as,

$$\hat{g}_R = g_R \bar{g}_R, \qquad \hat{v}_R = v_R \bar{g}_R, \qquad \rho = \frac{\gamma_R}{\lambda_R}. \tag{3.49}$$

Rewriting the Z factors in terms of these new parameters we have,

$$\begin{aligned}
Z_{\tilde{s}}^{1/2} Z_s^{1/2} &= 1 + \frac{\hat{g}_R}{8\epsilon} + O(\hat{g}_R^2), && (3.50)\\
Z_\lambda &= 1 + \frac{1}{16\epsilon}\hat{g}_R + O(\hat{g}_R^2), && (3.51)\\
Z_\tau &= 1 + \frac{1}{4\epsilon}\hat{g}_R + O(\hat{g}_R^2); Y_\tau = \frac{w_R}{2\epsilon} + O(w_R^2), && (3.52)\\
Z_g &= 1 + \frac{1}{2\epsilon}\hat{g}_R + w_R\hat{v}_R\frac{1}{\epsilon}\hat{g}_R^{-1} + O(\hat{g}_R^2), && (3.53)\\
Z_{\bar{g}} &= 1 + \frac{1}{2\epsilon}\hat{g}_R + O(\hat{g}_R^2), && (3.54)\\
Z_v &= 1 + \frac{w_R}{(1+\rho)\epsilon} + \frac{\rho\hat{v}_R}{2(1+\rho)\epsilon} + \frac{u_R}{2\epsilon} + O(\hat{v}^2), && (3.55)\\
Z_w &= 1 + \frac{(2w_R)}{(1+\rho)\epsilon} + \frac{\hat{g}_R}{4\epsilon} + \frac{\rho\hat{v}_R}{(1+\rho)\epsilon} + \frac{u_R}{2\epsilon} + O(w_R^2). && (3.56)
\end{aligned}$$

The variation of the non-linear coupling constants with the scale transformation μ is given by the beta functions. The beta functions are defined as the logarithmic derivative of the renormalized coupling constants with respect to the momentum scale μ keeping the bare values of the respective parameters fixed. The zeros of the beta functions are the fixed points of interest. Hence

$$\beta_\circ = \mu\partial_\mu \circ |_{bare}, \tag{3.57}$$

where $\circ$ stands for one of the nonlinear couplings, u_R, g_R, $\bar{g}_R$, v_R, w_R. The β functions for our model are

$$\begin{aligned}
\beta_u &= -\epsilon u_R + \frac{3u_R^2}{2}, && (3.58)\\
\beta_{\hat{g}} &= -\epsilon\hat{g}_R + \frac{3\hat{g}_R^2}{4} + \hat{v}_R w_R, && (3.59)\\
\beta_{\hat{v}} &= -\epsilon\hat{v}_R + \hat{v}_R\left[\frac{5\hat{g}_R}{16} + \frac{w_R}{1+\rho} + \frac{\rho\hat{v}_R}{2(1+\rho)} + \frac{u_R}{2}\right], && (3.60)\\
\beta w &= -\epsilon w_R + w_R\left[\frac{3\hat{g}_R}{16} + \frac{2w_R}{1+\rho} + \frac{\rho\hat{v}_R}{(1+\rho)} + \frac{u_R}{2}\right]. && (3.61)
\end{aligned}$$

For detailed calculations please see the appendix. We also evaluate the flow equation for the ratio of time scales ρ.

$$\begin{aligned}
\beta_\rho &= \mu\partial_\mu\rho = \frac{\gamma_R}{\lambda_R}\mu\partial_\mu \ln\gamma_R - \frac{\gamma_R}{\lambda_R}\mu\partial_\mu \ln\lambda_R\\
&= \frac{\gamma_R}{\lambda_R}\mu\partial_\mu \ln(Z_\phi^{-1/2} Z_{\tilde{\phi}}^{1/2} Z_\gamma^{-1}\gamma) - \frac{\gamma_R}{\lambda_R}\mu\partial_\mu \ln(Z_S^{1/2} Z_{\tilde{s}}^{1/2} Z_\lambda^{-1}\lambda)\\
&= \frac{\gamma_R}{\lambda_R}[-\frac{1}{2}\zeta_\phi + \frac{1}{2}\zeta_{\tilde{\phi}} - \zeta_\gamma] - \frac{\gamma_R}{\lambda_R}[\frac{1}{2}\zeta_s + \frac{1}{2}\zeta_{\tilde{s}} - \zeta_\lambda]\\
&= -\frac{\gamma_R}{\lambda_R}[\frac{1}{2}\zeta_s + \frac{1}{2}\zeta_{\tilde{s}} - \zeta_\lambda]\\
&= \rho[\frac{\hat{g}_R}{8} - \frac{\hat{g}_R}{16}] = \rho\frac{\hat{g}_R}{16}. && (3.62)
\end{aligned}$$

3.2 Fixed Points

The β functions describe how the dimensionless non-linear marginal coupling constants transform under scale transformation. In order to access the scale invariant regime, we have to look for the zeros of the β function. Not all zeros of the β function are infrared (IR) stable. The positive value of the derivative of the β function at the fixed point gives us the IR stable fixed point. The zeros of the β function are given by

$$\begin{aligned} 0 &= -\epsilon u_R + \frac{3u_R^2}{2} && (3.63)\\ 0 &= -\epsilon \hat{g}_R + \frac{3\hat{g}_R^2}{4} + \hat{v}_R w_R && (3.64)\\ 0 &= -\epsilon \hat{v}_R + \hat{v}_R\left(\frac{5\hat{g}_R}{16} + \frac{w_R}{1+\rho} + \frac{\rho\hat{v}_R}{2(1+\rho)} + \frac{u_R}{2}\right) && (3.65)\\ 0 &= -\epsilon w_R + w_R\left(\frac{3\hat{g}_R}{16} + \frac{2w_R}{1+\rho} + \frac{\rho\hat{v}_R}{(1+\rho)} + \frac{u_R}{2}\right) && (3.66)\\ 0 &= \rho\frac{\hat{g}_R}{16}. && (3.67) \end{aligned}$$

From Eqn (3.63) we see that there are only two solutions for u_R^*. They are, $u_R^* = 0$, $\frac{2\epsilon}{3}$. Now $\partial_{u_R}\beta_u|_{u_R^*}$ are $-\epsilon$ and $-\epsilon + 3 * \frac{2\epsilon}{3} = \epsilon$. Hence $u_R^* = \frac{2\epsilon}{3}$ is the IR stable fixed point. From Eqn (3.62) we see that, a non zero value of ρ implies $\hat{g}_R^* = 0$. Substituting these values for u_R and $\hat{g}_R$ we have

$$\begin{aligned} \hat{v}_R w_R &= 0 && (3.68)\\ -\epsilon\hat{v}_R + \hat{v}_R\left(\frac{w_R}{1+\rho} + \frac{\rho\hat{v}_R}{2(1+\rho)} + \frac{\epsilon}{3}\right) &= 0 && (3.69)\\ -\epsilon w_R + w_R\left(\frac{2w_R}{1+\rho} + \frac{\rho\hat{v}_R}{(1+\rho)} + \frac{\epsilon}{3}\right) &= 0 \quad . && (3.70) \end{aligned}$$

There are three possible solutions for $\hat{v}_R^*$ and w_R^*.
i) $\hat{v}_R^* = 0$, $w_R^* = 0$.
ii) $\hat{v}_R^* = 0$, $-\frac{2\epsilon}{3} + \frac{2w_R}{1+\rho} = 0 \Rightarrow w_R^* = \frac{\epsilon(1+\rho)}{3}$.
iii) $w_R^* = 0$, $-\frac{2\epsilon}{3} + \frac{(\rho\hat{v}_R)}{2(1+\rho)} = 0 \Rightarrow \hat{v}_R^* = \frac{4\epsilon(1+\rho)}{3\rho}$.

The matrix of the partial derivatives of the β function is,

$$M = \begin{pmatrix} \partial_{\hat{g}_R}\beta_{\hat{g}} & \partial_{\hat{v}_R}\beta_{\hat{g}} & \partial_{w_R}\beta_{\hat{g}} \\ \partial_{\hat{g}_R}\beta_{\hat{v}} & \partial_{\hat{v}_R}\beta_{\hat{v}} & \partial_{w_R}\beta_{\hat{v}} \\ \partial_{\hat{g}_R}\beta_{w} & \partial_{\hat{v}_R}\beta_{w} & \partial_{w_R}\beta_{w} \end{pmatrix},$$

which, for our purpose takes the form

$$M = \begin{pmatrix} -\epsilon + \frac{3\hat{g}_R}{2} & w_R & \hat{v}_R \\ \frac{5\hat{v}_R}{16} & -\frac{2\epsilon}{3} + \frac{5\hat{g}_R}{16} + \frac{w_R}{1+\rho} + \frac{\rho\hat{v}_R}{1+\rho} & \frac{\hat{v}_R}{1+\rho} \\ \frac{3w_R}{16} & \frac{\rho w_R}{1+\rho} & -\frac{2\epsilon}{3} + \frac{3\hat{g}_R}{16} + \frac{4w_R}{1+\rho} + \frac{\rho\hat{v}_R}{1+\rho} \end{pmatrix}.$$

Plugging in the solution i) in the above matrix we have

$$M_i = \begin{pmatrix} -\epsilon & 0 & 0 \\ 0 & -\frac{2\epsilon}{3} & 0 \\ 0 & 0 & -\frac{2\epsilon}{3} \end{pmatrix}.$$

The solution i) is completely unstable in all directions. For the second solution we have

$$M_{ii} = \begin{pmatrix} -\epsilon & \frac{\epsilon(1+\rho)}{3} & 0 \\ 0 & -\frac{\epsilon}{3} & 0 \\ \frac{\epsilon(1+\rho)}{16} & \frac{\rho\epsilon}{3} & \frac{2\epsilon}{3} \end{pmatrix}.$$

The above matrix has two negative eigenvalues $-\epsilon$ and $-\frac{\epsilon}{3}$ respectively. Thus it is unstable in $\hat{g}_R$ and $\hat{v}_R$ directions. The third solution leads to

$$M_{iii} = \begin{pmatrix} -\epsilon & 0 & \frac{4\epsilon(1+\rho)}{3\rho} \\ \frac{5\epsilon(1+\rho)}{12\rho} & \frac{2\epsilon}{3} & \frac{4\epsilon}{3\rho} \\ 0 & 0 & \frac{2\epsilon}{3} \end{pmatrix}.$$

This matrix also has a negative eigenvalue of $-\epsilon$, hence the solution is unstable in the $\hat{g}_R$ direction. So we conclude that in the critical infrared limit the stable fixed point solutions of Eqn (3.62) and Eqn (3.63) are

$$u_R^* = \frac{2\epsilon}{3}, \qquad \rho^* = 0. \tag{3.71}$$

We can plug those values in the β functions and look for IR stable solutions for $\hat{g}_R$, $\hat{v}_R$ and w_R. The β function is given by

$$0 = -\epsilon\hat{g}_R + \frac{3\hat{g}_R^2}{4} + \hat{v}_R w_R \tag{3.72}$$

$$0 = -\frac{2\epsilon\hat{v}_R}{3} + \hat{v}_R\left(\frac{5\hat{g}_R}{16} + w_R\right) \tag{3.73}$$

$$0 = -\frac{2\epsilon w_R}{3} + w_R\left(\frac{3\hat{g}_R}{16} + 2w_R\right). \tag{3.74}$$

There are three possible solutions to the above simultaneous equations. Only one of them is fully coupled though.
iv) $\hat{v}_R^* = 0$, $w_R^* = 0$, $\hat{g}_R^* = \frac{4\epsilon}{3}$.
v) $\hat{v}_R^* = 0$, $\hat{g}_R^* = \frac{4\epsilon}{3}$, $0 = -\frac{2\epsilon}{3} + \frac{\epsilon}{4} + 2w_R \Rightarrow w_R^* = \frac{5\epsilon}{24}$.
vi)$\hat{g}_R^* = \frac{32\epsilon}{21}$, $w_R^* = \frac{4\epsilon}{21}$, $\hat{v}_R^* = -\frac{8\epsilon}{7}$.

We are in a position to check for the stability of these solutions. The stability matrix is

$$M = \begin{pmatrix} -\epsilon + \frac{3\hat{g}_R}{2} & w_R & \hat{v}_R \\ \frac{5\hat{v}_R}{16} & -\frac{2\epsilon}{3} + \frac{5\hat{g}_R}{16} + w_R & \hat{v}_R \\ \frac{3w_R}{16} & 0 & -\frac{2\epsilon}{3} + \frac{3\hat{g}_R}{16} + 4w_R \end{pmatrix}.$$

The stability matrix for solution iv) is

$$M_{iv} = \begin{pmatrix} +\epsilon & 0 & 0 \\ 0 & -\frac{\epsilon}{4} & 0 \\ 0 & 0 & -\frac{5\epsilon}{12} \end{pmatrix}.$$

The solution iv) is unstable in $\hat{v}_R$ and w_R directions. The matrix M for solution v) is

$$M_v = \begin{pmatrix} +\epsilon & \frac{5\epsilon}{24} & 0 \\ 0 & -\frac{\epsilon}{24} & 0 \\ \frac{5\epsilon}{16*8} & 0 & \frac{11\epsilon}{12} \end{pmatrix}.$$

The solution is unstable in $\hat{v}_R$ direction.
The last solution is a fully coupled fixed point. The stability matrix has three eigenvalues with positive real parts indicating that this fixed point is IR stable. However, the fact that it is associated with $\rho^* = 0$ raises an important issue. Physically, $\rho \to 0$ implies that the dynamics of model A freezes on the time scale of the population dynamics fields, i.e. they now evolve in an environment characterized by quenched disorder. The key question, of course, is how to incorporate this quenched disorder into the directed percolation functional. In a first attempt [38], a time-delocalized vertex, of the form

$$-\frac{\lambda^2}{2} f_3 \int d^d r \left[\int dt \ \tilde{s}(x,t) s(x,t) \right]^2$$

is added to the action. This vertex arises from an additional quenched contribution in the correlations of a Langevin noise:

$$\langle \zeta(x,t)\zeta(x',t') \rangle = \lambda \left\{ g s(x,t)\delta(t-t') + f_3 s(x,t)s(x',t') \right\} \delta(x-x')$$

with $f_3 > 0$ due to positivity. Including this vertex into the DP action and performing the RG analysis [38], one finds only unphysical fixed points. Integrating the Wilson β-function for the new coupling directly yields a run-away solution. It is possible that the transition into the absorbing state, in the presence of the Model A background, becomes first order.

There is, however, another possibility of incorporating the frozen background, and the details here are left to future work. If we consider the Model A functional at its critical point, the Model A fields develop power law correlations. In other words, not only are the fluctuations of the environment quenched, but they also carry long-ranged correlations. In the most naive approach, one might expect these to modify the critical parameter of the DP fields, i.e.,

$$\tau = \tau_0 + f_4 \left(\overline{\psi(x)\psi(x')} \right)$$

where the overbar denotes a (critical) average within the Model A dynamics. With $\overline{\psi(x)\psi(x')} \sim |x-x'|^{2-d-\eta}$ (where η is the usual correlation exponent), one now has to consider the DP action in the presence of this correlated quenched randomness. The technical tools for this analysis have been developed [39] and can be carried over to models describing scale invariant behavior far from equilibrium [40]. However, the details remain to be worked out.

Chapter 4

Totally Asymmetric Simple Exclusion Process

4.1 Introduction

Our second project is on a specific type of driven diffusive model, namely the *Totally Asymmetric Simple Exclusion Process* (TASEP) model. This model will be my primary focus for the rest of the discussion. TASEP was originally proposed by MacDonalds and Gibbs in context of protein synthesis [4] and by Spitzer [5] in the context of stochastic interacting particle models. The model has found applications in diverse fields like molecular motors moving on micro tubules [41, 42], traffic [43], single-file diffusion [44], and economics [45]. In the long-time and large scale limit, the TASEP is described by a noisy Burgers equation [46], or similarly by the Kardar-Parisi-Zhang equation [47]. Hence it should come as no surprise that the TASEP model shares some generic features with the asymptotic properties of directed polymers in a random medium. Our work is primarily motivated by the work of Adams et al. [6]. We will postpone any discussion of our work until chapter 5. In this chapter we will introduce the model and summarize some generic features. We will also report the findings of Adams et al. [6], and point out the open question they posed.

4.2 Model

In the standard TASEP model the particles are allowed to hop unidirectionally with a unit rate along a one-dimensional lattice [5, 48]. The lattice sites are labeled by integers, $i \in \{0, 2M-1\}$. The lattice constant is $a = L/2M$. The particles are subjected to hardcore repulsion, so that at a given instant of time two particles cannot occupy the same lattice site. The evolution of the occupation η_i in a given time interval dt, is given

by

$$\eta_i(t+dt) = \begin{cases} \eta_i(t) & \text{with probability 1-2dt} \\ \eta_{i-1}(t) + \eta_i(t) - \eta_{i-1}(t)\eta_i(t) & \text{with probability dt} \\ \eta_i(t)\eta_{i+1}(t) & \text{with probability dt,} \end{cases} \tag{4.1}$$

where the first line accounts for the failure to update both the $(i-1,i)$ and $(i,i+1)$ bonds. The second line represents the update of the $(i-1,i)^{th}$ bond and the third line corresponds to the update of the $(i,i+1)^{th}$ bond (see [49]). In conclusion, the equation governing the evolution of the average occupation is

$$\frac{d\langle\eta_i\rangle}{dt} = \langle\eta_{i-1}\rangle - \langle\eta_i\rangle - \langle\eta_{i-1}\eta_i\rangle + \langle\eta_i\eta_{i+1}\rangle. \tag{4.2}$$

We can see from the above equation that the time evolution of the one-point correlation function depends on the two-point correlation function and it can be shown that the two-point correlation function depends on the three-point function. This hierarchical structure, is well known as the BBGKY hierarchy. Fortunately however, this model can be solved exactly and the stationary probability distribution can be found for arbitrary system sizes.

4.3 The Steady State for TASEP on a Ring

In the case of the periodic TASEP, the steady state is not difficult to find. For a system with L sites containing a constant number of particles N, $L!/N!(L-N)!$ distinct configurations exist. All these configurations are equally likely. The reason for this is, if R is the total number of clusters (i.e. an array of occupied sites without an unoccupied site in between the first and the last occupied site) in a given configuration C, then in unit time, the outflux of probability from configuration C is $R(C)P(C)$ (the first particle in each cluster hops). The influx of probability is $\sum_{C'} P(C')$ where the sum runs over just R configurations (because C''s can be realized by moving the last particle of each cluster in C one step backward) [5, 50]. The stationarity condition thus demands that all the configurations have equal weight. The steady state probability distribution is

$$P_{\text{steady}} = \frac{N!(L-N)!}{L!}. \tag{4.3}$$

This discussion can be found in [49]. It then follows that the one-point and two-point functions are

$$\langle\eta_i\rangle = \frac{N}{L}, \qquad \langle\eta_i\eta_j\rangle_{i\neq j} = \frac{N(N-1)}{L(L-1)}. \tag{4.4}$$

Other exactly calculated observables are the average velocity of a particle, and the diffusion constant of a tagged particle on a ring [51, 52, 53, 54]. The velocity V and the diffusion constant Δ are given by

$$V = \lim_{t\to\infty} \frac{\langle Y_t\rangle}{t}, \qquad \Delta = \lim_{t\to\infty} \frac{\langle Y_t^2\rangle - \langle Y_t\rangle^2}{t}, \tag{4.5}$$

where Y_t is the number of hops the particle has undergone in time t. The exact calculation yields [54]

$$V = \frac{L-N}{L-1}, \qquad \Delta = \frac{(2L-3)!}{(2N-1)!(2L-2N-1)!}\left[\frac{(N-1)!(L-N)!}{(L-1)!}\right]^2. \tag{4.6}$$

In the thermodynamic limit $\Delta \sim L^{-1/2}$, showing that the second moment of the fluctuation in the distance traveled by the tagged particle is subdiffusive.

4.4 Interface Equivalence

The TASEP can be mapped to an interface growth model that belongs to the Kardar-Parisi-Zhang (KPZ) universality class [47]. The methods discussed here can be found in [55]. At a given instant of time t the microscopic state of the system is completely characterized by the set of occupation numbers $\eta_i \in \{0, 1\}$. The rate of change of the occupation index follows a continuity equation inside the bulk given by

$$\partial_t \eta_i(t) = J_{i-1}(t) - J_i(t), \tag{4.7}$$

where $J_i = \eta_i(1 - \eta_{i+1})$ is the current, flowing out of the i^{th} site. If one chooses to ignore all the fluctuation effects completely, the equation governing the evolution of the average local density $\bar{\rho}_i(t) = \langle \eta_i(t) \rangle$ is the same as Eqn (4.7). The $\langle ... \rangle$ stands for the average of the occupation number at a given location i. To do so we have to take the average of Eqn (4.7) and ignore all the correlation effects (i.e. $\langle \eta_i(t)\eta_{i+1}(t) \rangle = \langle \eta_i(t) \rangle \langle \eta_{i+1} \rangle$). This approximation is generally called the *mean field* approximation. In this case the rate equation reduces to

$$\bar{\rho}_i(1 - \bar{\rho}_{i+1}) = J. \tag{4.8}$$

It turns out, the mean field approximation is exact for the periodic TASEP (for a review see [56]). In order to derive the full stochastic equation of motion for the TASEP, we express the occupation density and the current density as a sum of a deterministic and a fluctuating part

$$\begin{aligned} \rho_i &= \bar{\rho}_i + \delta\rho_i \\ J_i &= \rho_i(1 - \rho_{i+1}) + \delta J_i. \end{aligned} \tag{4.9}$$

The method is very commonly used in context of electron transport [57]. The steady state density is assumed to be spatially translation invariant (i.e. $\bar{\rho}_i = \bar{\rho}$). The Eqn (4.7), due to Eqn (4.9), can be expressed as

$$\partial_t \delta\rho_i(t) = (1 - \bar{\rho})[\delta\rho_{i-1} - \delta\rho_i] - \bar{\rho}[\delta\rho_i - \delta\rho_{i+1}] + \delta\rho_i[\delta\rho_{i+1} - \delta\rho_{i-1}] - \delta J_i + \delta J_{i-1}. \tag{4.10}$$

The current fluctuations obey the Gaussian statistics, such that

$$\langle \delta J_i(t) \delta J_j(t') \rangle = Var[J]\delta_{i,j}\delta(t - t'), \tag{4.11}$$

where

$$Var[J] = \bar{\rho}(1-\bar{\rho})[1-\bar{\rho}(1-\bar{\rho})]. \tag{4.12}$$

The expression for the variance of J can be obtained by observing that $J_i^2 = J_i$, so that $Var[J] = \langle J\rangle(1-\langle J\rangle)$. In the continuum limit Eqn (4.10) yields the well known stochastic equation of motion [55, 58]

$$\partial_t\phi(x,t) + (v - 2\phi(x,t))\partial_x\phi(x,t) = \frac{1}{2}\partial_x^2\phi(x,t) - \partial_x\xi(x,t). \tag{4.13}$$

Eqn (4.13) has been derived by setting $x = ia$ and by introducing the fields

$$\phi(x,t) = \delta\rho_i(t) \qquad \text{and} \qquad \xi(x,t) = \delta J_i(t). \tag{4.14}$$

The partial derivative in front of ξ is due to the fact that, inside the bulk, the particle number is locally conserved. The lengths are measured in units of lattice spacing a. The noise ξ is a Gaussian white noise with noise strength equal to $Var[J]$. The collective drift velocity is $v = 1 - 2\bar{\rho}$ and changes its sign at $\bar{\rho} = \frac{1}{2}$. For a TASEP on a ring, the drift term can be eliminated by a Galilean transformation $x^{'} \to x - vt$. The ensuing equation for the time evolution of the fluctuation is known as the noisy Burgers equation [46]. In 1-d, the Burgers equation can be recast into the KPZ equation for surface growth upon introducing a new field h via $\phi = \partial_x h$. The KPZ equation is

$$\frac{\partial h(x,t)}{\partial t} = \frac{1}{2}\frac{\partial^2 h(x,t)}{\partial x^2} + \lambda\left(\frac{\partial h(x,t)}{\partial x}\right)^2 + \xi(x,t), \tag{4.15}$$

where λ is the anharmonic coupling strength. For the symmetric exclusion process, where the probability to hop forward is equal to the probability to hop backward, the interface does not move but fluctuates about the equilibrium profile. The time evolution of the fluctuation is not governed by the KPZ growth equation but rather by the Edwards-Wilkinson (EW) equation [59],

$$\frac{\partial h(x,t)}{\partial t} = \frac{1}{2}\frac{\partial^2 h(x,t)}{\partial x^2} + \xi(x,t). \tag{4.16}$$

The Eqn (4.15) can be generalized to include higher order nonlinearities. The general form is given by

$$\frac{\partial h(x,t)}{\partial t} = \frac{1}{2}\frac{\partial^2 h(x,t)}{\partial x^2} + \sum_{n=0}^{\infty}\lambda_n\left(\frac{\partial h(x,t)}{\partial x}\right)^n + \xi(x,t). \tag{4.17}$$

In absence of the constant and the drift term in Eqn (4.17) the two point correlation function takes the form [55, 58, 60, 61]

$$C(x,t) \sim x^{2\chi-2}G\left(\frac{t}{x^z}\right), \tag{4.18}$$

where χ and z are the roughness [70] and the dynamic exponent respectively. The scaling function $G(s)$ goes to a constant as $s \to 0$, implying $C(x,0) \sim x^{2\chi-2}$ [55]. As $s \to \infty$ the

scaling function behaves as $G(s) \to s^{(2\chi-2)/z}$, implying $C(0,t) \sim t^{(2\chi-2)/z}$. We can define another exponent called the growth exponent β related to the two other exponents by a scaling law $z = \chi/\beta$.
In the RG sense these two equations, the EW and KPZ, have two distinct fixed points. The EW fixed point, in one dimension, is characterized by the critical exponents $\beta = 1/4$ and $z = 2$ [59]. The Edwards-Wilkinson fixed point also characterizes the systems with odd order non-linearity in the rate equation, starting with the cubic term. The cubic term is marginally irrelevant at the EW fixed point.
The presence of the $(\partial h/\partial x)^2$ term in the rate equation however, breaks the $h \to -h$ symmetry, leading to a new universality class. The coupling λ is a relevant coupling for the EW fixed point and hence the RG flow takes the system away to a new fixed point called the KPZ fixed point. The exponents for the KPZ fixed point, in one dimension, are $\beta = 1/3$ and $z = 3/2$ [47].

4.5 Steady State for an Open TASEP

An open TASEP is a generalization of the closed TASEP. The extension of the periodic TASEP is achieved by coupling the system to two particle baths that are maintained at fixed densities $\rho_{\text{left}} = \alpha$ and $\rho_{\text{right}} = 1 - \beta$. A particle can hop into the system with a rate α from the left reservoir only if the zeroth site is unoccupied and a particle can leave the last occupied site with a rate β on the right. The stationary probabilities for the steady state for the open TASEP can be calculated exactly [62, 63]. The time evolution, Eqn (4.2), of the occupation number for the bulk remains invariant, at the boundary, however, they are modified to incorporate the coupling of the two reservoirs to the system.

$$\frac{d\langle\eta_0\rangle}{dt} = \alpha\langle(1-\eta_0)\rangle - \langle\eta_0(1-\eta_1)\rangle \tag{4.19}$$

$$\frac{\langle\eta_{2M-1}\rangle}{dt} = \langle\eta_{2M-2}(1-\eta_{2M-1})\rangle - \beta\langle\eta_{2M-1}\rangle. \tag{4.20}$$

The stationary state of this model has been extensively studied. In the open system three phases have been identified. The phase diagram of the TASEP model is shown in Fig (4.1). The phases are known as the *high-density* (HD), *low-density* (LD) and the *max-current* (MC) phases. The high density and the low density phases are related to one another by particle-hole symmetry. The system undergoes a discontinuous transition along the co-existence line $\alpha = \beta < 1/2$, while the lines $\alpha = 1/2 \leq \beta$ and $\beta = 1/2 \leq \alpha$ mark continuous transitions. In the thermodynamic limit the bulk density $\bar{\rho}_i =< \eta_i >$ is given by $\rho_{\text{left}} = \alpha$, $\rho_{\text{right}} = 1 - \beta$ and $1/2$ for low-density, high-density and max-current phases respectively. On the line $\alpha = \beta < 1/2$, both the HD and the LD phases co-exist. [62, 63].

The dynamic properties of the TASEP model are, however, a very nontrivial issue. The largest relaxation time for the closed TASEP has been derived [63, 64, 65, 66]. The dynamic exponent was found to be $z = 3/2$. For the open system no exact has yet been found but there are strong evidences that $z = 3/2$ for the largest relaxation time for the

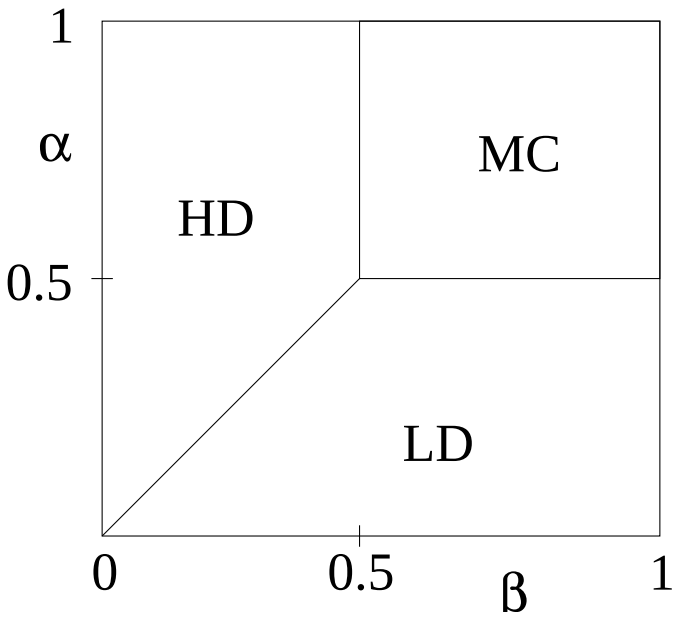

Figure 4.1: The phase diagram of an open TASEP. The high density, low density and the maximal current phases are represented by acronyms HD, LD and MC respectively.

max current phase [67].

4.6 The Power Spectrum

This section predominantly contains the discussion of the power spectrum. A power spectrum gives the distribution of the signal's power in a given frequency bin. It is a positive real valued function of the frequency variable associated with a stationary stochastic process. If the signal $f(t)$ is square integrable then the associated power spectrum $I(\omega)$ is defined as

$$I(\omega) = \left| \frac{1}{\sqrt{2\pi}} \int_{-\infty}^{\infty} f(t) e^{-i\omega t} dt \right|^2 . \tag{4.21}$$

For a stochastic process the signal $f(t)$ is a random variable. Therefore Eqn (4.21) has to be modified. The power spectrum for an underlying stochastic process is defined as

$$I(\omega) = \left\langle \left| \frac{1}{\sqrt{2\pi}} \int_{-\infty}^{\infty} f(t) e^{-i\omega t} dt \right|^2 \right\rangle . \tag{4.22}$$

The angular brackets represent averaging over the total number of realizations in the steady state. If the signal takes only discrete values, the above definition of the power spectrum can be generalized to the discrete case as well.
The power spectrum in context of the open TASEP model has been studied by Pierobon et al. [55]. They have looked at the power spectrum of a local density fluctuation in the co-existence phase. David Adams et al. [6] studied the power spectrum of the total

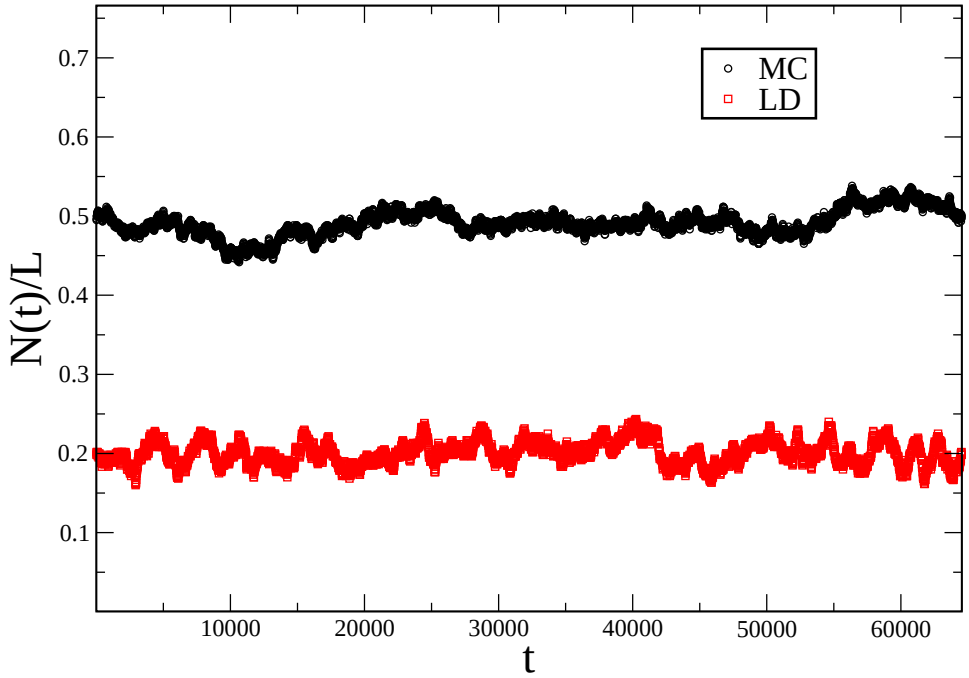

Figure 4.2: Typical time series for $N(t)$, for $L = 600$, in the two distinct regimes: MC and LD. The data have been generated by us but a similar image was originally published in [6].

number of particles of an open TASEP in its different phases. If $N(t)$ is the total number of particles inside the lattice at time t, the power spectrum is defined as $I(\omega) = \langle|\tilde{N}(\omega)|^2\rangle$, $N(\omega)$ being the Fourier transform of $N(t)$. A typical time series for the total occupancy, $N(t)$, for an open TASEP of system size $L = 600$ is shown in Fig (4.2), for two different regimes. The representative values of α and β are $(0.2, 0.7)$ and $(0.7, 0.7)$ for the low density and the max current phases, respectively. Fig (4.3) shows the power spectrum for the total occupancy in the MC and low density phases. Due to the particle hole symmetry, the power spectrum in the high density phase is not shown explicitly. For a discrete time-series $N(t)$, the Fourier transform $\tilde{N}(\omega)$ is defined as: $\tilde{N}(\omega) = \sum_{t=1}^{T} N(t)e^{-i\omega t}$, where T is the total span of measurement in the steady state and $\omega = 2\pi m/T$ with $m = 0, 1....T-1$. The power spectrum in the MC phase shows a power law decay except for very high and very low values of ω. The decay exponent was reported to be 1.62 [6]. The flat part of the graph for small values of ω is due to the finite system size L, where there is a crossover. The theoretical discussion on the scaling form of the power spectrum in MC and co-existence phases can be found in [6].
In spite of the fact that $N(t)$ in the low density phase shows no interesting features, the power spectrum exhibits pronounced oscillations that eventually decay into a power law for large ω. This feature was not observed before and called for some careful study. In order to explain the unexpected oscillations the authors resort to the linearized biased coarse grained Langevin equation

$$\partial_t\phi(x,t) + v\partial_x\phi = D\partial_x^2\phi - \partial_x\xi. \tag{4.23}$$

The choice of neglecting the non-linear term can be physically motivated. The non-

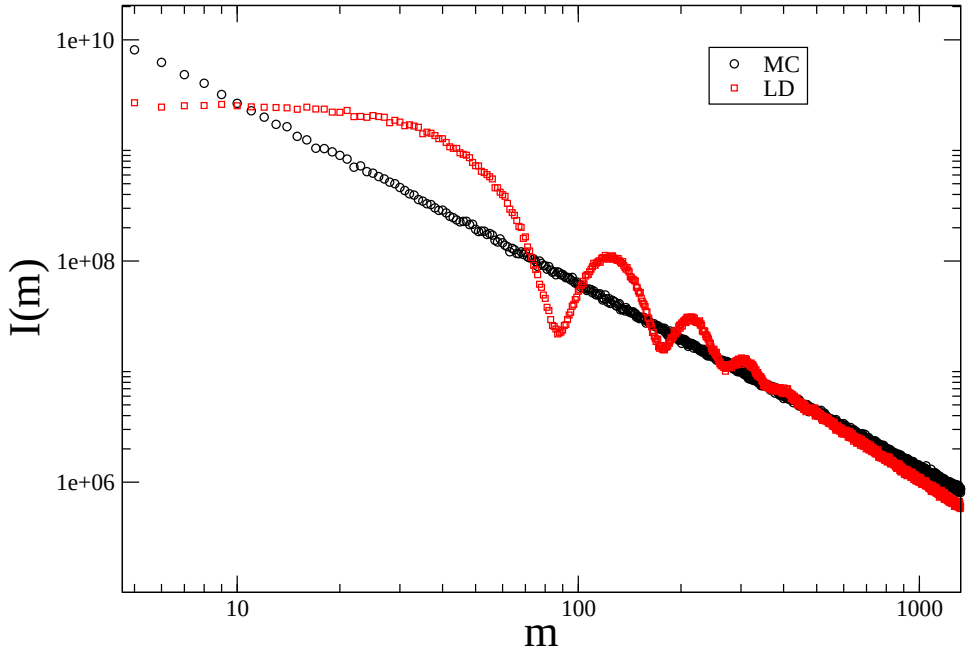

Figure 4.3: The power spectrum of an open TASEP in the MC phase is shown in black. The rates $\alpha = 0.6$ and $\beta = 0.7$. The system size is $L = 600$. We show the power spectrum of an open TASEP of the same length in the LD phase in red. The rates are $\alpha = 0.1$ and $\beta = 0.7$. The data have been generated by us but a similar image was originally published in [6].

linearity becomes crucial when the drift v is small, like around the phase boundary $\alpha = 1/2 \leq \beta$ or $\beta = 1/2 \leq \alpha$. But in the LD phase the density of the particles is small, and non-linearity can be ignored safely. Under this approximation the power spectrum can be computed exactly [6]. It is given by

$$I(\omega) = \frac{8ADT}{v^3} \mathrm{Re}\left[\frac{e^{ik_+ L} - 1}{R(1-R)^2} + \frac{e^{ik_-^* L} - 1}{R^*(1+R^*)^2}\right], \tag{4.24}$$

where $R = \sqrt{1 - 4iD\omega/v^2}$ and $k_\pm = iv(-1 \pm R)/2D$. The quantity A is the noise strength given by $\langle \xi(x,t)\xi(x',t')\rangle = A\delta(x-x')\delta(t-t')$. It appears that the noise strength A is equal to $Var[J]$ in Eqn (4.11). Since the steady state distribution of an open TASEP is not a product measure, it remains to be checked if A is indeed equal to $Var[J]$. For the time being we will keep it as A. T is the total span of time over which the data for $N(t)$ have been recorded. The power spectrum can be studied for three different regions ; a) $\omega \to 0$, b) $\omega \ll v^2/D$, c) $\omega \to \infty$. In the first limit the power spectrum goes to a constant and can be used to fit A, for the third region it decays to a power law. Detailed discussion of all these three regions are in [6]. The region that directly concerns our work is the second region $\omega \ll v^2/D$. In this region, the power spectrum shows pronounced oscillation and is given by the expression [6]

$$I(\omega) = \frac{2AvT}{D\omega^2}[1 - e^{-\frac{D\omega^2 L}{v^3}} \cos(\omega L/v)]. \tag{4.25}$$

We can see that Eqn (4.25) is oscillatory. The minima are integer multiples of vT/L

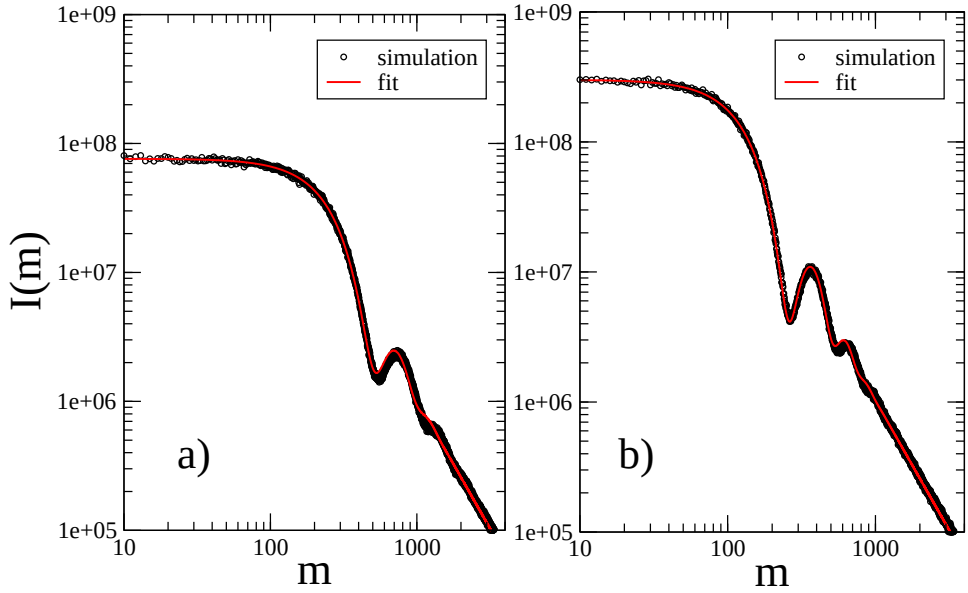

Figure 4.4: Fit for the linear theory using A and D as a fitting parameter a) L=100 , b) L = 200. The parameters are $\alpha = 0.1$ and $\beta = 0.7$. $\omega = 2\pi m/T$.

in m, where $\omega = 2\pi m/T$. The location of the minima falls off inversely as the system size and goes up linearly with the average drift velocity v, which in turn falls off linearly with density. The authors of Ref [6] used Eqn (4.24) to fit the simulation data for the power spectrum. In the theory, the quantities A and D are used as the fitting parameters. Since the entrance rate α is the bulk density in the low density phase, the average drift velocity v is not a fitting parameter but a constant. We show two typical fits in Fig (4.4) for system sizes $L = 100$ and 200 respectively. The data have been generated by us but we have used the fitting function given by Eqn (4.25). The density is $\alpha = 0.1$. The fits show surprisingly good agreement, which reverberates the fact that the linear theory in essence has captured all the essential features of the power spectrum. But naively one would expect the diffusion constant to be 1/2 from Eqn (4.13), instead Adams et al. found the diffusion constant to be enhanced from its "bare value". They did not proceed further to explain the strange "renormalization" of the diffusion constant.

Fascinated by this observation, we decided to have a closer look at the oscillations. We will employ the standard Monte-Carlo technique to find out the nature of dependence these oscillations have on the system size and density. The potential boundary effects will be explored by introducing another length scale, namely the window size. A window is a segement of the whole lattice. The power spectrum computed inside the window, embedded deep in the bulk, is free of boundary effects. The results will give us deeper insights into the observed behavior of the power spectrum. Then we will extend our analysis for the case of periodic TASEP. The power spectrum will be computed inside the window. The similarities and dissimilarities to the open TASEP case will be analysed by a linear theory. We will see that the problem of enhanced diffusion constant is not confined to open TASEP only. It is shared generically by both closed and open TASEP.

We will try to understand the riddle of enhanced diffusion by looking at the full non-linear theory.

Chapter 5

Simulation Results and Theoretical Outlook

The last chapter laid the groundwork for our work which we are going to discuss in detail in this chapter. To restate, pronounced oscillations in the power spectrum of the total occupancy in the low density phase of an open TASEP was reported by Adams et al. [6]. A linear theory was brought in to explain the oscillations. The authors found encouraging agreement with the simulation data at the cost of an enhanced diffusion constant D. This surprising enhancement of the diffusion constant had not been reported previously and called for a detailed study. Motivated by their finding, we will look for an explanation for the enhanced diffusion constant. The two most intuitive predictions for the cause of the mismatch are a) potential boundary effects have been ignored, b) only a linearized version of a more correct non-linear theory has been considered. In this chapter these possibilities will be explored in order. We will carry out rigorous Monte-Carlo simulations to reconfirm the finding of Adams et al. [6] as well as seek an answer to the question posed above. A theoretical explanation will be provided for our new observations.

5.1 Simulation and Results

We performed Monte Carlo simulations using sequential updates. In all our simulations, we have started off with an empty lattice. In each time step, we make $N(t) + 1$ random attempts to move the particles. After a sufficiently long time, the system settles into a time-independent distribution P_{steady}, the exact form of which is also known [62, 63]. We discarded the first $200,000$ time steps to ensure that the system is given enough time to settle down to a steady state. Then, the data for $N(t)$, i.e. the total number of particles at a given instant of time t, was recorded for a total time of $T = 65536$. This choice of T helps in defining the discrete Fourier transform of the signal $N(t)$: $\tilde{N}(\omega) = \sum_{t=1}^{T} N(t)e^{-i\omega t}$, where $\omega = \frac{2\pi m}{T}$. The power spectrum is calculated using a fast Fourier transform routine [68].

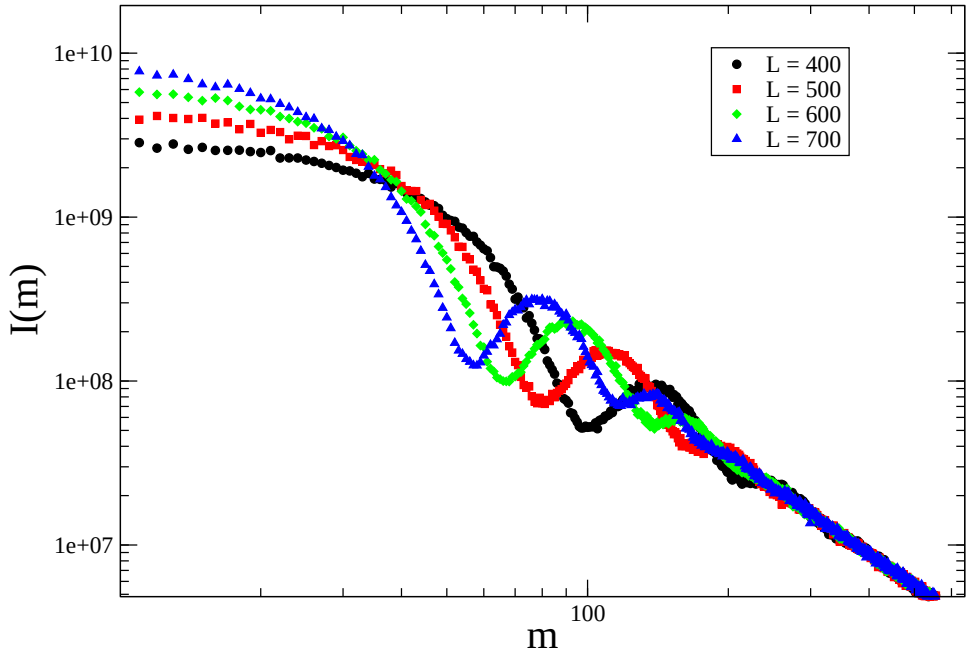

Figure 5.1: Log-log plot of the power spectrum for the open TASEP in the low density phase for different system sizes L. $\alpha = 0.2$ and $\beta = 0.7$.

5.1.1 Dependence on System Size

We choose representative entrance and exit rates $\alpha = 0.2$ and $\beta = 0.7$ respectively. We took data for different system sizes starting from $L = 100$ to $L = 1000$. A few representative plots are shown in Fig (5.1) above.

The plots show oscillations, that eventually decay into a power law. As can be seen, the locations of the minima shift to the left with increasing system size. The location of the first minimum as a function of system size is shown in Fig (5.2). The locations of all the other minima show similar variation with the system size. As the minima are not sharp, the error bars in the Fig (5.2) are obtained by visually inspecting the range of points lying in the near neighborhood of the actual minima. The simulations were done for a fixed density. The location of the first minimum falls off as $1/L^{\delta}$. The decay exponent, extracted from fitting the data points shown in black in Fig (5.2), was found to be $\delta = 1.1$. If however, we choose to fit a function of the form A_0/L, the kind of fit we will get is shown in blue in Fig (5.2). The value of A_0 is set to 39321.6, as from Eqn (4.25) we know $A_0 = vT$, where $v = 0.6$ and $T = 65536$. The blue plot shows deviations from the data points for small values of system size L, but fits the data better for large L. This tells us that the agreement of the linear theory with the simulation data is better for large system sizes. We also observe, that the oscillations decay faster with growing system size. In the limit $L \to \infty$ all the oscillations will have been shifted all the way to the left and one would only expect to see the power law decay. This is also consistent with the fact, that in the thermodynamic limit we can eliminate the drift term in Eqn (4.13) by a Galilean transformation, so that the power spectrum resembles the power spectrum of the max current phase. This re-establishes the fact that the location of the minima of the power

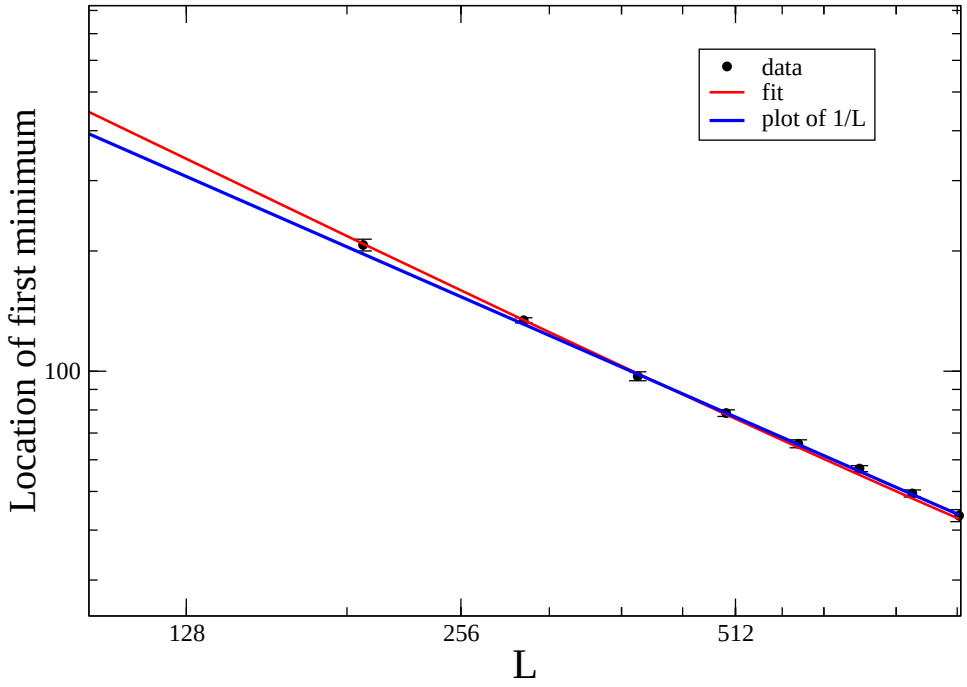

Figure 5.2: Log-log plot of the location of the first minimum for different system sizes L starting from 100 up to 900. $\alpha = 0.2$ and $\beta = 0.7$. The red line is the best fit, to a function of the form C_0/L^{δ}. The blue line is a plot of A_0/L

spectrum indeed falls off as $1/L$.

5.1.2 Dependence on Density

The effects of the entrance and the exit rates are encapsulated in the average density of particles. In the low density phase the entrance rate fixes the average density whereas in the high density phase, it is the exit rate that determines it. We can see the effect of α, by looking at the variation of the power spectrum of a fixed system size as a function of density. Fig (5.3) shows that the minima shift to the right as we lower the density. The oscillations also become more and more pronounced. The location of the first and the second minima for different densities are shown in the Fig (5.4). A linear fit gives a reasonable agreement.

From Eqn (4.25) we see that the locations of the minima, if plotted in m, are integer multiples of Tv/L, where $v = 1-2\bar{\rho}$. This prediction is compared to our data shown in Fig (5.4). The predicted functions are plotted in Fig (5.4a) and (5.4b), the functional form of which are $163.84 - 327.68\bar{\rho}$ and $327.68 - 655.36\bar{\rho}$. Our data shows good agreement for the location of the first minimum. The deviation for the second minimum for higher values of density should not be considered as an inconsistency in the theory. The higher the density gets, the oscillations decay faster to a power law (Eqn (4.25)), making it difficult to pin-point with accuracy the location of subsequent minima.

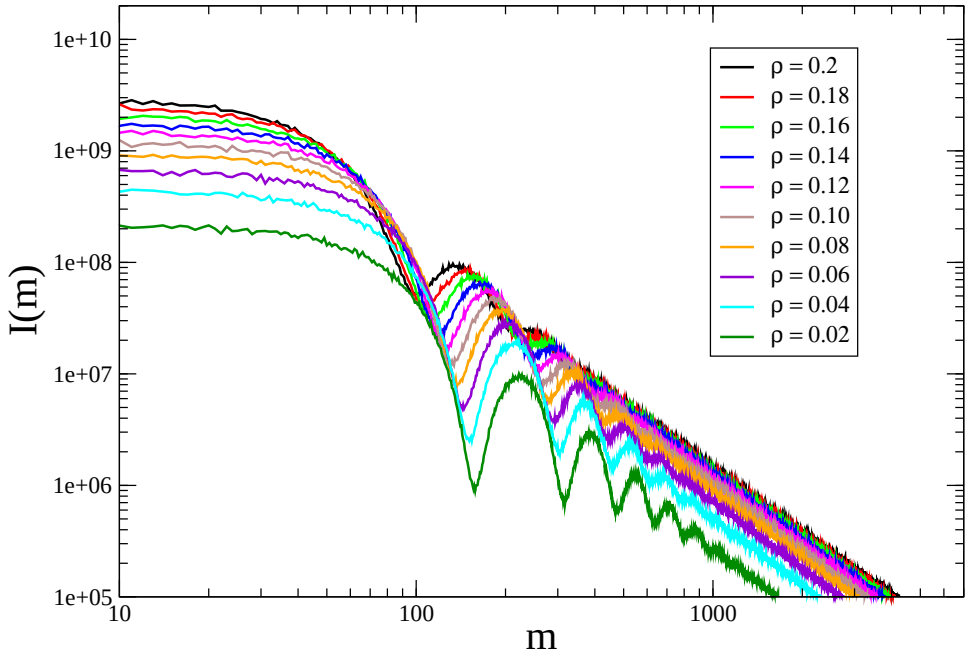

Figure 5.3: Log-log plot of the power spectrum of an open TASEP of length $L = 400$ for different densities.

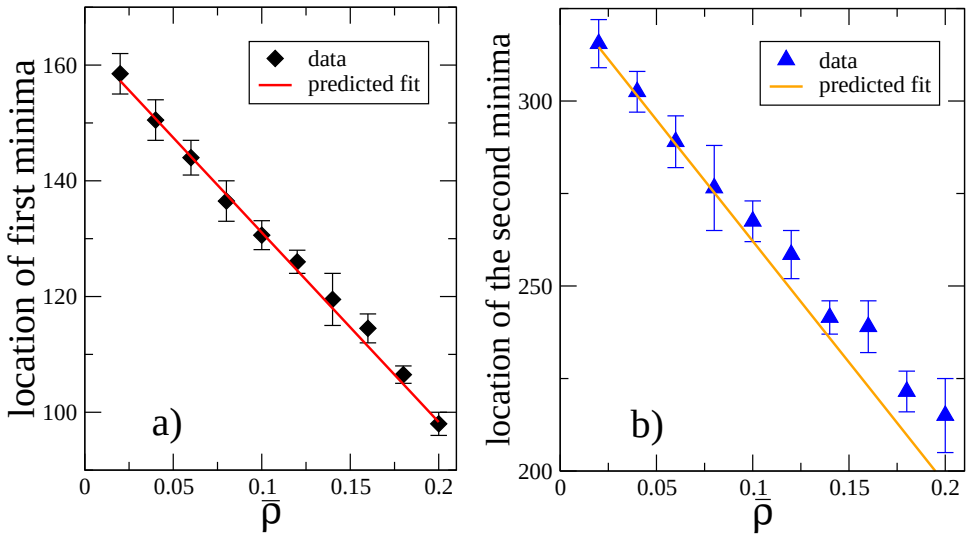

Figure 5.4: Linear plot of a) location of the first minimum and b) location of the second minimum as a function of ρ for system size $L = 400$. The parameters are $\alpha = 0.2$ and $\beta = 0.7$. A linear function was used to fit the above data, the functional form of which was obtained from Eqn (4.25). For the left panel the plot is for the function $163.84 - 327.68\bar{\rho}$. For the right panel the plot is for function $327.68 - 655.36\bar{\rho}$. $T = 65536$.

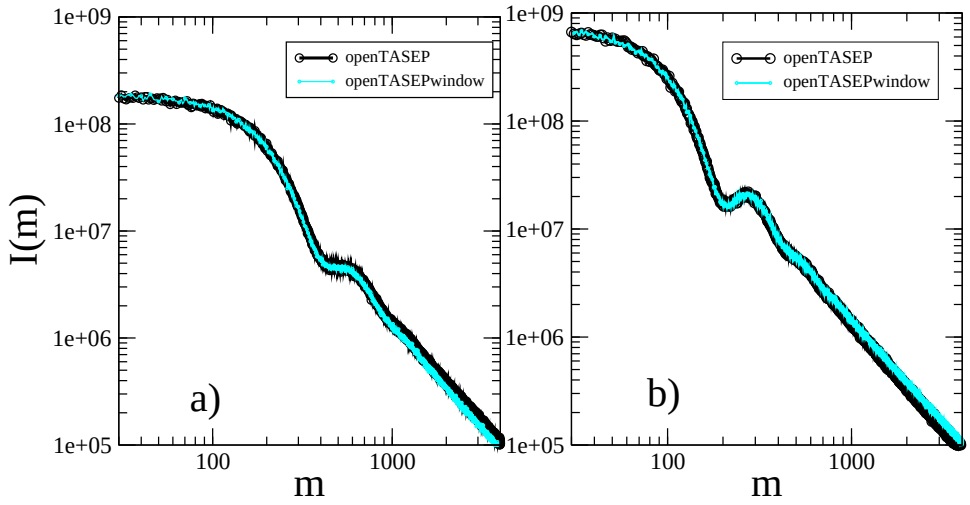

Figure 5.5: Log-log plot of the power spectrum. a) Open TASEP of length $L = 100$ and an open TASEP of length $L = 2000$ with a window of length $l = 100$. b) Open TASEP of length $L = 200$ and an open TASEP of length $L = 2000$ with a window of length $l = 200$. The parameters are $\alpha = 0.2$ and $\beta = 0.7$. For the TASEPs with the windows, the power spectra are calculated only inside the window and not for the whole system.

5.1.3 Effect of the Boundary

Up till now we have not addressed the boundary effects. A natural question is: are the boundary effects responsible for this mysterious enhancement of the diffusion constant ? We introduce a length scale l, which we call the window size. A window is a segment of an open TASEP. The window can be placed anywhere on an open lattice and the power spectrum can be studied for the window only. The motivation is to study the power spectrum of the bulk. We can place a window in the middle of the lattice and study the power spectrum inside the window, thus minimizing substantially the effects of the boundary. We can place the window near the boundary as well and compare the power spectrum with the one where the window is placed deep inside the bulk. Any substantial deviation in the nature of the two power spectra can be attributed to the boundary effects. If however, the two power spectra do not deviate, we can conclude that the effect of the boundary is insignificant. In Fig (5.5) we compare the power spectra of two open TASEPs, one with the window and the other without. The window size of one is chosen to be equal to the system size of the other. The density is $\rho = 0.2$ and the windows are placed in the middle of the lattice.

The graphs coincide making it abundantly clear that boundaries do not have much influence on the power spectrum under consideration. The oscillations do not depend in any way on the boundaries. The role of the boundary is to fix the average density. Fig (5.6) shows the power spectra for the windows placed at different locations on a much larger lattice. In this case the average density is chosen to be $\rho = 0.01$. The power spectrum overlap for different locations of the window. This tells us that enhancement of the diffusion constant cannot be boundary induced.

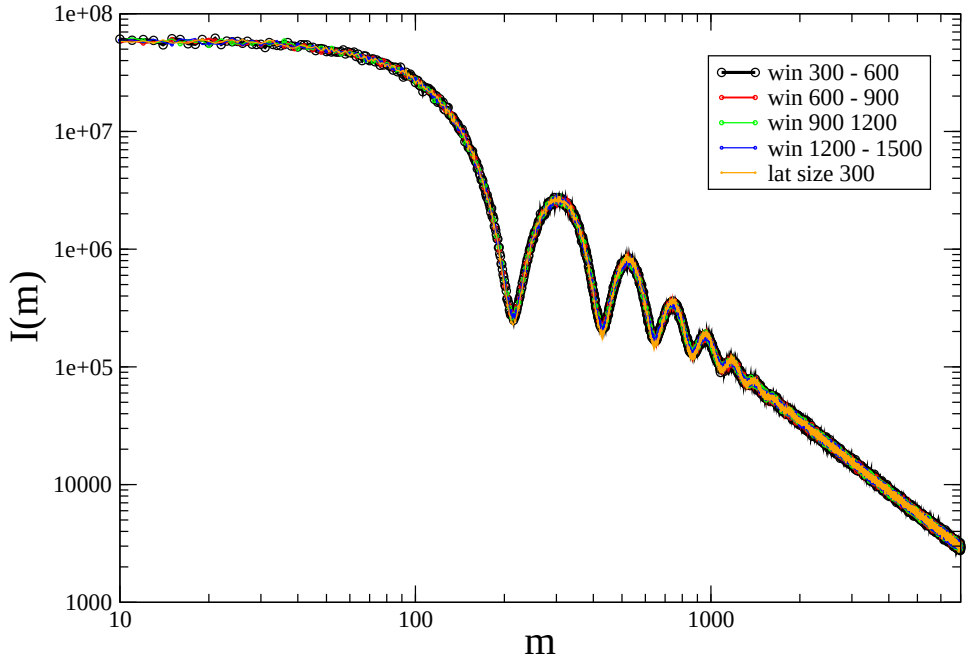

Figure 5.6: Log-log plot of the power spectrum of an open TASEP of $L = 2000$ and $l = 300$ placed at different locations starting from lattice site 300 to lattice site 1500. The plot also shows the graph for $L = 300$. The parameters are $\alpha = 0.01$ and $\beta = 0.7$.

5.1.4 Periodic TASEP with a Window in the Middle

The findings above prompted us to look at the closed TASEP. We expect similar signatures to be present in the power spectrum computed inside a window of a closed TASEP. We consider a periodic TASEP with a window in the middle and repeat the same exercise. Fig (5.7) shows the plot of the power spectrum of the periodic TASEP along with the power spectrum for the open TASEP. Again the window size is equal to the length of the open TASEP. Two different system sizes are presented.

Fig (5.7) demonstrates that the power spectrum for the periodic TASEP starts off with some initial oscillations and then falls onto the curve for the open TASEP. The oscillations for the larger values of frequency ω are the same for both the periodic and the open TASEP. We would argue that the small ω oscillations are an artifact of the periodic boundary condition. The physical origin of the large ω oscillations can be attributed to the time it takes for the fluctuation to sweep across the window [6, 69]. In the case of the periodic TASEP, however, the fluctuation that leaves the window re-enters the window after traversing through the rest of the lattice, giving rise to the small ω oscillations. Our claim has been verified in Fig (5.8) and (5.9) .

Fig (5.8a) shows data for periodic systems of varying length L yet fixed window size. Clearly, there are distinct differences between the different systems for small values of ω. In contrast, the large ω behaviors follow each other very faithfully. The system size dominates the small ω behavior but leaves the remainder of the spectrum unaffected. Replotting the data as a function of ωL, as shown in Fig (5.8b), collapses the location of the maxima for the small ω sector of the different curves. Similarly, Fig. (5.9a) shows

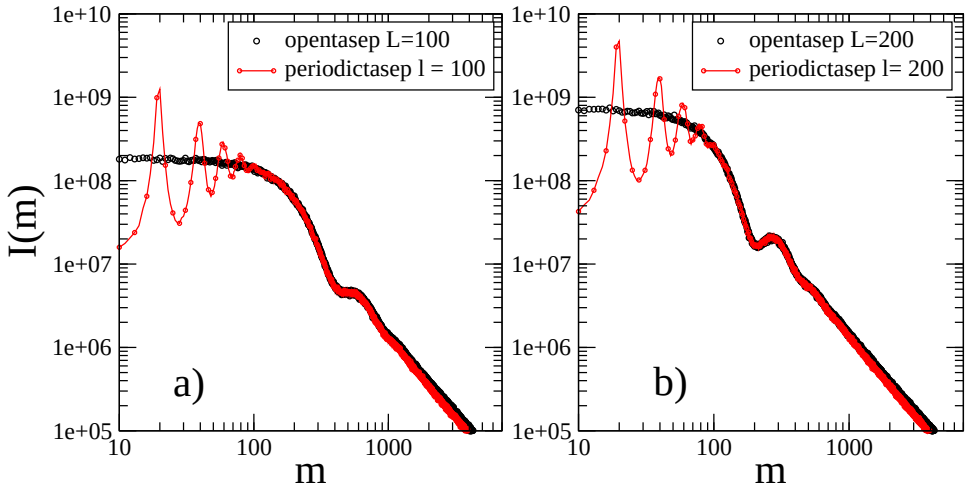

Figure 5.7: Log-log plot of the power spectrum of an a) open TASEP of $L = 100$ and a periodic TASEP of window $l = 100$ b) open TASEP of $L = 200$ and a periodic TASEP of window $l = 200$, $\rho = \alpha = 0.2$. The system size of the periodic TASEP is $L = 2000$.

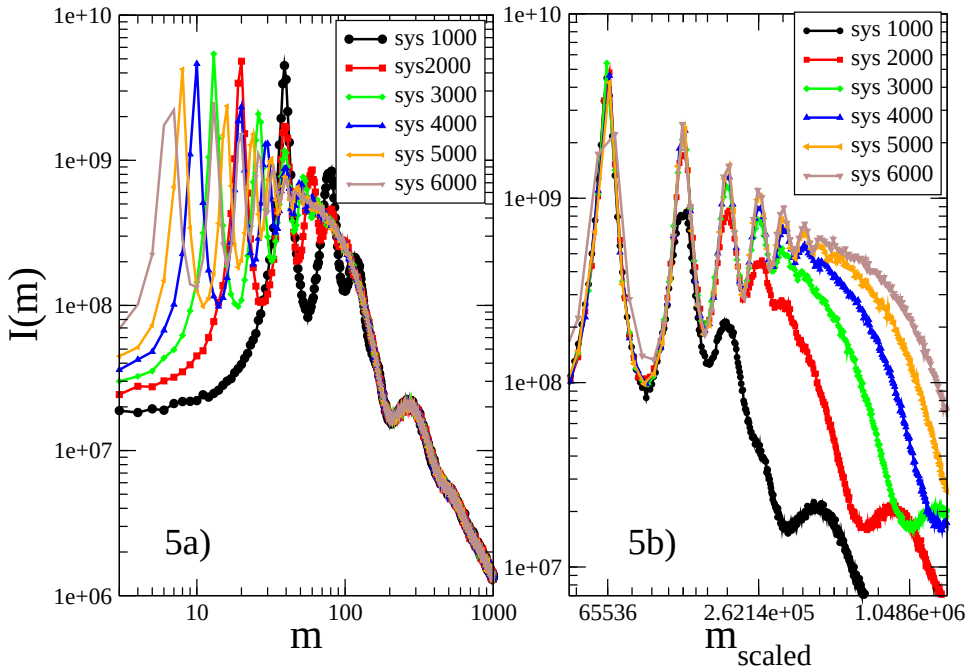

Figure 5.8: Log-log plot of the power spectrum of a periodic TASEP a) window $l = 200$ for different system sizes b) the same graph with x-axis rescaled as ωL. The sector displayed, shows the location of small ω oscillations collapse. $\rho = 0.2$.

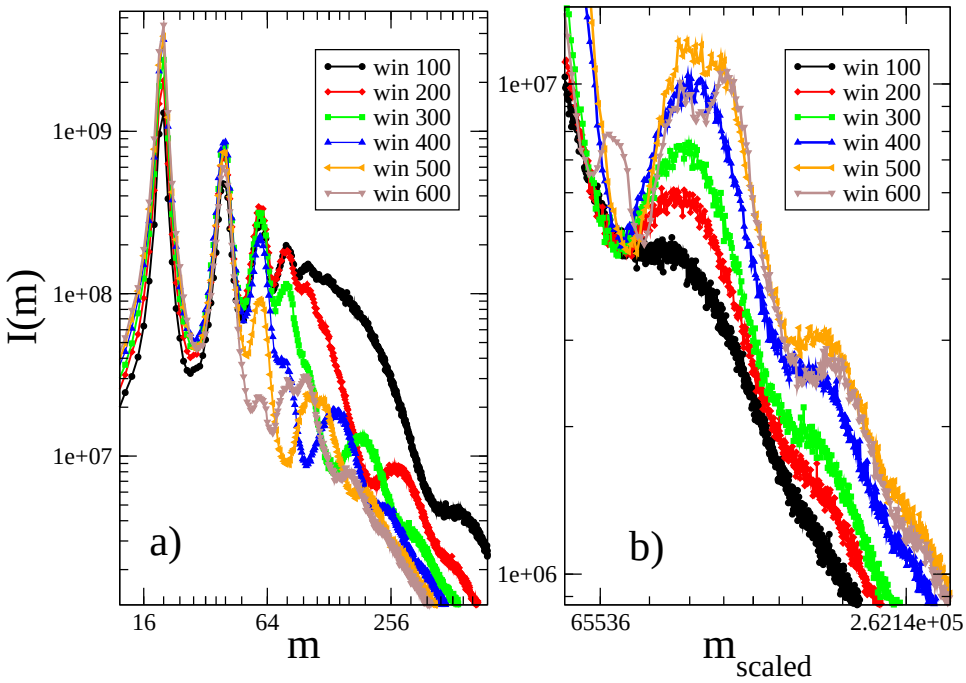

Figure 5.9: Log-log plot of the power spectrum of a periodic TASEP a) system size $L = 2000$ for different window sizes b) the same graph with x-axis rescaled as ωl. The sector displayed, shows the location of large ω oscillations collapse. $\rho = 0.2$.

data for different l at the same L. When replotted as a function of ωl, the location of the minima for the large ω part of the spectra coincides reasonably well. This is illustrated in Fig (5.9b).

5.1.5 Density Dependence of the Power Spectrum of a TASEP on a Ring with a Window in the Middle

This section is devoted to explore the density dependence of the power spectrum inside a window placed on a ring. In Fig (5.10) we explore how the power spectrum of a periodic TASEP depends on its density. A system size of $L = 2000$ and a window size of $l = 400$ are chosen and held fixed while the density is steadily lowered. We can see, the lower the densities get, the more shifted the plots are as a whole to the right, implying that the fluctuations take, on an average, a smaller time to sweep the lattice as well as the window. In other words, the average drift increases as we lower the density. A similar study can be undertaken on the location of the maxima for the small ω oscillations for different densities. The plots are shown in Fig (5.11). We show a linear fit along with the plots. The linear fits are in good agreement with the data.

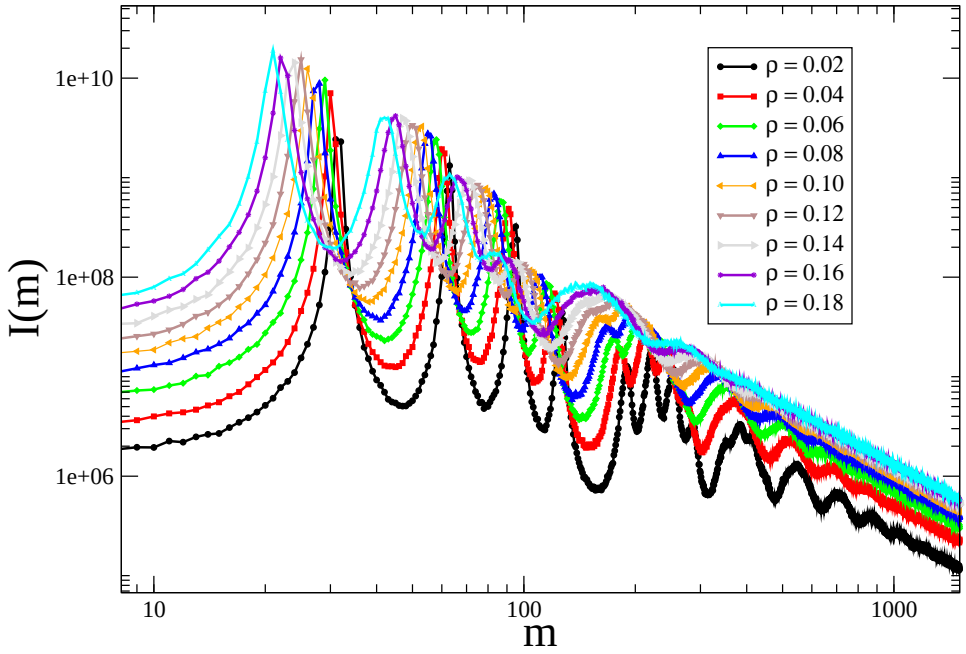

Figure 5.10: Log-log plot of the power spectrum of a periodic TASEP of length $L = 2000$ and window size $l = 400$ for different densities.

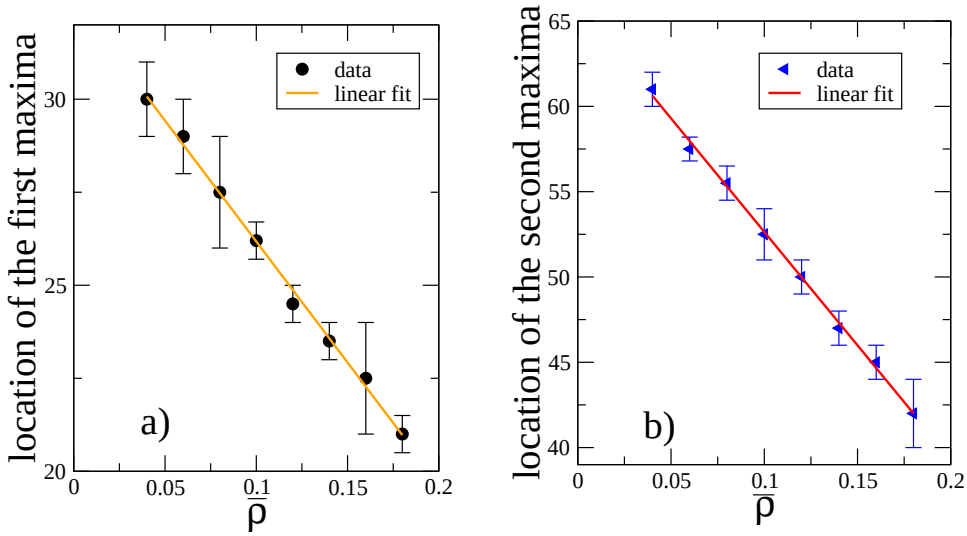

Figure 5.11: Linear plot of a) location of the first maximum b) location of the second maximum as a function of ρ for window size $l = 400$ of a periodic TASEP.

5.2 Linear Theory

In order to explain the power spectrum of the periodic TASEP we propose a discrete linear theory, much in the same spirit of the calculations done by Adams et al. [6]. For a discrete finite system the momentum integral has to be replaced by a discrete sum whose upper and lower limit are fixed by the lattice constant and the system size respectively. The system we will look at is of length L, while the power spectrum will be calculated inside a window of size l embedded in the bulk. The power spectrum can be obtained from the equation for the fluctuation ϕ around $\bar{\rho}$ [55]

$$\phi(x,t+1)-\phi(x,t) = (1-\bar{\rho})[\phi(x-1,t)-\phi(x,t)]-\bar{\rho}[\phi(x,t)-\phi(x+1,t)]-\xi(x,t)+\xi(x-1,t). \tag{5.1}$$

ξ is a Gaussian white noise. We can write ϕ in Fourier space as

$$\phi(x,t) = \frac{1}{LT}\sum_{k=0}^{L-1}\sum_{\omega} e^{i(q_k x+\omega t)}\tilde{\phi}(q_k,\omega), \tag{5.2}$$

where $q_k = (2\pi k)/L$. We find,

$$\begin{aligned}\phi(x,t+1) &= \frac{1}{LT}\sum_{k=0}^{L-1}\sum_{\omega} e^{i(q_k x+\omega(t+1))}\tilde{\phi}(q_k,\omega) \\ &= \frac{1}{LT}\sum_{k}\sum_{\omega} e^{i(q_k x+\omega t)}e^{i\omega}\tilde{\phi}(q_k,\omega).\end{aligned} \tag{5.3}$$

Substituting Eqn (5.2) in Eqn (5.1) we have

$$\begin{aligned}[e^{i\omega}-1]\tilde{\phi}(q_k,\omega) &= (1-\bar{\rho})[e^{-iq_k}-1]\tilde{\phi}(q_k,\omega) - \bar{\rho}[1-e^{iq_k}]\tilde{\phi}(q_k,\omega) \\ &+ [e^{-iq_k}-1]\tilde{\xi}(q_k,\omega),\end{aligned} \tag{5.4}$$

$$\tilde{\phi}(q_k,\omega) = \frac{(e^{-iq_k}-1)\tilde{\xi}(q_k,\omega)}{e^{i\omega}-1-(1-\bar{\rho})[e^{-iq_k}-1]+\bar{\rho}[1-e^{iq_k}]}. \tag{5.5}$$

Now,

$$-(1-\bar{\rho})[e^{-iq_k}-1]+\bar{\rho}[1-e^{iq_k}] = 1-\cos(q_k)+i\sin(q_k)(1-2\bar{\rho}).$$

Substituting it in the Eqn (5.5) we have

$$\tilde{\phi}(q_k,\omega) = \frac{(e^{-iq_k}-1)\tilde{\xi}(q_k,\omega)}{e^{i\omega}-1+1-\cos(q_k)+iv\sin(q_k)}. \tag{5.6}$$

Now, $N_{seg}(t) = \bar{\rho}l+\sum_x \phi(x,t)$, where N_{seg} is the total occupancy in the segment of length l. Substituting Eqn (5.6) in the expression for the N_{seg} we have

$$N_{seg}(t) = \bar{\rho}l + \frac{1}{LT}\sum_{x=0}^{l-1}\sum_{k,\omega} e^{i(q_k x+\omega t)}\tilde{\phi}(q_k,\omega). \tag{5.7}$$

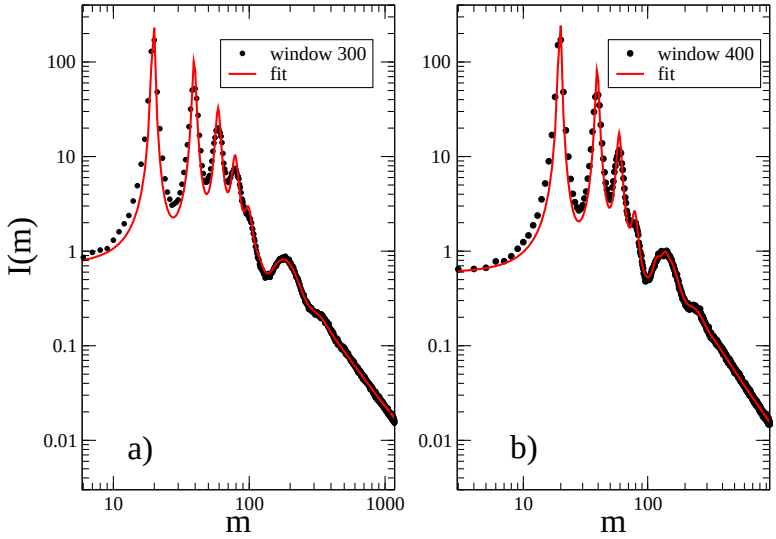

Figure 5.12: Log-log plot of the power spectrum of a periodic TASEP along with its fit for $L = 2000$, a) window size $l = 300$ b) window $l = 400$, $\bar{\rho} = 0.2$ with D as a fitting parameter. $D = 6.0$ and 6.4 respectively for a) and b)

The Fourier Transform $\tilde{N}_{seg}(\omega')$ is equal to $\sum_t e^{-i\omega' t} N_{seg}(t)$.
Therefore,

$$\begin{aligned}
\tilde{N}_{seg}(\omega') &= \frac{1}{LT}\sum_t e^{-i\omega' t}\sum_{x=0}^{l-1}\sum_{k,\omega} e^{i(q_k x+\omega t)}\frac{(e^{-iq_k}-1)\tilde{\xi}(q_k,\omega)}{e^{i\omega}-1+D(1-\cos(q_k))+iv\sin(q_k)},\\
&= \frac{1}{LT}\sum_{k,\omega,t} e^{-i\omega' t}e^{i\omega t}\frac{(e^{-iq_k}-1)\tilde{\xi}(q_k,\omega)}{e^{i\omega}-1+D(1-\cos(q_k))+iv\sin(q_k)}\frac{1-e^{iq_k l}}{1-e^{iq_k}},\\
&= \frac{1}{LT}\sum_{k,\omega} T\delta_{\omega,\omega'}\frac{(e^{-iq_k}-1)\tilde{\xi}(q_k,\omega)}{e^{i\omega}-1+D(1-\cos(q_k))+iv\sin(q_k)}\frac{1-e^{iq_k l}}{1-e^{iq_k}},\\
&= \frac{1}{L}\sum_{k}\frac{(e^{-iq_k}-1)\tilde{\xi}(q_k,\omega)}{e^{i\omega}-1+D(1-\cos(q_k))+iv\sin(q_k)}\frac{1-e^{iq_k l}}{1-e^{iq_k}}. \qquad (5.8)
\end{aligned}$$

The resulting $I(\omega) = \langle|\tilde{N}_{seg}(\omega)|^2\rangle$ after averaging over noise is

$$I(\omega) = \frac{2AT}{L}\sum_k \frac{1-\cos(q_k l)}{(\cos(\omega)-1+D(1-\cos(q_k)))^2+(\sin(\omega)+v\sin(q_k))^2}. \qquad (5.9)$$

The two-point noise correlator was written as $\langle\xi(q_k,\omega)\xi^*(q_{k'},\omega)\rangle = ALT\delta_{k,k'}$, where A is the noise strength. The constant D in our case is equal to 1. But in previous studies, D was found to be seriously enhanced due to interaction [6, 69]. This is the reason why we chose to keep D unspecified. It will be a fitting parameter of our theory. The discrete sum has been computed numerically. We show fits with D as the fitting parameter in Fig (5.12).

Fig (5.12) shows that our linear theory captures all the essential details. The noise

strength A and the diffusion constant D are the parameters of our theory.

5.3 The Fitting Parameter D

This section is dedicated to the discussion of the fitting parameter D, the diffusion constant. We have extracted the nature of variation of D as a function of system size L and the density ρ for an open TASEP. The variation of the diffusion constant D for the case of a periodic TASEP has not been presented here. This should not be considered as a loss of generality as we showed that the boundaries do not have any role to play in this reported deviation of the diffusion constant. We observe that the only place in Eqn (4.25) where the diffusion constant D appears by itself is in the exponential. Thus the diffusion constant actually dictates how fast the oscillations are going to die off to a power law. This gave us a reason not to fit the whole data set for the power spectrum but only a truncated portion of it. We keep the data for $0 \ll \omega \ll v^2/D$ in the truncated data set. The truncated portion contains the oscillations and arguably will present us with a more reliable value of the diffusion constant. We adopt two different methods : a) we fit the log of the truncated data set with the log of the fitting function b) we fit the data set with the fitting function. The reason for adopting the first method is to reduce the relative error associated with the data points whose values are orders of magnitude different. A comparative plot is shown in Fig (5.13).
Fig (5.13) delineates the differences in the results. While method (b) gave us a linear variation of the diffusion constant with the system size, method (a) predicts something fairly different. Looking at Fig (5.13a) it is obvious that the plots are in fact not linear but a power law. We have shown three fits as well. We have fitted the plots in the Fig (5.13a) by the functional form, $A_0 + A_1 * x^{\delta}$. The value of δ is found to be roughly around 0.3. As the second method puts equal emphasis on all the data points, it is reasonable to trust Fig (5.13a) more.

We have shown that the power spectrum for an open TASEP of length L is identical to the power spectrum in a window of size l as long as the window size l is equal to L. This is true irrespective of the boundary condition. We can have an open TASEP with the window l in the middle or a closed TASEP with the window in the middle, the nature of variation of the power spectrum for large frequencies is exactly the same. The closed TASEP however shows some deviations for smaller values of ω. We conclude that the boundaries do not play a pronounced role in this surprising dependence of the diffusion constant D on the window size l. Moreover we also observe from Fig (5.13) the higher the value of the density ρ, the higher the diffusion constant. In fact, for a very low density of $\rho = 0.01$, the diffusion constant D is more or less close to 0.5, the "unrenormalized bare value". Now, a higher density induces a stronger hardcore repulsion. The non-linear term in the equation of motion is due to exclusion. So it is not unnatural to believe that the mysterious behavior of the diffusion constant can be due to the non-linear term, which we have ignored so far. We will seek the correction to the diffusion constant in the non-linear

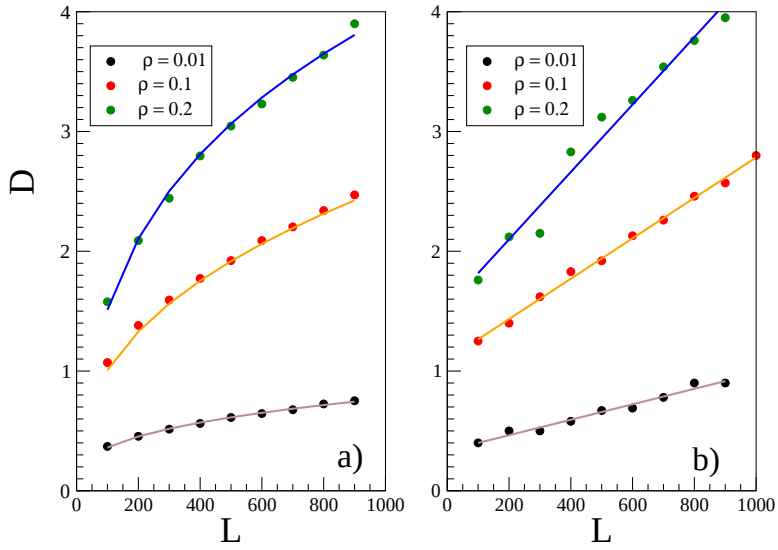

Figure 5.13: The dots are the extracted values of the diffusion constant D. The solid lines are fits. a) Linear plot of the diffusion constant Vs the system size for three different densities. The diffusion constant is extracted by fitting the log of Eqn (4.25). to the log of the data obtained from simulation. The three plots are fitted with a power law of the form $y = A + Bx^{\delta}$. The exponents for the three data sets are roughly 0.3. b) Linear plot of the diffusion constant as a function of the system size for three different densities. The diffusion constant is extracted by fitting the function above to the raw data.

term.

5.4 Perturbation Theory

We saw in the sections above that the oscillations are not a boundary induced phenomenon and that the fitting functions does not explicitly carry any information about the boundary. We will seek an answer to the riddle by taking into account the nonlinearity. Similar enhancement of the diffusion constant was also reported by [6, 69]. Starting from the well known Langevin Eqn (4.10), we will construct the dynamic functional. Then, we will compute the two-point vertex function to one-loop order. The diffusion constant in Fourier space is the coefficient of the square of the external momentum Q. The correction to the diffusion constant will be sought for in the coefficient of Q^2 to one-loop order. There is however another approach that we can undertake. This method relies on the calculation of the whole power spectrum order by order. Then, the corrected power spectrum can be used to fit the simulation data. Since the variation of the fitting parameters would not be extracted from fitting a linear theory to the simulation data but by fitting the entire nonlinear theory, the correction obtained by this method will be more reliable. Though the second approach is more systematic, the calculation is much involved. We will undertake the first approach in this dissertation.
Since the strange behavior of the diffusion constant is fairly generic for both open and closed TASEP, we will confine our self to the periodic boundary condition only. This

section will be devoted to calculating the effect of nonlinearity in continuum.
In what follows we will briefly motivate the *Janssen-De Dominicis* functional for the construction of dynamic field theory. Then we will write down the action for the TASEP model and then we will employ perturbation theory to evaluate the vertex function.
We start off with the continuous rate equation for the variation of the fluctuating field ϕ, Eqn (4.13). In place of 1/2 we put a constant D. The average of an observable is the ensemble average over all noise realizations. So if O is an observable, $\langle O\rangle_\zeta \propto \int D[\zeta]O[\phi(\zeta)]W[\zeta]$, where $W[\zeta]$ is the noise distribution. In our case $\zeta = \partial_x\xi$. It is easy to transform from the variable $\{\zeta\} = \{\phi\}$ keeping in mind the constraint given by Eqn (4.13) that ϕ has to obey throughout space-time. This constraint can be imposed in the form of a delta-function at every point in space and time. After performing a Hubbard-Stratonovich type of transformation which replaces the delta-function by an exponential, followed by the noise integral, we can write the expression for the average in the form of a path integral, $\langle O\rangle_\zeta \propto \int D[\tilde{\phi}]\int D[\phi]O[\phi]e^{-S[\tilde{\phi},\phi]}$. S is the action. The notation $\tilde{\phi}$ is for the auxiliary field [28] and should not be confused with the $\tilde{\phi}$ discussed in the section on linear theory. There, it was just the Fourier transform of the field ϕ. The action, in our case is given by

$$S[\tilde{\phi},\phi] = \int dx \int dt \left(\tilde{\phi}\left[\partial_t\phi - F[\phi]\right] - \tilde{\phi}\mathbf{L}\tilde{\phi}\right), \tag{5.10}$$

where $F[\phi] = D\nabla^2\phi - (v-\phi)\partial_x\phi$, and $\mathbf{L} = -A\partial_x^2$, such that $\langle\zeta(x,t)\zeta(x^{'},t^{'})\rangle = 2\mathbf{L}\delta(x - x^{'})\delta(t-t^{'})$. The double derivative in front of the delta function is because ζ is a conserved noise. The bilinear part is

$$S_0[\tilde{\phi},\phi] = \int dx \int dt \left(\tilde{\phi}(x,t)\left[\partial_t\phi(x,t) - D\nabla^2\phi(x,t) + v\partial_x\phi(x,t)\right] - \tilde{\phi}(x,t)\mathbf{L}\tilde{\phi}(x,t)\right). \tag{5.11}$$

The interaction part is given by

$$S_{\rm int}[\tilde{\phi},\phi] = -u\int dx \int dt \left(\tilde{\phi}(x,t)\phi(x,t)\partial_x\phi(x,t)\right). \tag{5.12}$$

where u parametrizes the strength of the bias and is formally called the three-point coupling constant in the field theory nomenclature. It is more convenient to write the bilinear part of the action in the momentum space. The propagator G_0 and the noise correlator C_0 can be read off straightaway.

$$\begin{aligned} G_0(q_k,\omega) &= \frac{1}{-i\omega + Dk^2 + ikv}, \\ C_0(q_k,\omega) &= -2Ak^2|G_0(q_k,\omega)|^2. \end{aligned} \tag{5.13}$$

We take the non-linear part of the action $S_{\rm int}[\tilde{\phi},\phi] = -u\int dx\int dt\tilde{\phi}\phi\partial_x\phi$ and integrate it by parts yielding, $S_{\rm int} = \frac{u}{2}\int dx\int dt(\partial_x\tilde{\phi})\phi^2$. The interaction vertex in Fourier space comes with a factor of ik because of the derivative. The quantity of interest is the two-point vertex function as a function of the external momentum and frequency. We calculate just the one-loop contribution. The one-loop contribution to the two-point vertex function is shown in Fig (5.14). The directed arrows are the propagators. The propagators with a bar on them are associated with a factor of ik. The generalized loop momentum is

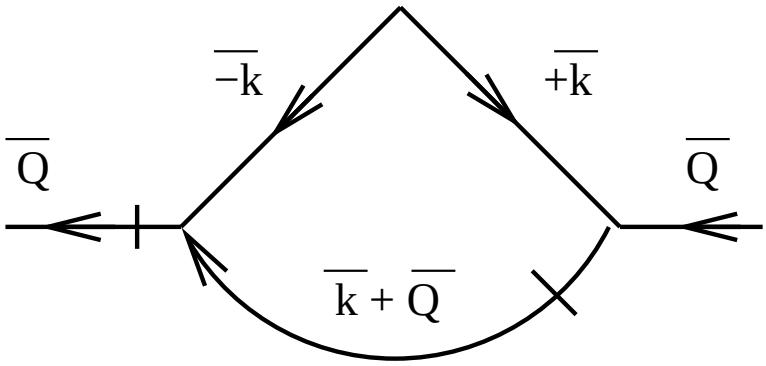

Figure 5.14: Two point Feynman graph to one loop order.

$\bar{k} = \{k, \omega\}$ whereas $\bar{Q} = \{Q, \omega_e\}$ is the generalized external momentum. The correction to the tree level graph is proportional to

$$\text{correction} \propto Qu^2 \int_{2\pi/L}^{\infty} \frac{dk}{2\pi} \int \frac{d\omega}{2\pi} \frac{2(Q+k)Ak^2}{(i\omega + \Gamma)(-i\omega + \Gamma^*)(i\omega + \Gamma')}, \tag{5.14}$$

where $\Gamma = Dk^2 - ivk$ and $\Gamma' = D(Q+k)^2 - iv(Q+k)$, the diagram is evaluated for $\omega_e = 0$. After performing the integral over frequency we are left with

$$\text{correction} \propto \frac{QAu^2}{D} \int \frac{dk}{2\pi} \frac{Q+k}{2Dk^2 + DQ^2 + 2DQk - ivk}. \tag{5.15}$$

We will only focus on the $O(Q^2)$ contribution as it corrects the bare value of the diffusion constant. To $O(Q^2)$ we have

$$\text{correction} \propto \frac{QAu^2}{D} \int \frac{dk}{2\pi} \left[\frac{Q}{2Dk^2} - \frac{Q}{2Dk^2} + \frac{ivQ}{4D^2k^3} \right]. \tag{5.16}$$

So we see that the terms which go as L drops off. The term we are left with is

$$\text{correction} \propto \frac{ivQ^2u^2A}{4D^3} \int \frac{dk}{2\pi} \frac{1}{k^3}. \tag{5.17}$$

But the integrand is odd in k. Under the periodic boundary condition, the range of integration can be symmetrized. Hence the integral above will be zero. The correction to the diffusion constant from the continuum theory is zero.
There may be a reason why this is so. The most obvious reason could be that the inherent discreteness of the dynamics and the model has been neglected in favor of the continuum limit. As the lattice constant goes to zero the interactions become far more local than what we observe in our simulation. The natural check will be to extend the calculation for a discrete geometry.

5.5 The Discrete Case

We start off with the discrete Langevin equation

$$\begin{aligned}\partial_t\phi_p(t) &= (1-\bar{\rho})[\phi_{p-1}(t)-\phi_p(t)]-\bar{\rho}[\phi_p(t)-\phi_{p+1}(t)]+\phi_p(t)[\phi_{p+1}(t)-\phi_{p-1}(t)]\\ &\quad -[\xi_p(t)-\xi_{p-1}(t)],\end{aligned} \tag{5.18}$$

with noise correlation

$$\langle\xi_p(t)\xi_l(t^{'})\rangle = A\delta_{p,l}\delta(t-t^{'}). \tag{5.19}$$

The action can be constructed from the Langevin equation by introducing *Martin-Siggia-Rose* [28] response field $\tilde{\phi}$. Keeping in mind $x_p = pL/2M$ and $q_k = 2\pi k/L$, p and k being integers, we find the Gaussian action to be

$$\begin{aligned}S_0[\tilde{\phi},\phi] &= \sum_{p=0}^{2M-1}\int dt\tilde{\phi}_p(t)[\partial_t\phi_p+\bar{\rho}[\phi_p-\phi_{p+1}]-(1-\bar{\rho})[\phi_{p-1}-\phi_p]\\ &\quad -(\tilde{\phi}_p-\tilde{\phi}_{p-1})A(\tilde{\phi}_p-\tilde{\phi}_{p-1})].\end{aligned} \tag{5.20}$$

The solution to this equation in Fourier space is

$$\begin{aligned}S_0[\tilde{\phi},\phi] &= \frac{1}{2M}\sum_k\int\frac{d\omega}{2\pi}\tilde{\phi}(q_{-k},-\omega)[-i\omega+\bar{\rho}(1-e^{iq_k})-(1-\bar{\rho})(e^{-iq_k}-1)]\phi(q_k,\omega)\\ &\quad -\frac{2A}{2M}\sum_k\int\frac{d\omega}{2\pi}\tilde{\phi}(q_{-k},-\omega)(1-\cos q_k)\tilde{\phi}(q_k,\omega),\end{aligned} \tag{5.21}$$

where

$$\phi(x_p,t) = \frac{1}{2M}\int\frac{d\omega}{2\pi}\sum_{k=0}\phi(q_k,\omega)e^{i(x_pq_k-\omega t)}, \tag{5.22}$$

and

$$\tilde{\phi}(x_p,t) = \frac{1}{2M}\int\frac{d\omega}{2\pi}\sum_{k=0}\tilde{\phi}(q_k,\omega)e^{i(x_pq_k-\omega t)}. \tag{5.23}$$

It is easy to read off the Gaussian propagator(G_0) and noise correlation(C_0) from S_0 in the Fourier space

$$\begin{aligned}G_0(q_k,\omega) &= \frac{2M}{1-i\omega-\cos(q_k)+i(1-2\bar{\rho})\sin(q_k)},\\ &= \tilde{G_0}2M,\end{aligned}$$

where $\tilde{G_0} = 1/(1-i\omega-\cos(q_k)+i(1-2\bar{\rho})\sin(q_k))$.

$$\begin{aligned}C_0(q_k,\omega) &= -8MA(1-\cos q_k)|\tilde{G_0}(q_k,\omega)|^2\\ &= \tilde{C_0}2M,\end{aligned} \tag{5.24}$$

where $\tilde{C_0} = -4A(1-\cos q_k)|\tilde{G_0}(q_k,\omega)|^2$. The interaction action

$$S_{\text{int}}[\tilde{\phi},\phi] = -u\sum_p\int dt\tilde{\phi}(x_p,t)\phi(x_p,t)[\phi(x_{p+1},t)-\phi(x_{p-1},t)], \tag{5.25}$$

has been replaced by $+u/2\sum_p \int dt\phi(x_p,t)\phi(x_p,t)[\tilde{\phi}(x_{p+1},t) - \tilde{\phi}(x_{p-1},t)]$. This gives a factor of $i\sin(q_k)$ in Fourier space and checks out with the continuum limit where the derivative in $\phi\partial_x\phi$ pulls down a factor of ik. The three-point coupling constant is u. We calculate diagrams to one-loop order. The diagram is evaluated for $\omega_e = 0$ and for small values of the external momentum Q_{k_e}. Σ to one-loop order is shown in Fig (5.14). The directed arrows are the propagators and the pointed peak at the top is the noise correlator. Whereever there is a bar, there is $i\sin$ associated to that leg. The diagrams comes with a combinatoric factor of $8 * 1/8$ (8 came from the Wick's theorem and $1/8$ from expanding the interaction in a series). Rules are : a) with every vertex we attach a factor $2iu\sin(q_k)$, where q_k is the momentum, b) for every directed line we assign a $\tilde{G_0}(-q_k,-\omega)$, c) for every noise correlator we attach a factor of $-4A(1-\cos(q_k))$. We will keep terms which are $O(Q_{k_e}^2)$ only. The expression for the diagram is

$$\begin{aligned}\text{Dia} &= \frac{1}{2M}\sum_k \int \frac{d\omega}{2\pi} \frac{-(2iu)^2\sin(Q_{k_e})\sin(q_k+Q_{k_e})4A(1-\cos q_k)}{[1-i\omega-\cos(q_k)+i(1-2\bar{\rho})\sin(q_k)][1+i\omega-\cos(q_k)-i(1-2\bar{\rho})\sin(q_k)]} \\ &* \frac{1}{1+i(\omega_e+\omega_k)-\cos(q_k+q_{k_e})-i(1-2\bar{\rho})\sin(q_k+Q_{k_e})}. \end{aligned} \tag{5.26}$$

The final form of the expression after the frequency integral and assuming $k_e \simeq 0$ is

$$\text{Dia} = \frac{8u^2AQ_{k_e}}{2M}\sum_{k=1}^{2M-1} \frac{\sin(q_k)+Q_{k_e}\cos(q_k)}{2(1-cos(q_k))+Q_{k_e}(sin(q_k)-ivcos(q_k))}, \tag{5.27}$$

where $v = 1-2\bar{\rho}$. Therefore the expression to $O(Q_{k_e}^2)$ is

$$\text{Dia} = -2u^2AQ_{k_e}^2 \tag{5.28}$$

For detailed calculations please refer to the appendix. The correction to the two-point function $\Gamma_{1,1}$, to the one-loop order, goes as the system size. Looking at the bare propagator and the correction term, the diffusion constant can be extracted to the one-loop order. We find

$$\text{D}_{\text{eff}} = \frac{1}{2} + 2u^2A \tag{5.29}$$

Our analytic calculation does not reconcile our simulation result. The simulation result, appears to indicate a non-linear variation of the diffusion constant with the system size which eventually goes to the bare value of $1/2$ as the density and the system size goes to zero. Our analytical calculation on the other hand predicts a constant shift in the diffusion constant to one-loop order and does not show any dependence on the system size. Recently however, we have discovered that the cancellation of the $1/k^2$ contribution in the continuum theory appears to be a mere coincidence. The terms only cancel if we choose to distribute the momentum the way it is shown in Fig (5.14) [71]. We continue to explore the consequences of this finding.

The reason for the mismatch can be due to one of the following other reasons as well : we have fitted a linear theory to the simulation data and we have argued that the enhanced diffusion constant encapsulates all the non-linear effects of the full stochastic differential

equation. It is far more insightful to actually compute the power spectrum order by order and compare the analytic result with the simulation. This will give us a better idea about how the non-linearity actually influences the parameters of our theory. These are among the few avenues we have to pursue to understand the riddle better.

To summarize, we have performed simulations of the power spectrum of the total occupancy in the low density phase. We have outlined the effects of changing system size, density, and boundaries on the oscillations that we observed in the power spectrum. We showed that the oscillations decay faster to a power law with increasing system size. The location of the minima shifts to the left as well. Lowering the density shifts the location of the minima to the right. It appears that the oscillations are not boundary induced and they are fairly generic for both open and closed TASEP. A linear theory was put forward, which accounts for the observed phenomena. The fitting parameter of our theory, namely the diffusion constant D is off it's bare value. In order to answer this puzzle, we resorted to dynamic field theory. The one-loop calculation for the two-point vertex function was performed on a lattice and in a continuum. The correction to the diffusion constant still falls short of capturing the nature of variation of the diffusion constant that we observed in our simulation.

Chapter 6

Summary and Conclusion

This thesis presents two seemingly disparate topics, namely, an analysis of a transition from an active to an absorbing state in a reaction diffusion model and a study of the occupancy power spectrum associated with a driven diffusive system. However, the two topics are linked, both conceptually and methodically: Both describe far-from-equilibrium phenomena where the dynamics of the system plays a critical role, and both are analyzed using field theoretic techniques. For the first model, we perform a full renormalization group analysis, while for the second model, a simple perturbative calculation suffices. For the latter case, Monte Carlo simulations provide the initial insights which guide the theoretical approach.

The first part of the thesis investigates the stability of the ordinary directed percolation (DP) fixed point when the field describing the evolving population is coupled to a fluctuating background, modeled by model A dynamics. The DP problem is arguably the simplest model which exhibits an active to absorbing state transition. Characterized by a scalar order parameter, this transition defines a very fundamental universality class in non-equilibrium critical phenomena. Most transitions into absorbing states fall into this class unless the order parameter has a different symmetry or the state space separates into disjoint subspaces. The stability of the DP fixed point, with respect to various perturbations such as frozen randomness or a non-critical diffusive density, has already been studied, but its coupling to a *critical* fluctuating field has not yet been explored. In the classification of Halerpin and Hohenberg, Model A describes the dynamics of a non-conserved scalar field with Ising-like $\mathbb{Z}_2$ symmetry.

In Chapter 2, we reviewed briefly how the DP action can be derived within the standard Doi-Peliti [14, 15] formalism. This approach relies on second quantized ladder operators to cast the master equation in the form of an imaginary time Schödinger equation. Using a representation in terms of coherent states, a path integral formulation can be obtained (for general review, see [13]). The model A action is well known, describing the non-conserved relaxational dynamics associated with the Landau-Ginzburg-Wilson (LGW) Hamiltonian. It can be expressed in terms of a Langevin equation for the (coarse-grained) order parameter field, with the LGW Hamiltonian providing the thermodynamic force which drives the order parameter field towards the minima of the potential. The fast

degrees of freedom are modeled in the form of a white noise, with average zero and delta-correlated second moment. The Langevin action is then recast as a dynamic functional, following the standard Janssen-De Dominicis approach for construction of a dynamic field theory. As an aside, we should note that the DP action can be obtained in a similar fashion; however, in this approach, the noice correlations do not emerge as naturally as they do in the Doi-Peliti formalism.

The upper critical dimension for both theories is four. Once the dynamic functional of both model components is known, we can look for new novel marginal couplings at four dimensions. We found two new marginal couplings. The stability of the DP fixed point was explored following standard RG techniques, namely, dimensional regularization, ϵ expansion and minimal subtraction. A key result of this analysis is the observation that the Model A dynamics freezes on the time scale of the DP fields, so that the DP fields evolve in a quenched (but highly correlated) background. The effect of a quenched random background, distributed according to a (time-independent) Gaussian, has been considered further by Janssen. He found that the beta functions have only runaway solutions in the physical domain, suggesting that the transition becomes first order. However, this approach does not reflect the full *critical* correlations of the Model A fields. While the problem of a quenched random background with power law correlations can, in principle, be analyzed, it is beyond the scope of this work.

The second part of the thesis focuses on the TASEP model. This model, originally introduced in the context of protein production from messenger RNA [McDonald Gibbs] and also as a stochastic model in pure mathematics, has found applications in diverse disciplines. For both periodic and open boundary conditions, the steady-state configurational probability distribution is exactly known. While uniform for the periodic case, it displays considerable richness for the open case, such as multiple phases, phase co-existence and first and second order phase transitions. The phase diagram is controlled by the entrance (α) and exit rates (β).

While dynamic exponents and local spatio-temporal correlations had been investigated before, the power spectrum associated with a *global* quantity, namely, the total occupancy $N(t)$ of an open TASEP, was studied only recently [6]. The key result was the discovery of damped oscillations, decaying into a power law, characterizing the low density phase. A linearized version of the stochastic equation of motion for the fluctuation of the local density was brought to bear in order to capture the oscillations. This simple theory shows good agreement with Monte Carlo simulations, provided the (theoretical) diffusion coefficient, D, is adjusted appropriately. In this thesis, we provide a detailed analysis of this fitting procedure, exploring how D depends on system size, total average density, and boundary conditions. Using Monte Carlo simulations, we find that D increases rapidly with system size and density, indicating that the interactions (exclusion) plays an important role. To elucidate the role of the boundary conditions, we compare power spectrum data for three cases: the occupancy of an open TASEP of length L, the occupancy of a *window* of width L in a much larger open TASEP, and the occupancy of a window of width L in a much larger *periodic* TASEP. We find that the first two cases are essentially indistinguishable while the third case displays the same ω-dependence for all but the smallest ω. The discrepancies there can be traced to the fact that the periodic boundary

conditions allow a density fluctuation to traverse the window multiple times. A linear theory was again put forward to explain both sets of oscillations in the periodic TASEP and captured the observed phenomena well. Again, however, the fitting parameter (diffusion constant D) were found to deviate substantially from their naive "unrenormalized values". Since the Monte Carlo results suggest that the exclusion interaction comes into play, we computed the first order correction to D from the full nonlinear theory, based on a one-loop calculation of the diffusion propagator in a finite system. Unfortunately, the results were inconclusive: it appears that the thermodynamic limit ($L \to \infty$) does not commute with differentiation with respect to external wave vector. A more careful analysis of the perturbation analysis for the finite system, and of the details of how to take the thermodynamic limit, is required. Alternatively, the whole power spectrum should be calculated order by order and then fitted to the data. This would provide a more systematic view of how the nonlinearity affects the whole function. We plan to pursue this avenue in the future.

Bibliography

[1] C. W. Gardiner, *Handbook of Stochastic Methods*, (Springer, Berlin 1983).

[2] P. Grassberger and K. Sundermeyer, *Phys. Lett. B*, **77**, 220 (1978).

[3] P. Grassberger and A. de La Torre, *Ann. Phys.* (New York), 373 (1979).

[4] C. Macdonald, J. Gibbs and A. Pipkin, *Biopolymers*, **6**, 1 (1968).

[5] F. Spitzer, *Adv. Math*, **5**, 246 (1970).

[6] D. A. Adams, B. Schmittmann and R. K. P. Zia, *Phys. Rev. Lett*, **99**, 020601 (2007).

[7] P. C. Hohenberg and B. I. Halperin, *Rev. Mod. Phys.*, **49**, 435 (1977).

[8] H. K. Janssen 1979, *Dynamical critical phenomena and related topics, Lecture Notes in Physics*, **104**, eds. C. P. Enz (Springer, Heidelberg), 26.

[9] D. E. Wolf, M. Schreckenberg and A. Bachem, *Traffic and granular flow, World Scientific, Singapore*, (1996).

[10] T. E. Harris, *Ann. Prob.*, **2**, 969 (1974).

[11] R. Bausch, H. K. Janssen and H. Wagner, *Z. Phys. B*, **24**, 113 (1976).

[12] D. C. Mattis and M. L. Glasser, *Rev. Mod. Phys*, **70**, 979 (1998).

[13] U. C. Täuber, M. Howard and B. P. Lee, *J. Phys. A: Math Gen.*, **38**, R79 (2005).

[14] M. Doi, *J. Phys. A: Math. Gen.*, **9**, 1465 (1976).

[15] L. Peliti, *J. Phys*, **46**, 1469 (1985).

[16] J. L. Cardy and R. L. Sugar, *J. Phys. A*, **13**, L423 (1980).

[17] H. K. Janssen, *Z. Phys. B*, **42**, 151 (1981).

[18] P. Grassberger, *Z. Phys. B*, **47**, 365 (1982).

[19] H. Hinrichsen, *Adv. Phys.*, **49**, 815 (2000).

[20] H. K. Janssen and U. C. Täuber, *Ann. Phys.*, **315**, 147 (2005).

[21] D. Stauffer and A. Aharony, *Introduction to percolation Theory, second ed., Taylor and Francis, London*, (1994).

[22] S. R. Broadbent and J. M. Hammersley, *Proc. Camb. Phil. Soc.*, **53**, 629 (1957).

[23] P. Ramond, *Field theory- a modern primer*, (1981).

[24] C. Itzykson and J. M. Drouffe, *Statistical field theory*, (Cambridge University Press, Cambridge), (1989).

[25] M. Le Bellac, *Quantum and statistical field theory*, (Oxford University Press, Oxford), (1991).

[26] J. Cardy, *Scaling and renormalization in statistical physics*, (Cambridge University Press, Cambridge), (1996).

[27] B. I. Halperin and P. C. Hohenberg and S. K. Ma, *Phys. Rev. Lett.*, **29**, 1548 (1972).

[28] P. C. Martin, E. D. Siggia and H. A. Rose, *Phys. Rev. A*, **8**, 423 (1973).

[29] H. K. Janssen, *Z. Phys. B*, **23**, 377 (1976).

[30] C. De Dominicis, *J. Physique Colloque*, **37**, C2247 (1976).

[31] U. C. Täuber, *Critical dynamics: a field theory approach to equilibrium and non-equilibrium scaling behavior*, in preparation (to be published at Cambridge University Press, Cambridge) for completed chapters, see
http://www.phys.vt.edu/∼ tauber/utaeuber.html

[32] K. G. Wilson and M. E. Fisher, *Phys. Rev. Lett.*, **28**, 240 (1972).

[33] H.K. Janssen, *Phys. Rev. E*, **55**, 6253 (1997).

[34] A. G. Moreira and R. Dickman, *Phys. Rev. E*, **54**, R3090 (1996).

[35] R. Kree, B. Schaub and B. Schmittmann, *Phys. Rev. A*, **39**, 2214 (1989).

[36] F. van Wijland, K. Oerding and H. J .Hilhorst, *Physica A*, **251**, 179 (1998).

[37] S. Mukherjee, H. K. Janssen, B. Schmittmann, *Physica A*, **384**, Issue 1, 82 (2007).

[38] H . K. Janssen, *private communication*, unpublished.

[39] J. Honkonen and M.Y. Nalimov, *J. Phys. A: Math. Gen.*, **22**, 751 (1989).

[40] H.K. Janssen and B. Schmittmann, *J. Stat. Phys*, **95**, 569 (1999).

[41] A. Parmeggiani, T. Franosch and E. Frey, *Phys. Rev. Lett.*, **90**, 086601 (2003).

[42] R. Lipowsky, S.Klumpp and T. Nieuwenhuizen, *Phys. Rev. Lett*, **87**, 108101, (2001).

[43] D. Chowdhury, L. Santen and A. Schadschneider, *Phys. Rep*, **329**, 199 (2000).

[44] Q. Wei, C. Bechinger and P. Leiderer, *Science*, **287**, 625 (2000).

[45] R. Willmann, G. Schütz and D. Challet, *J. Phys. A* **316**, 413 (2002).

[46] J. M. Burgers, *The Nonlinear Diffusion Equation*, (Riedel, Boston), (1974).

[47] M. Kardar, G. Parisi and Y. C. Zhang, *Phys. Rev. Lett.*, **56**, 889 (1986).

[48] J. Krug, *Phys. Rev. Lett.*, **67**, 1882 (1991).

[49] B. Derrida, *Physics Report*, **301**, 65 (1998).

[50] P. Meakin, P. Ramanlal, L. M. Sander and R. C. Ball, *Phys. Rev. A*, **34**, 5091 (1986).

[51] A. De. Masi, P. A. Ferrari, *J. Statist. Phys.*, (1985). **38** 603.

[52] R. Kutner, H. van Beijeren, *J. Statist. Phys.*, (1985). **39** 317.

[53] S. N. Majumdar and M. Burma, *Phys. Rev. B*, **44**, 5306 (1991).

[54] B. Derrida, M. R. Evans and D. Mukamel, *J. Phys. A*, **26**, 4911 (1993).

[55] P. Pierobon, A. Parmeggiani, F. von Oppen and E. Frey, *Phys. Rev. E*, **72**, 036123 (2005).

[56] G. E. Schütz, *Integrable stochastic many-body systems, Habilitationsschrift, Universität Bonn*, 1998.

[57] M. Kogan and A. Y. Shul'man, *Sov. Phys. JETP*, **29**, 3 (1969).

[58] H. K. Janssen and B. Schmittmann, *Z. Phys. B*, **63**, 517 (1986).
For general review, see B. Schmittmann and R. K. P. Zia, *Statistical Mechanics of Driven Diffusive Systems.*, **17** of Phase Transition and Critical Phenomena, eds C. Domb and J. L. Lebowitz (Academic, New York), (1995).

[59] S. F. Edwards and D. R. Wilkinson, *Proc. R. Soc. London, Ser. A*, **381**, 17 (1982).

[60] D. Forster, D. R. Nelson and M. J. Stephen, *Phys. Rev. A*, **16**, 732 (1977).

[61] S. Gupta, S. N. Majumdar, C. Godréche and M. Burma, *Phys. Rev. E*, **76**, 021112 (2007).

[62] B. Derrida, E. Domany and D. Mukhamel, *J. Stat. Phys.*, **69**, 667 (1992).

[63] B. Derrida, M. R. Evans, V. Hakim and V. Pasquier, *J. Phys. A*, **26**, 1493 (1993).

[64] D. Dhar, *Phase Transition*, **9**, 1 (1987).

[65] L. H. Gwa and H. Spohn, *Phys. Rev. A*, **46**, 844 (1992).

[66] B. Derrida, J. Lebowitz and E. Speer, *Phys. Rev. Lett*, **87**, 150601 (2001).

[67] Z. Nagy, C. Appert and L. Santen, *J. Stat. Phys.*, **109**, 623 (2002).

[68] W. H. Press, S. A. Teukolsky, W. T. Vetterling and B. P. Flannery, *Numerical Recipe in C The Art of Scientific Computing Second Edition*, (Cambridge University Press), (1992).

[69] A. G. Angel and R. K. P. Zia *http://arxiv.org/pdf/0811.1977* (2008).

[70] A. L. Barabasi and H. E. Stanley 1995 *Fractal Concepts in Surface Growth* (Cambridge University Press).

[71] S. Mukherjee and B. Schmittmann, in preparation.

Appendix A

Detailed Calculation of the Beta Function

$$\beta_\circ = \mu\partial_\mu \circ |_{bare}, \tag{A.1}$$

where $\circ$ stands for one of the nonlinear couplings, u_R, g_R, $\bar{g}_R$, v_R, w_R.

$$\begin{aligned}
\beta_u &= \mu\partial_\mu u_R = \mu\partial_\mu [Z_\phi^2 Z_\gamma^1 Z_u^{-1} u\mu^{-\epsilon} G_\epsilon] \\
&= -\epsilon u_R + 2Z_\phi^2 [Z_\phi^{-1}\mu\partial_\mu Z_\phi] Z_\gamma Z_u^{-1} u G_\epsilon \mu^{-\epsilon} + ... \\
&= -\epsilon u_R + 2u_R \mu\partial_\mu \ln Z_\phi + ...
\end{aligned}$$

These finite logarithmic derivatives are the Wilson's functions and will be denoted by ζ. In terms of the Wilson's function we have,

$$\beta_u = -\epsilon u_R + u_R[2\zeta_\phi + \zeta_\gamma - \zeta_u]. \tag{A.2}$$

Similarly the other β functions are,

$$\begin{aligned}
\beta_g &= \mu\partial_\mu [Z_s^{1/2} Z_\lambda Z_g^{-1} g\mu^{-\epsilon/2}\sqrt{G_\epsilon}] \\
&= -\frac{\epsilon g_R}{2} + g_R[\zeta_s/2 + \zeta_\lambda - \zeta_g],
\end{aligned} \tag{A.3}$$

$$\begin{aligned}
\beta_{\bar{g}} &= \mu\partial_\mu [Z_{\tilde{s}}^{1/2} Z_\lambda Z_{\bar{g}}^{-1} \bar{g}\mu^{-\epsilon/2}\sqrt{G_\epsilon}] \\
&= -\frac{\epsilon \bar{g}_R}{2} + \bar{g}_R[\zeta_{\tilde{s}}/2 + \zeta_\lambda - \zeta_{\bar{g}}],
\end{aligned} \tag{A.4}$$

$$\begin{aligned}
\beta_v &= \mu\partial_\mu [Z_\phi Z_s^{1/2} Z_\gamma Z_v^{-1} v\mu^{-\epsilon/2}\sqrt{G_\epsilon}] \\
&= -\frac{\epsilon v_R}{2} + v_R[\zeta_\phi + \zeta_s/2 + \zeta_\gamma - \zeta_v],
\end{aligned} \tag{A.5}$$

$$\begin{aligned}
\beta_w &= \mu\partial_\mu [Z_\phi Z_\lambda Z_w^{-1} w\mu^{-\epsilon} G_\epsilon] \\
&= -\epsilon w_R + w_R[\zeta_\phi + \zeta_\lambda - \zeta_w],
\end{aligned} \tag{A.6}$$

$$\begin{aligned}\beta_{\hat{g}} &= g_R\{-\frac{\epsilon\bar{g}_R}{2}+\bar{g}_R[\zeta_{\tilde{s}}/2+\zeta_\lambda-\zeta_{\bar{g}}]\}+\bar{g}_R\{-\frac{\epsilon g_R}{2}+g_R[\zeta_s/2+\zeta_\lambda-\zeta_g]\}\\ &= -\epsilon\hat{g}_R+\hat{g}_R[\frac{1}{2}(\zeta_{\tilde{s}}+\zeta_s)+2\zeta_\lambda-\zeta_{\bar{g}}-\zeta_g], \qquad (A.7)\end{aligned}$$

$$\begin{aligned}\beta_{\hat{v}} &= v_R\{-\frac{\epsilon\bar{g}_R}{2}+\bar{g}_R[\zeta_{\tilde{s}}/2+\zeta_\lambda-\zeta_{\bar{g}}]\}+\bar{g}_R\{-\frac{\epsilon v_R}{2}+v_R[\zeta_\phi+\zeta_s/2+\zeta_\gamma-\zeta_v]\}\\ &= -\epsilon\hat{v}_R+\hat{v}_R\{\frac{1}{2}(\zeta_{\tilde{s}}+\zeta_s)+\zeta_\phi+\zeta_\gamma+\zeta_\lambda-\zeta_{\bar{g}}-\zeta_v\}. \qquad (A.8)\end{aligned}$$

The Wilson functions to one loop order are,

$$\zeta_\phi=\zeta_{\tilde{\phi}}=\zeta_\gamma=0 \qquad (A.9)$$

$$(A.10)$$

$$\begin{aligned}\zeta_u &= \mu\partial_\mu\ln Z_u=\mu\partial_\mu\ln(1+\frac{3u_R}{2\epsilon})\\ &= \frac{3}{2\epsilon}\beta_u\\ &= -\frac{3u_R}{2}+O(u_R^2), \qquad (A.11)\end{aligned}$$

$$\begin{aligned}\zeta_{\tilde{s}}+\zeta_s &= \mu\partial_\mu\ln Z_{\tilde{s}}+\mu\partial_\mu\ln Z_s=\mu\partial_\mu\ln(Z_{\tilde{s}}Z_s)=2\mu\partial_\mu\ln(Z_{\tilde{s}}Z_s)^{1/2}\\ &= 2\mu\partial_\mu\ln(1+\frac{g_R\bar{g}_R}{8\epsilon})=\frac{1}{4\epsilon}\beta_{\hat{g}}\\ &= -\frac{\hat{g}_R}{4}+O(\hat{g}_R^2), \qquad (A.12)\end{aligned}$$

$$\begin{aligned}\zeta_\lambda &= \mu\partial_\mu\ln Z_\lambda=\mu\partial_\mu\ln(1+\frac{1}{16\epsilon}g_R\bar{g}_R).\\ &= \frac{1}{16\epsilon}\beta_{\hat{g}}=-\frac{\hat{g}_R}{16}+O(\hat{g}_R^2), \qquad (A.13)\end{aligned}$$

$$\begin{aligned}\zeta_{\bar{g}} &= \mu\partial_\mu\ln Z_{\bar{g}}=\mu\partial_\mu\ln(1+\frac{1}{2\epsilon}g_R\bar{g}_R)=\frac{1}{2\epsilon}\beta_{\hat{g}}\\ &= -\frac{\hat{g}_R}{2}+O(\hat{g}_R^2), \qquad (A.14)\end{aligned}$$

$$\begin{aligned}\zeta_g &= \mu\partial_\mu Z_g=\mu\partial_\mu\ln(1+\frac{1}{2\epsilon}g_R\bar{g}_R+w_Rv_R\frac{1}{\epsilon}g_R^{-1})\\ &= \mu\partial_\mu(\frac{1}{2\epsilon}g_R\bar{g}_R+\frac{w_Rv_R\bar{g}_R}{\epsilon g_R\bar{g}_R})\\ &= \frac{1}{2\epsilon}\beta_{\hat{g}}+\frac{\hat{v}_R\beta_w}{\hat{g}_R\epsilon}+\frac{w_R\beta_{\hat{v}}}{\epsilon\hat{g}_R}-\frac{w_R\hat{v}_R}{\epsilon\hat{g}_R^2}\beta_{\hat{g}}\\ &= -\frac{\hat{g}_R}{2}-\frac{\hat{v}_Rw_R}{\hat{g}_R}-\frac{w_R\hat{v}_R}{\hat{g}_R}+\frac{w_R\hat{v}_R}{\hat{g}_R}\\ &= -\frac{\hat{g}_R}{2}-\frac{\hat{v}_Rw_R}{\hat{g}_R}+O(\hat{g}_R^2), \qquad (A.15)\end{aligned}$$

$$\begin{aligned}
\zeta_v &= \mu\partial_\mu \ln Z_v = \mu\partial_\mu \ln(1+\frac{w_R}{1+\rho}\frac{1}{\epsilon}+\frac{(\rho v_R)(\bar{g}_R)}{2(1+\rho)}\frac{1}{\epsilon}+\frac{u_R}{2\epsilon}) \\
&= \mu\partial_\mu(\frac{w_R}{1+\rho}\frac{1}{\epsilon}+\frac{(\rho\hat{v}_R)}{2(1+\rho)}\frac{1}{\epsilon}+\frac{u_R}{2\epsilon}) \\
&= \frac{\beta_w}{1+\rho}\frac{1}{\epsilon}+\frac{(\rho\beta_{\hat{v}})}{2(1+\rho)}\frac{1}{\epsilon}+\frac{\beta_u}{2\epsilon} \\
&= -\frac{w_R}{1+\rho}-\frac{(\rho\hat{v}_R)}{2(1+\rho)}-\frac{u_R}{2} \\
&= -\frac{w_R}{1+\rho}-\frac{(\rho\hat{v}_R)}{2(1+\rho)}-\frac{u_R}{2}+O(\hat{v}_R^2), \qquad \text{(A.16)}
\end{aligned}$$

$$\begin{aligned}
\zeta_w &= \mu\partial_\mu \ln Z_w = \mu\partial_\mu \ln(1+\frac{2w_R}{1+\rho}\frac{1}{\epsilon}+\frac{g_R\bar{g}_R}{4}\frac{1}{\epsilon}+\frac{(\rho v_R)(\bar{g}_R)}{(1+\rho)}\frac{1}{\epsilon}+\frac{u_R}{2}\frac{1}{\epsilon}) \\
&= \mu\partial_\mu(\frac{(2w_R)}{1+\rho}\frac{1}{\epsilon}+\frac{\hat{g}_R}{4\epsilon}+\frac{\rho\hat{v}_R}{(1+\rho)}\frac{1}{\epsilon}+\frac{u_R}{2}\frac{1}{\epsilon}) \\
&= \frac{2\beta_w}{1+\rho}\frac{1}{\epsilon}+\frac{\beta_{\hat{g}}}{4\epsilon}+\frac{\rho\beta_{\hat{v}}}{(1+\rho)}\frac{1}{\epsilon}+\frac{\beta_u}{2}\frac{1}{\epsilon} \\
&= -\frac{2w_R}{1+\rho}-\frac{\hat{g}_R}{4}-\frac{\rho\hat{v}_R}{(1+\rho)}-\frac{u_R}{2}+O(w_R^2). \qquad \text{(A.17)}
\end{aligned}$$

Hence the Gell-Mann-Low functions to 1 loop order are,

$$\begin{aligned}
\beta_u &= -\epsilon u_R + u_R[2\zeta_\phi+\zeta_\gamma-\zeta_u] = -\epsilon u_R + u_R[-(-\frac{3u_R}{2})] \\
&= -\epsilon u_R+\frac{3u_R^2}{2}, \qquad \text{(A.18)}
\end{aligned}$$

$$\begin{aligned}
\beta_{\hat{g}} &= -\epsilon\hat{g}_R+\hat{g}_R[\frac{1}{2}(\zeta_{\tilde{s}}+\zeta_s)+2\zeta_\lambda-\zeta_{\bar{g}}-\zeta_g] \\
&= -\epsilon\hat{g}_R+\hat{g}_R[\frac{1}{2}(-\frac{\hat{g}_R}{4})+2(-\frac{\hat{g}_R}{16})-(-\frac{\hat{g}_R}{2})-(-\frac{\hat{g}_R}{2}-\frac{\hat{v}_R w_R}{\hat{g}_R})] \\
&= -\epsilon\hat{g}_R+\hat{g}_R[-\frac{\hat{g}_R}{4}+\hat{g}_R+\frac{\hat{v}_R w_R}{\hat{g}_R}] \\
&= -\epsilon\hat{g}_R+\hat{g}_R[\frac{3\hat{g}_R}{4}+\frac{\hat{v}_R w_R}{\hat{g}_R}] \\
&= -\epsilon\hat{g}_R+\frac{3\hat{g}_R^2}{4}+\hat{v}_R w_R, \qquad \text{(A.19)}
\end{aligned}$$

$$\begin{aligned}
\beta_{\hat{v}} &= -\epsilon\hat{v}_R+\hat{v}_R\{\frac{1}{2}(\zeta_{\tilde{s}}+\zeta_s)+\zeta_\phi+\zeta_\gamma+\zeta_\lambda-\zeta_{\bar{g}}-\zeta_v\} \\
&= -\epsilon\hat{v}_R+\hat{v}_R\{\frac{1}{2}(-\frac{\hat{g}_R}{4})+(-\frac{\hat{g}_R}{16})-(-\frac{\hat{g}_R}{2})-(-\frac{w_R}{1+\rho}-\frac{(\rho\hat{v}_R)}{2(1+\rho)}-\frac{u_R}{2})\} \\
&= -\epsilon\hat{v}_R+\hat{v}_R\{-\frac{\hat{g}_R}{8}-\frac{\hat{g}_R}{16}+\frac{\hat{g}_R}{2}+\frac{w_R}{1+\rho}+\frac{(\rho\hat{v}_R)}{2(1+\rho)}+\frac{u_R}{2}\} \\
&= -\epsilon\hat{v}_R+\hat{v}_R\{\frac{5\hat{g}_R}{16}+\frac{w_R}{1+\rho}+\frac{(\rho\hat{v}_R)}{2(1+\rho)}+\frac{u_R}{2}\}, \qquad \text{(A.20)}
\end{aligned}$$

$$\begin{aligned}\beta_w &= -\epsilon w_R + w_R[\zeta_\phi + \zeta_\lambda - \zeta_w] = -\epsilon w_R + w_R[-\frac{\hat{g}_R}{16} - (-\frac{2w_R}{1+\rho} - \frac{\hat{g}_R}{4} - \frac{\rho\hat{v}_R}{(1+\rho)} - \frac{u_R}{2})] \\ &= -\epsilon w_R + w_R[-\frac{\hat{g}_R}{16} + \frac{2w_R}{1+\rho} + \frac{\hat{g}_R}{4} + \frac{\rho\hat{v}_R}{(1+\rho)} + \frac{u_R}{2}] \\ &= -\epsilon w_R + w_R[\frac{3\hat{g}_R}{16} + \frac{2w_R}{1+\rho} + \frac{\rho\hat{v}_R}{(1+\rho)} + \frac{u_R}{2}]. \end{aligned} \tag{A.21}$$

Appendix B

Calculation of the Diagram (5.14) to One-Loop Order

The expression for the diagram is

$$\begin{aligned}\text{Dia} &= \frac{1}{2M}\sum_k \int \frac{d\omega}{2\pi} \frac{-(2iu)^2 \sin(Q_{k_e})\sin(q_k+Q_{k_e})4A(1-\cos(q_k))}{[1-i\omega-\cos(q_k)+i(1-2\bar{\rho})\sin(q_k)][1+i\omega-\cos(q_k)-i(1-2\bar{\rho})\sin(q_k)]} \\ &* \frac{1}{1+i(\omega_e+\omega_k)-\cos(q_k+Q_{k_e})-i(1-2\bar{\rho})\sin(q_k+Q_{k_e})}. \end{aligned} \tag{B.1}$$

Lets do the ω integral first. Let define $v = 1-2\bar{\rho}$. The ω integral is given by

$$I_\omega = \int \frac{d\omega}{2\pi} \frac{-i}{[\omega+i\Gamma][\omega-i\Gamma^*][\omega-i\Gamma_1^*]}, \tag{B.2}$$

Where $\Gamma = 1-\cos(q_k)+iv\sin(q_k)$ and $\Gamma_1^* = 1-\cos(q_k+Q_{K_e})-iv\sin(q_k+Q_{k_e})$.

The singularity in the lower half plane is at $\omega = v\sin(q_k)+i(\cos(q_k)-1)$. After performing the contour integral we have

$$I_\omega = \frac{1}{2(1-\cos(q_k))[(1-\cos(q_k))+(1-\cos(Q_{k_e}+q_k))+iv\sin(q_k)-iv\sin(Q_{k_e}+q_k)]}. \tag{B.3}$$

Assuming the external momentum $K_e \simeq 0$ we can approximate

$$\cos(Q_{k_e}+q_k) = \cos(q_k) - Q_{k_e}\sin(q_k), \tag{B.4}$$

$$\sin(Q_{k_e}+q_k) = \sin(q_k) + Q_{k_e}\cos(q_k). \tag{B.5}$$

Under this assumption the expression for I_ω reduces to

$$I_\omega = \frac{1}{2(1-\cos(q_k))\{2(1-\cos(q_k))+Q_{k_e}\sin(q_k)-ivQ_{k_e}\cos(q_k)\}}. \tag{B.6}$$

So the entire diagram looks like

$$\text{Dia} = \frac{8u^2AQ_{k_e}}{2M}\sum_k \frac{\sin(q_k) + Q_{k_e}\cos(q_k)}{2(1-\cos(q_k)) - ivQ_{k_e}\cos(q_k) + Q_{k_e}\sin(q_k)}, \tag{B.7}$$

$$\text{Dia} = \frac{8u^2AQ_{k_e}}{2M}\sum_k \frac{(\sin(q_k) + Q_{k_e}\cos(q_k))\left(1 - \frac{Q_{k_e}}{2(1-\cos(q_k))}(\sin(q_k) + iv\cos(q_k))\right)}{2(1-\cos(q_k))}. \tag{B.8}$$

Extracting the terms to $O(Q_{k_e}^2)$ we have

$$\text{correction} = \frac{8u^2AQ_{k_e}^2}{2M}\sum_k \frac{1}{2(1-\cos(q_k))}\left[cos(q_k) - \frac{sin^2(q_k)}{2(1-\cos(q_k))}\right]. \tag{B.9}$$

The term $\sin(q_k)\cos(q_k)/4(1-\cos(q_k))^2$ has been dropped, as it is an odd term and would drop out under periodic boundary condition. Simplifying the expression in Eqn (B.9) and then carrying out the summation we have

$$\text{correction} = \frac{2u^2AQ_{k_e}^2}{2M}(-2M) \tag{B.10}$$

Therefore

$$\text{correction} = -2u^2AQ_{k_e}^2 \tag{B.11}$$